HIGH-INTENSITY FOCUSED ULTRASOUND (HIFU) INDUCED HYPERECHOIC REGIONS FOR THE ULTRASOUND GUIDANCE OF HIFU THERAPY

Brian Alan Rabkin

A dissertation submitted in partial fulfillment of the requirements for the degree of

Doctor of Philosophy

University of Washington

2004

Program Authorized to Offer Degree: Department of Bioengineering

UMI Number: 3151654

INFORMATION TO USERS

The quality of this reproduction is dependent upon the quality of the copy submitted. Broken or indistinct print, colored or poor quality illustrations and photographs, print bleed-through, substandard margins, and improper alignment can adversely affect reproduction.

In the unlikely event that the author did not send a complete manuscript and there are missing pages, these will be noted. Also, if unauthorized copyright material had to be removed, a note will indicate the deletion.
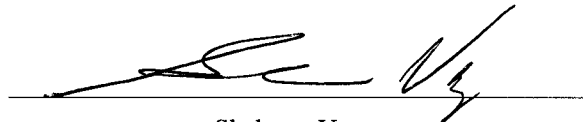
UMI®

UMI Microform 3151654

University of Washington

Graduate School

This is to certify that I have examined this copy of a doctoral dissertation by
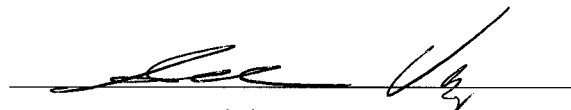
Brian Alan Rabkin

and have found that it is complete and satisfactory in all respects,
and that any and all revisions required by the final
examining committee have been made.
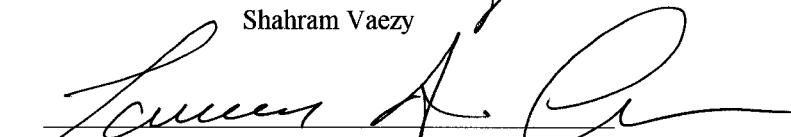
Chair of Supervisory Committee:

_____

Shahram Vaezy

Reading Committee:

_____

Shahram Vaezy

_____

Lawrence A. Crum

_____

Thomas J. Matula

Date: December 10, 2004

University of Washington

Abstract

High-Intensity Focused Ultrasound (HIFU) Induced Hyperechoic Regions for the Ultrasound
Guidance of HIFU Therapy

Brian Alan Rabkin

Chair of the Supervisory Committee:
Shahram Vaezy, Associate Professor
Department of Bioengineering

*High Intensity Focused Ultrasound (HIFU) treatment of soft tissues has been shown to result in a
hyperechoic region in B-mode ultrasound (US) images. The goals of this project were to gain an
understanding of the mechanisms involved in the production of a hyperechoic region and to
assess the use of the hyperechoic region as a targeting method for ensuring the proper placement
of the HIFU focus prior to commencement of therapy. The objectives of this dissertation were to:
(1) confirm if cavitation is involved in the appearance of a hyperechoic region; (2) determine if
there is a relationship between temperature change and the formation of a hyperechoic region;
and (3) determine if a hyperechoic region can be used for targeting of the HIFU focal region by
assessing the extent of tissue damage involved.*

*For studying the involvement of cavitation during the appearance of a hyperechoic region, a US-
system was developed. The system consisted of (1) a single-element HIFU transducer (3.3 MHz)
placed coaxially to (2) a broadband single element unfocused cavitation detector, (0.5-5.5 MHz)
and coplanar with (3) an imaging probe (bandwidth of 5-9 MHz). A thermocouple was located
near the HIFU focus for thermal measurements. HIFU at 220 - 1710 W/cm^2 was applied for 10 s
to porcine muscle in-vivo. Cavitation activity was detected by both active and passive cavitation
detection methods with good correlation during the formation of a hyperechoic region in a
diagnostic US image. Thermal measurements showed the initial formation of bubbles at the
HIFU focus to be due to acoustic cavitation alone or in conjunction with boiling. In addition, the
formation of a hyperechoic region resulted in bubble-enhanced heating at the treatment site.*

*The short- and long-term (0 h – 14 days) tissue damage associated with the production of a
hyperechoic region useful for targeting of the HIFU treatment site was evaluated in vivo in rabbit*

muscle. Short duration HIFU pulses (31.25 and 62.5 ms at 4390 and 3660 W/cm², respectively) were found to produce immediate damage to cells and blood vessels within the HIFU focus in 32.5% of 120 samples, followed by normal tissue healing.

TABLE OF CONTENTS

ii

ABBREVIATIONS

ACD	Active Cavitation Detection
AE	Acoustic Energy
DC	Duty Cycle
f_0	Fundamental Insonation Frequency
HIFU	High Intensity Focused Ultrasound
I	Intensity
IC	Inertial Cavitation
PCD	Passive Cavitation Detection
PRF	Pulse Repetition Frequency
RF	Radio Frequency Signal
RMS	Root Mean Square
SATA	Spatial Average Temporal Average
SATP	Spatial Average Temporal Peak
SC	Stable Cavitation
US	Ultrasound

LIST OF FIGURES

LIST OF TABLES

Acknowledgements

The author wishes to express sincere appreciation of the people that have aided in both the completion of this thesis and for the completion of a doctorate degree in Bioengineering. I would especially like to thank my advisor, Professor Shahram Vaezy, for being a friend and mentor from well before I had the wonderful opportunity of joining his group. I am also thankful for the support and friendship I received from my colleagues at the Center for Industrial and Medical Ultrasound (CIMU) and the Department of Bioengineering.

I would especially like to thank my colleagues that had a direct influence on the research and outcome of this thesis: my advisor and mentor Shahram Vaezy; fellow graduate student/post-doc and friend, Vesna Zderic, for her hard work and advice; animal technician Frank Starr III, for his humor and expertise; electronic technician, Terry Myntii, for his help and work with electronic components; veterinarians and experts on any thing observable with a microscope, Sue Knoblaugh and Denny Liggitt, for helping me with the histological analysis; friend, former lab mate, and Fourier transform expert, Tobias Mann, who's help was beyond valuable for the analysis of RF signals; thermal monitoring expert, fellow graduate student, Ajay Anand, for lending an ear or two; fellow graduate student, Neil Own, for his expertise on image processing; an outstanding graduate student, Robyn Greaby, for her expertise and patience; Larry Crum and Tom Matula for thier advice and help when it came to the detection of bubbles; and, my friend, Anne Boyd for all her patience and editorial comments.

Dedication

I dedicate this thesis to my family which has given me love, joy, and support throughout my life.

1. INTRODUCTION

1.1. MOTIVATION

High Intensity Focused Ultrasound (HIFU) has been explored for its therapeutic use in the treatment of malignant and benign tumors (Gianfelice et al. 2003; Hynynen et al. 2001; Rowland et al. 1997; Van Leenders et al. 2000; Wu et al. 2002; Wu et al. 2003), hemostasis (Delon-Martin et al. 1995; Hynynen et al. 1996; Martin et al. 1999; Vaezy et al. 2001), and the transfection of DNA (Miller and Song 2003). The main advantage of HIFU is its non-invasive nature; the focus where therapy occurs can be placed deep within a patient's body without affecting the intervening tissue layers. In order to utilize this advantage, the development of a real-time targeting and monitoring method for the initial placement of the focus at the appropriate therapy site and the observation of changes to tissue during treatment is required.

Current methods of guiding and monitoring transcutaneous applications of HIFU for non-invasive therapies include magnetic resonance imaging (MRI) and diagnostic ultrasound (US) imaging techniques. While MRI provides excellent soft tissue contrast and the ability to measure temperatures at the HIFU treatment site, it has several drawbacks including its overall expense, its non-portability, the need to use special HIFU equipment that does not interfere with the magnetic field, and the slow rate of image presentation – reported as 5-10 sec after HIFU exposure (Bohris et al. 2001; Righetti et al. 1999). US guidance of HIFU therapy has been used because of the portability, low cost, real-time image processing, simple integration with HIFU instruments, and extensive availability of diagnostic US (Vaezy et al. 2001; Wu et al. 2003). The use of US visualization for the guidance and monitoring of HIFU therapies most often relies on the appearance of a hyperechoic region in the US image (Fry et al. 1995; ter Haar et al. 1989; Wu et al. 2003). A hyperechoic region is an area of increased echogenicity that appears in an US image as a bright obvious change in grey-scale within the target tissue during HIFU treatment.

The mechanisms involved in the appearance of a hyperechoic region at the HIFU exposure site are still unclear (Wu, et al. 2003). It has been postulated that the formation of a hyperechoic region results from bubble activity generated during HIFU treatment (Bailey et al. 2001; ter Haar

et al. 1989; Vaezy et al. 2001; Wu et al. 2003). Determining whether bubbles are involved in the appearance of a hyperechoic region is important because, when bubbles are present in an ultrasound field they will be driven into motion by the mechanical action of the ultrasound and can result in an increased rate of heating and/or mechanical damage to the surrounding tissue (Church 2002; Leighton 1994). Tissue damage, in the form of pitting, rupture, and tearing of tissue can result from shear forces, microstreaming, shock waves, and fluid microjets produced by the stable oscillation and/or inertial collapse of bubbles in an acoustic field (Barkman et al. 1999; Clarke and ter Haar 1997; Vaezy et al. 2001; Poliachik et. al 2001). Once the mechanisms involved in, and the bioeffects that result from the appearance of a hyperechoic region have been determined, the appearance of a hyperechoic region can be better utilized for the guidance and monitoring of HIFU therapies.

1.2. OBJECTIVE

This dissertation describes investigations into the source of hyperechoic regions in B-mode diagnostic ultrasound images during the visualization of HIFU therapy. The role of bubbles in the generation of hyperechoic regions and the thermal and/or mechanical mechanisms involved in their inception were studied. Also the short- and long-term damage associated with the production of a hyperechoic region produced primarily by acoustic cavitation was examined.

1.3. RESEARCH GOALS

The HIFU treatment site has been shown to occur outside of the geometric focus of the transducer (Bailey et al. 2001; Clarke and ter Haar 1997; Hynynen 1991; Watkin et al. 1996). Hynynen (1991) observed the appearance of hyperechoic regions originating outside of the HIFU focus and close to tissue discontinuities such as muscle group interfaces and blood vessels. This was attributed to the preferential occurrence of cavitation damage close to blood vessels and other tissue interfaces (Fry et al. 1970; NCRP 2002). Lesions have also been observed in the near field of the HIFU transducer proximal to the geometric focus (Bailey et al. 2001; Watkin et al. 1996). The position shift of the lesion towards the HIFU transducer was attributed to an increase in heating in the near field as a result of an increase in the absorption coefficient of tissue due to the

presence of bubbles and to a minor degree the non-linear propagation of the US waves (Bailey et al. 2001; Watkin et al. 1996). Therefore, a method of locating the HIFU focus within the desired treatment site prior to commencement of therapy is required.

The overall goal of this project is to assess the use of a HIFU-induced hyperechoic region in a B-mode US image as a targeting method for ensuring the proper placement of the HIFU focus within the desired treatment site prior to commencement of therapy. The objectives of this dissertation were to: (1) determine if cavitation is involved in the appearance of a hyperechoic region; (2) determine if there is a relationship between temperature change and the formation of a hyperechoic region; and (3) determine if a hyperechoic region can be used for targeting of the HIFU focal region by assessing the extent of tissue damage involved. The following specific aims were accomplished:

Specific Aim I: Determine the involvement of cavitation in the formation of a hyperechoic region during HIFU. This set of experiments was done to correlate the onset of a hyperechoic region with the onset of cavitation as determined by active and passive cavitation detection, *in vivo* (in pig muscle). The results of the following activities are discussed in Chapter 3:

1. Development and characterization of an integrated HIFU system (a) for real-time US visualization of the formation of HIFU lesions and (b) for measuring cavitation activity by active and passive cavitation detection at the HIFU focus during the appearance of a hyperechoic region.

2. Determination of the relationship between the onset of cavitation and the appearance of a hyperechoic region at the HIFU focus over a range of HIFU intensities *in vivo* in pig muscle.

Specific Aim II: Determine the relationship between the temperature at the HIFU focus with the formation of a hyperechoic region at different HIFU intensities *in vivo*. This set of experiments was done to correlate changes in tissue temperature at the HIFU focus with the appearance of cavitation and the formation of a hyperechoic region at the focus. The results of the following experiments are discussed in Chapter 4:

1. Incorporation of a thermocouple for measuring the temperature at the HIFU focus into the system developed in Chapter 3.

2. Determination of the relationship between the rate of tissue temperature increase at different HIFU intensities, the presence of cavitation (by PCD), and the appearance of a hyperechoic region *in vivo* in pig muscle.

Specific Aim III: Determine if hyperechoic regions can be produced *in vivo* without tissue damage. This set of experiments was done to determine the HIFU parameters for producing a hyperechoic region with short exposures *in vivo* in rabbit muscle and assessing the short- and long-term tissue damage at the lesion sites:

1. An integrated HIFU system was developed for real-time US visualization of the formation of HIFU lesions for transcutaneous applications in rabbit thigh muscles.

2. The HIFU intensity values were determined for the formation of a hyperechoic region within a relatively short HIFU exposure (< 0.5 and < 1.0 s) in rabbit thigh muscle *in vivo*.

3. The short- and long-term tissue damage induced during the production of a hyperechoic region by short transcutaneous HIFU exposures useful determining the treatment site in an US image, was determined (using the parameters determined in sub aim 2). Histological and morphological assessments of tissue damage were done 0 hour, 4 hhour, 2, 7 and 14 days post HIFU exposures that resulted in the production of a hyperechoic region in rabbit thigh muscle *in vivo*.

1.4.   SIGNIFICANCE

HIFU therapy is gaining acceptance as a modality for the treatment of malignant and benign cancers (Wu, et al. 2004; Mulcahy et al. 2004; Chapelon et al. 1999). In addition to the use of HIFU for cancer therapy, HIFU has been studied for its use in the cessation of bleeding during hemostasis (Martin et al. 1999; Vaezy et al. 2001, Vaezy et al. 1998). Because US is portable, low cost, simple to integrate with HIFU instruments, extensively available, and a real-time

imaging modality, it has been extensively used for the guidance and monitoring of HIFU therapies. Since the use of US visualization for the guidance and monitoring of HIFU therapies most often relies on the appearance of a hyperechoic region in the US image (Fry et al. 1995; ter Haar et al. 1989; Wu et al. 2003) it is important to understand the mechanisms involved in the appearance of the hyperechoic region to improve treatment planning, guidance, and monitoring.

1.5.   ORGANIZATION OF THE DISSERTATION

In Chapter 2, a description of the predominant mechanisms, thermal and cavitation, that produce tissue damage during HIFU therapy. This is followed by a description of the HIFU in current clinical research and the current state of knowledge regarding the role of bubbles in the appearance of a hyperechoic region in an US image at the HIFU treatment site.

Chapter 3 presents a study done to determine if cavitation, and therefore bubbles, is involved in the formation of a hyperechoic region in an US image at the HIFU treatment site *in vivo*. An US system was developed for measuring the cavitation activity by both active and passive cavitation detection while recording changes in B-mode US image echogenicity at the HIFU focus during treatments. A study was conducted *in vivo* in the thigh and back muscles of 6 juvenile pigs for HIFU exposures of 10 s duration, 80% duty cycle, and *in situ* intensities of 220-1710 W/cm^2 at 3.32 MHz. Cavitation activity, with good correlation, was detected by both active and passive cavitation detection methods during the formation of a hyperechoic region at the site of HIFU treatment in the diagnostic US image.

A second *in vivo* study to further understand the involvement of bubbles during the appearance of a hyperechoic region is described in Chapter 4. During this study, thermal measurements were conducted at the HIFU focus, along with PCD, and measurements of changes in the echogenicity of the US image. To measure the thermal behavior of the tissue at the HIFU focus, a fine wire thermocouple was incorporated into the US system used in the study described in Chapter 3. The thermocouple was placed either at or near the HIFU focus during exposures with *in situ* intensities of 220-1710 W/cm^2 for 10 s treatment times. The appearance of a hyperechoic region was found to result from acoustic cavitation that in turn resulted in bubble-enhanced heating, and

to result from boiling and cavitation after the tissue at the HIFU focus achieved a temperature above 100°C.

Chapter 5 describes an *in vivo* study in rabbit thigh muscle for determining the short- and long-term (0 hours to 14 days) tissue damage associated with the production of a hyperechoic region adequate for targeting of the HIFU treatment site. An US-guided HIFU system that incorporated a curvilinear (CL10-5) imaging probe with a 3.2 MHz HIFU transducer was developed for transcutaneous application in rabbit thigh muscle. A set of preliminary studies was first performed to determine a low dose for the production of a hyperechoic region in the US image and to optimize a method for tissue harvesting during the survival study. During the survival study, HIFU exposures were conducted at intensities of 4390 and 3660 W/cm^2 and durations of 31.25 and 62.5 ms, respectively. A hyperechoic region appeared in 82% of the HIFU exposures and tissue damage was found in 39 of 120 samples in which the hyperechoic region occurred. Short-term damage, 0 and 4 h post treatment, was typified by intracellular cavities 4-25 μm in diameter, indicative of cavitation induced damage. From day 2 to 14, the treated site followed a normal healing process.

Chapter 6 is a summary of the research done towards completion of this thesis and a brief discussion of future studies needed prior to the use of hyperechoic regions for targeting of the HIFU focal site in the clinical setting.

2. HIGH INTENSITY FOCUSED ULTRASOUND

2.1.   BIOEFFECTS OF HIFU

Tissue damage at the HIFU focus can be restricted to a very well defined volume, typically the size of the focus, which has lead to its potential usefulness as a therapeutic modality for the treatment of tumors. During HIFU therapy, ultrasound waves are focused to a concentrated ellipsoid focal volume of approximately 1 mm by 10 mm depending on the frequency. HIFU intensities are typically between 1,000 to 10,000 W/cm^2 at frequencies between 0.75 to 5 MHz. The predominant causes of tissue damage, in the form of a lesion, by ultrasound at the HIFU focus results from the conversion of mechanical energy into heat and from cavitation. When ultrasound waves in the form of mechanical energy interact with tissue at the HIFU focus, absorption and scattering occur. The absorption of the US waves results in a rise in tissue temperature that is dependent on parameters specific to both the tissue and the US wave. In addition, cavitation – the formation and oscillation of bubbles – can result from the pressure fluctuations with each acoustic cycle. As the negative portion of the US pressure wave passes through tissue, either preexisting vapor or gas voids or gas that is drawn out of solution can begin to form bubbles and grow (Apfel and Holland 1991; Church 2002; Leighton 1994; Maris and Quan 1989). Different bioeffects can arise from thermal and non-thermal (cavitation) mechanisms at the HIFU focus.

The localized deposition of thermal energy results in the destruction of cells at a rate that is dose dependent. The rate of cell death depends upon the tissue type and condition of the cells. Injury to cells starts occurring when the tissue temperature is raised to 43°C, with cell death occurring after 30-60 minutes (Kennedy et al. 2003; ter Haar et al. 1988). As the temperature rises the extent of tissue damage and the time needed to cause irreversible cell death decreases exponentially (Vykhodtseva et al. 2000). For example, the temperature at the HIFU focus can reach 70°C within 1 s and result in coagulative necrosis of tissue in the focal volume(Chen et al. 1993).

Tissue damage from a purely thermal mechanism is well defined, adhering to the shape of the HIFU focus (Chen et al. 1993; Fry et al. 1955; Melodelima et al. 2003). In contrast, lesions produced in the presence of cavitation tend to form unpredictably with the majority of damage occurring closer to the HIFU source and tadpole-shaped lesions (Bailey et al. 2001; Chen et al. 2003; Malcolm and ter Haar 1996; Meaney et al. 2000; Watkin et al. 1996). Cavitation at the HIFU focus results in pitting, rupturing and tearing of tissue (Barkman et al. 1999; Clarke and ter Haar 1997; Vaezy et al. 2001). The formation of microbubbles in tissue during HIFU results in increased scattering and attenuation and an increase in the rate in which energy is deposited within tissue (Barkman et al. 1999; Clarke and ter Haar 1997; Holt and Roy 2001). This increase in the rate of energy deposition results in a bubble-enhanced rapid rise in temperature in an ultrasound field *in vitro* (Holt and Roy 2001; Watmough et al. 1993), *ex vivo* (Clarke and ter Haar 1997) and *in vivo* (Barkman et al. 1999; Hynynen 1991; Lele 1987; Sokka et al. 2002). Therefore, treatment parameters below that of the cavitation threshold are usually used to produce controlled coagulative necrotic lesions (Hynynen 1991; Malcolm and ter Haar 1996).

Indirect tissue damage outside of the HIFU treatment site has been reported when vessel occlusion within the treatment site has occurred. Necrosis and damage to adjacent tissues result from occluded blood vessels at the focus, and therefore a loss of blood perfusion to the adjacent tissues (Chen et al. 1999). Vascular damage can occur from either purely thermal or cavitation mechanisms (Miller and Gies 1998). Several studies have explored the use of HIFU induced vascular damage, specifically occlusion to restrict blood flow to tumors for therapeutic purposes (Wu et al. 2002; Wu et al. 2003) and for the stopping of bleeding during HIFU induced hemostasis (Martin et al. 1999; Vaezy et al. 1998).

2.2. HIFU IN THE CLINICAL SETTING

The ability of HIFU to treat tissue at a distance from the HIFU source, without causing damage to the intervening tissue, has resulted in an effort to develop HIFU for non-invasive surgery. This effort started in the 1950's when HIFU induced lesions were produced deep within the brains of cats and monkeys (Fry et al. 1955; Fry et al. 1954). Technological limitations resulted in little interested in HIFU for therapy during the 1960s, 1970, and 1980s. As technology has improved,

research into the usefulness of HIFU as a non-invasive surgical tool has grown dramatically. Currently, with over 1000 patients treated between December of 1997 and October of 2001, extensive clinical use of HIFU for the treatment of solid tumors has been conducted in China (Wu et al. 2004). HIFU treatment in China has included malignant and metastatic tumors of the liver, pancreas, bone, breast, and kidney, along with benign tumors in the uterine myoma, breast, and liver. HIFU has also been approved for clinical use out side of China in the non-invasive treatment of prostate cancer and benign prostatic hyperplasia (Chapelon et al. 1999; Sanghvi et al. 1999; Thuroff et al. 2003; Blana et al. 2004). Clinical trials are currently underway for the treatment of liver tumors (Kennedy et al. 2004) in the United Kingdom. HIFU has recently been approved for the treatment of benign uterine fibroids using MRI guidance in the United States (Mulcahy and Franklin 2004). Since HIFU is non invasive, the rate of recovery after HIFU treatment has been shown to be more rapid than conventional invasive surgical methods (Mulcahy and Franklin 2004; Wu et al. 2004). Although there has been concern over the likelihood of increasing the number of circulating tumor cells after HIFU ablation, a recent study has found that this does not occur and that there was also a reduction in the amount of circulating mRNA associated with the tumors after HIFU ablation (Wu et al. 2004).

2.3. EVIDENCE OF THE INVOLVEMENT OF BUBBLES DURING THE APPEARANCE OF A HYPERECHOIC REGION

Since the appearance of a hyperechoic region in an US image is most often used for the US guidance and monitoring of HIFU therapies, an understanding of the mechanisms involved in the appearance of a hyperechoic region is needed. A growing body of evidence suggests the presence of microbubbles at the focal site. First, during HIFU ablation, coagulative necrosis lesions could not be produced beyond the hyperechoic region. This was believed to result from the inability of US to pass through microbubbles (Fry et al. 1995). Second, bright speckle size spots, that were assumed to be bubbles, have been observed with real-time US monitoring escaping into the vascular system of the liver from the focal site during *in vivo* HIFU exposures (Vaezy et al. 2001). Third, the production of hyperechoic bright spots in the HIFU near field (between the HIFU focus and transducer) was observed only in tissues that shared the same vascular network with the tissue that the original hyperechoic region was formed within. It was, therefore,

concluded that bubbles were produced at the focus during the formation of the initial hyperechoic region and perfused to adjacent tissues in the near field, resulting in the production of an additional hyperechoic region (Fry et al. 1995). Fourth, backscattering of US has been shown not to change in a significant manner due to thermal coagulation of tissue in the absence of bubbles (Bush et al. 1993). During the studies described above, no measurements of acoustic emissions distinct to cavitation were performed.

Cavitation is typically measured by either passive cavitation detection (PCD) or active cavitation detection (ACD) (Leighton 1994; Chen et al. 2003; Roy et al. 1990; Fry et al. 1995). During PCD, the radio frequency (RF) signal of the detector is collected while the region of interest in the medium is being sonicated by a different source (Leighton 1994; Chen et al. 2003). With PCD, the two categories of cavitation, stable and inertial, can be distinguished by the frequency spectrum of the RF signal collected from the region of interest (Leighton 1994) . During stable cavitation (SC), the size of the bubble changes are relatively little with each acoustic cycle and the restoring force of the internal gas governs the bubble dynamics. SC can be detected as a peak in the frequency spectrum of a RF signal collected by PCD at the harmonics ($2f_0$, $3f_0$, etc.), subharmonics ($f_0/2$, $f_0/3$, etc.), and ultraharmonics ($3f_0/2$, $3f_0/2$, etc.), where f_0 is the insonation frequency. During inertial cavitation (IC), the bubbles grow relatively large in a few acoustic cycles and violently collapse. IC is detected by an increase in signal amplitude of the RF signal collected by PCD over a broad range of frequencies. During ACD, bubbles in the region of interest are interrogated with a short duration US pulse and the RF of the reflected signal is collected (Roy et al. 1990). The level of cavitation is determined by the amplitude of the collected RF signal.

There are a limited number of studies in which cavitation has been measured during the appearance of a hyperechoic region. During HIFU ablation of dog thigh muscle *in vivo*, Hynynen (1991) observed, in a few samples, that the hyperechoic region appeared after the first HIFU pulse in which inertial cavitation was detected. In a study to determine if cavitation occurred at the focal site of a lithotripter *in vivo*, Coleman et al. (1996), using a 1-MHz hydrophone, found that the acoustic emission distinct to cavitation at the shock wave focus correlated with the appearance of a hyperechoic region in the US images immediately post-treatment. As a result of this study, the presence of a hyperechoic region in an US image has been used to determine if cavitation occurred during lithotripsy (Tavakkoli et al. 1997). During the studies by Coleman et

al. (1996) and Hynynen (1991), the US imager was not synchronized with the cavitation detector and a very limited number of hyperechoic regions were studied. Therefore, further study is needed to confirm their results regarding the involvement of cavitation and bubbles in the appearance of a hyperechoic region.

3. INVOLVEMENT OF CAVITATION IN THE APPEARANCE OF A HYPERECHOIC REGION

This section presents a study in which cavitation activity – with good correlation – was detected *in vivo* during the formation of a hyperechoic region in a diagnostic US image at the site of HIFU treatment. Both active and passive cavitation detection (ACD and PCD, respectively) were performed using a system consisting of a HIFU transducer, a cavitation detector transducer, and an US-imaging probe that were all co-focal and synchronized. ACD consisted of measuring the changes in the peak-to-peak amplitude of the backscatter signal – an indicator of bubble activity – from the HIFU focal site. PCD consisted of measuring the levels of broadband and subharmonic noise from the fast Fourier transform (FFT) of the collected RF signal, as indicators of inertial and stable cavitation, respectively. HIFU exposures were performed *in vivo* in the back and outer thigh muscles of pigs while US images along with the RF signal from the cavitation detector were recorded.

The goal of this study was to determine the relationship between the onset of cavitation and the appearance of a hyperechoic region in an US image resulting from HIFU sonication. Completion of this aim involved the following steps:

1. **Device Development and Characterization:** An integrated US imaging, HIFU, and cavitation detection system was developed and evaluated *in vivo* in pig muscle.

2. *In Vivo* **Cavitation and US Measurements:** *In vivo* studies in a pig model were conducted to determine the relationship between the onset of cavitation (by ACD and PCD) and the appearance of a hyperechoic region.

3.1.   PRELIMINARY STUDIES

3.1.1.   DEVICE DEVELOPMENT

Two different approaches were taken for the development of an US system that could be used to study the involvement of cavitation in the appearance of a hyperechoic region in an US image *in vivo*. Both approaches integrated a HIFU transducer with an US imaging probe and an A-mode transducer – used for cavitation detection. The first approach incorporated the US system with a method for mechanically changing the HIFU focal depth. The second approach was constructed with a fixed focal depth and small overall footprint. This was developed after the first US system was deemed both unnecessary with respect to the variable focal depth and awkward to use in the *in vivo* setting. A description of the two US systems follows a description of the components used in both systems.

Both US systems incorporated a single-element 1.1 MHz concave air-backed HIFU transducer (focal depth of 6.3 cm and f-number of 0.9; Sonic Concepts, Woodinville, WA) driven at the frequency of its 3rd harmonic (3.32 MHz). The transducer was driven at the higher harmonic in order to increase the threshold intensity and/or sonication duration needed to produce a hyperechoic region. This provided a greater range of HIFU parameters to work within without producing a hyperechoic region and/or cavitation. The focus had a full-width half-maximum (FWHM) beam width and length of 0.45 mm and 4 mm, respectively, measured using a calibrated PVDF needle hydrophone (NTR Systems, Seattle, WA). The acoustic power was determined using a radiation force balance technique (Christensen 1988). The transducer was manufactured with a 2 cm-wide hole at its center for placing a cavitation detection transducer coaxial to the HIFU path (Figure 3-1). A B-mode diagnostic imaging probe was placed so that its imaging plane intersected the HIFU axis along its length, such that the HIFU focus was within the imaging plane. It was possible to perform both cavitation detection and imaging of the HIFU focal region simultaneously with this configuration. A broadband frequency (5-9 MHz) curved array probe (C9-5; Philips Medical Systems, Bothell, WA) was selected for imaging because of its small footprint (1.9 cm diameter). The axial and lateral resolution of the imager was measured at the

location of the HIFU focal site using a previously reported method (Elliott and Thrush 1996).

A pair of thin monofilament fibers (0.02 mm diameter) that were arranged in a V shape with known dimensions was scanned with the US imager along their axis (Figure 3-2a) using a high resolution translational stage. The distance between the fibers was measured at the position just prior to where the two strings could no longer be resolved. For determining the slice thickness of the imaging plane, a nylon bead (0.26 mm diameter) imbedded in an acoustically transparent 7% polyacrylamide gel (Prokop et al. 2003) was scanned across the US beam at the site of the HIFU focal region (Figure 3-2b). With the US imager setup with the same parameters used during the *in vivo* studies described in Section 3.2 (MI of 1.0 and imaging depth of 6.3 cm) the axial and lateral resolution were measured to be 0.77 mm and 1.83 mm, respectively, and the slice thickness was measured to be 15 mm.
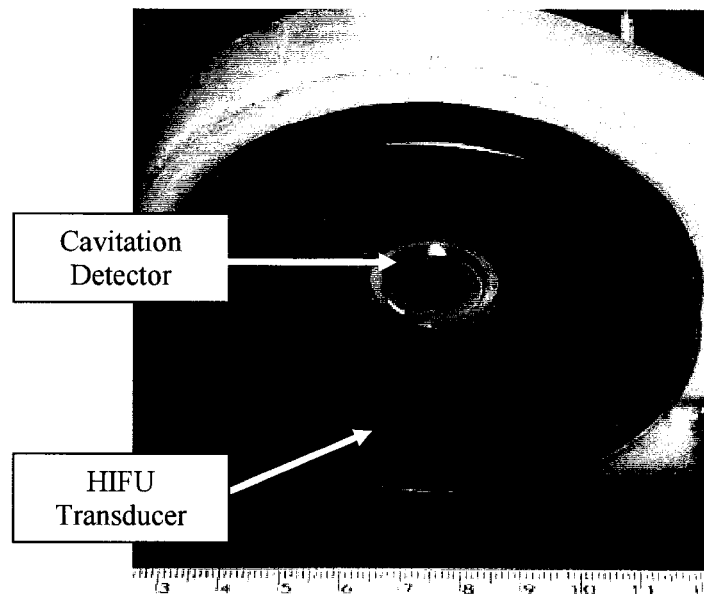
Figure 3-1: Photograph of the position of the cavitation detector within a hole in the HIFU transducer.
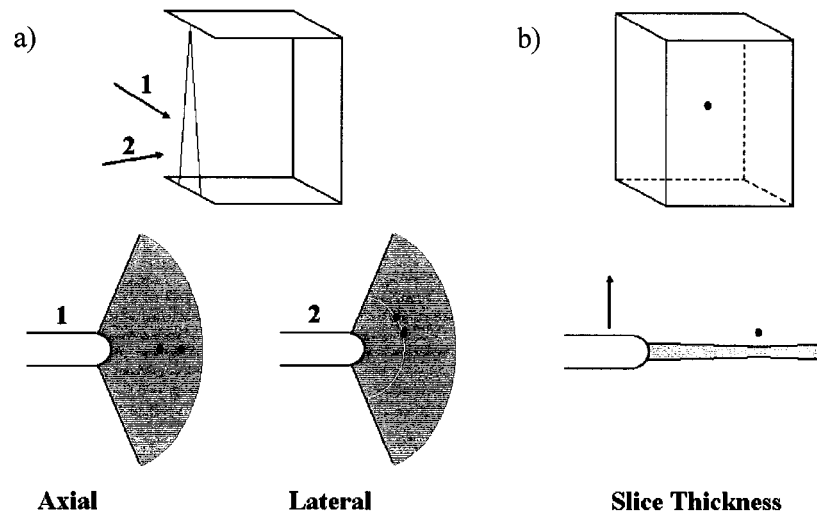
Figure 3-2: Experimental setup for measuring the (a) axial and lateral resolution, and (b) slice thickness of an US imaging probe at the HIFU focal site. For axial and lateral resolution a pair of thin monofilament fibers placed in a V, were scanned along their length and the distance between them measured at the location where they were still distinguishable from one another in an US image. For slice thickness, a small nylon bead imbedded in an acoustically transparent gel was scanned through the imaging plane and the distance across which the bead was visible in the US image was measured.

1st Generation Variable Depth US System

The first US system incorporated all three US devices (HIFU transducer, cavitation detector, and imaging probe) into a single unit (Figure 3-3) that was placed into a custom-built water collar (Figure 3-4). By submerging the US system inside the water collar, the focal depth of the HIFU transducer within tissue could be changed while retaining the focus within the image plane of the US imaging probe and coaxial to the cavitation detector. A gauge for changing the depth of the US system within the water-filled collar was placed between a metal plate attached to the water collar and the handle of the US system.

In vivo evaluation of this system on the thigh muscles of a pig (Figure 3-4) found the transducer awkward to couple to the muscle because of the large surface area of the water collar. It was hard to determine whether air remained trapped under the cellophane and under the transducer

prior to each HIFU exposure. The large footprint of the water cone reduced the total muscle area accessible for HIFU exposures because of the distance between the HIFU transducer's focus and the outer edge of the water collar, and because of the need to place the system on a relatively flat surface.
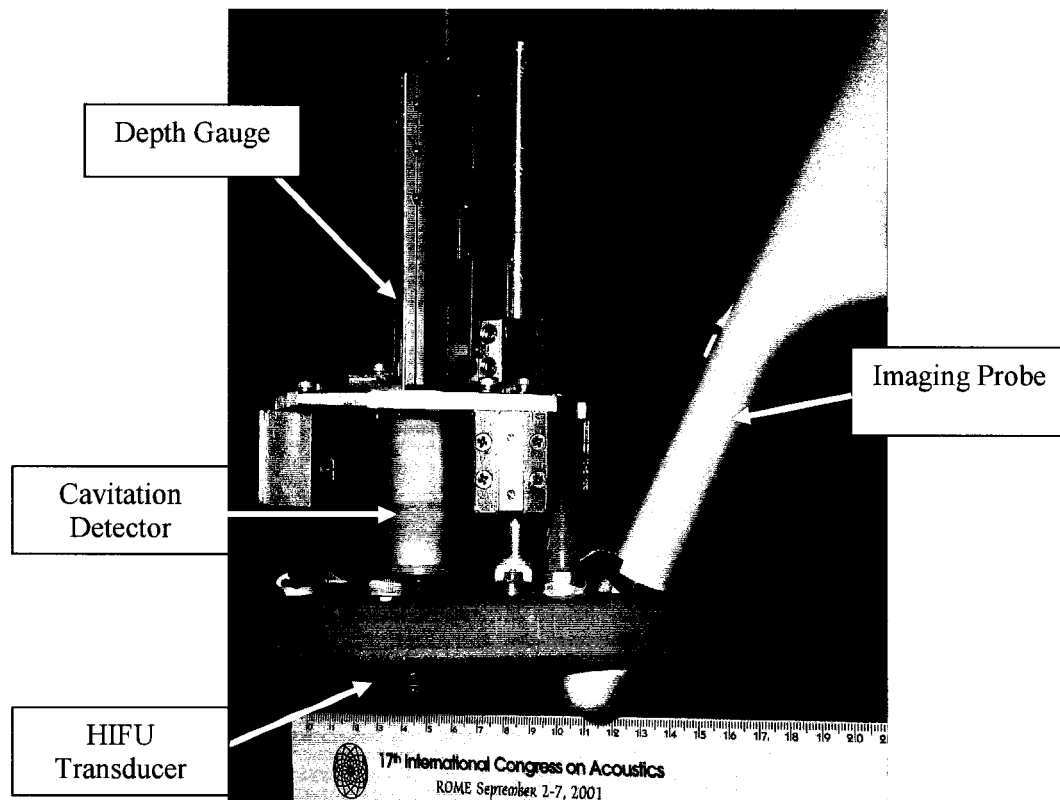
Figure 3-3: Photograph of the 1st generation US system that incorporated a 3.32 MHz air-backed HIFU transducer, cavitation detection transducer, and an US imaging probe. The US system was attached to a fine resolution (0.1 mm) gauge for adjusting the HIFU focal depth.
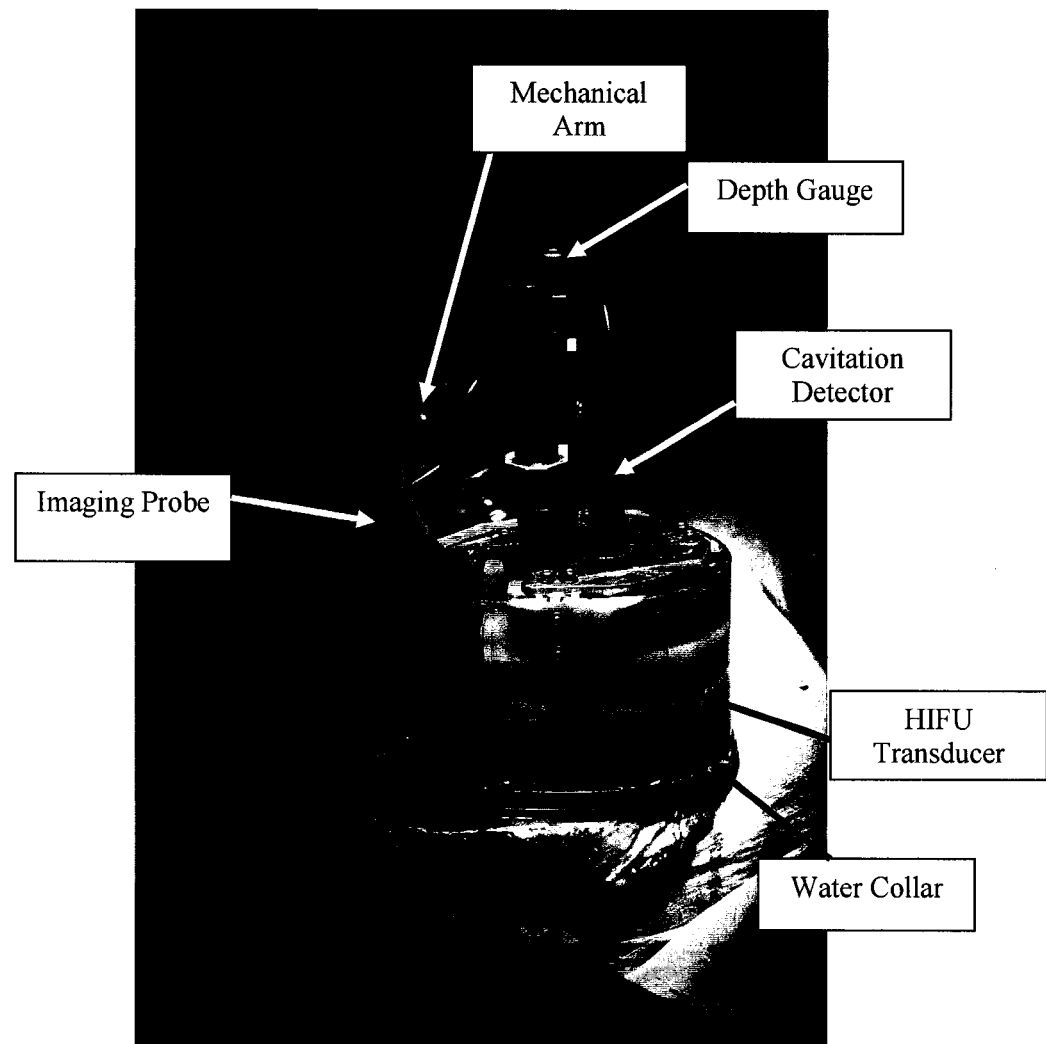
Figure 3-4: Photograph of the first US system, integrating a HIFU transducer with an imaging probe and cavitation detection, in use in an *in vivo* study. This system was designed with the integrated parts placed in a water collar, covered on the bottom with an acoustically transparent cellophane sheet, in order for the focal depth within the tissue to be adjustable by changing the depth of the US system within the water collar. The whole system was held in place on the pig's thigh by a custom-built mechanical arm.

2nd Generation Fixed Depth US System

The second approach for an integrated US system was constructed with a fixed focal depth and small overall footprint (Figure 3-5). A custom-built aluminum holder was made in the APEAL staff machine shop at the University of Washington for the attachment and alignment of the HIFU transducer with the US imager. The holder allowed for the variable depth of the US imager with respect to the HIFU transducer, while maintaining the HIFU focus within the US imaging plane. A custom-built polycarbonate cone (Figure 3-5) filled with degassed water and covered at the tip with a single-layered cellophane membrane was placed over the face of the HIFU transducer. This was used to couple the HIFU and cavitation detection transducer to the tissue and to set the HIFU transducer focus to a depth of 2 cm within the muscle. This US system was easier to couple to tissue, weighed significantly less, and had a significantly smaller overall footprint than the 1st generation US system.
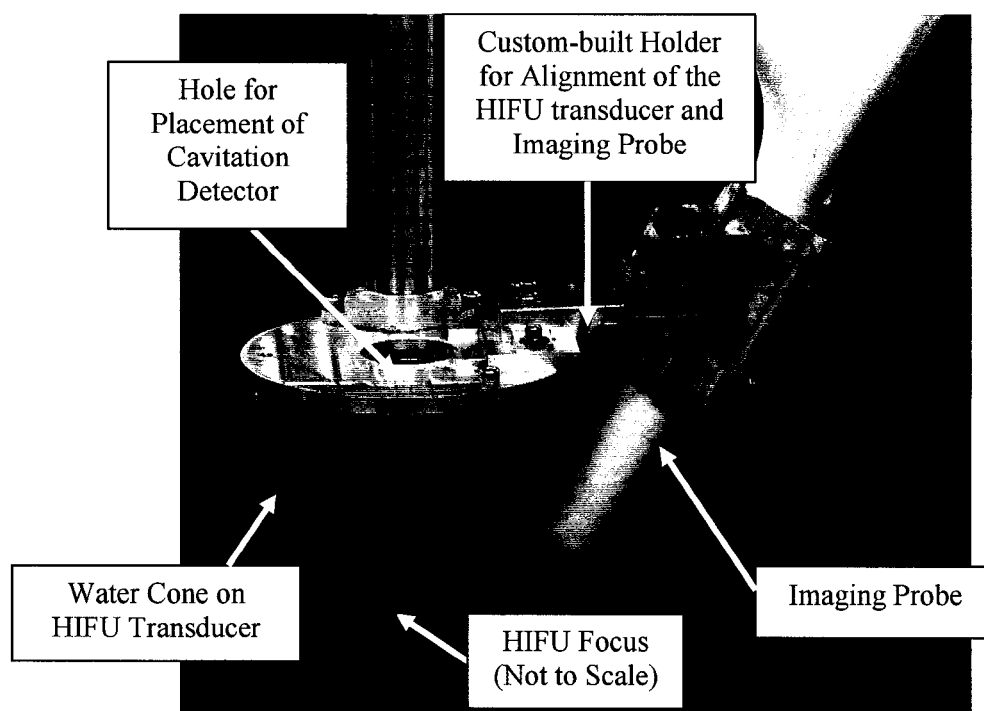
Figure 3-5: **Photograph of the 2nd generation US system that incorporated a HIFU transducer with an A-mode cavitation detector at its center and an US imaging probe. All US devices overlapped at the HIFU focus. A degassed water filled cone was placed over the HIFU transducer to set the depth of the transducers focus to 2 cm in tissue.**

3.2. INVOLVEMENT OF CAVITATION IN THE APPEARANCE OF A HYPERECHOIC REGION: *IN VIVO* RESULTS

A set of measurements of the change in cavitation activity (by ACD and PCD) and echogenicity in an US image were conducted *in vivo* at the HIFU focus. HIFU exposures were performed in the thigh muscles of pigs at *in situ* intensities of 220 – 1710 W/cm^2 for 10 s durations. This study was done to gain an understanding of the involvement of bubbles in the appearance of a hyperechoic region at the HIFU focus *in vivo*.

3.2.1. MATERIALS AND METHODS

Animal Model

Six juvenile pigs weighing 25-35 kg each were used. The experimental protocol was approved by the Animal Care Committee at the University of Washington and conducted according to the guidelines of the United States National Institutes of Health (NIH) for use of laboratory animals. Initial sedation of the pigs was done with an intramuscular (IM) injection of a mixture containing acepromazine (1 mg/kg) and ketamine (22 mg/kg). After transportation to the experimental room, a dose of 3.5-4 mL of ketamine/xylazine (1:8 ratio) was used to anesthetize each animal. A tracheal tube was then introduced for maintenance of anesthesia (isofluorane 1-3%) during the experiment.

HIFU exposures were performed in the muscles located adjacent to the spine (longissimus thoracis) and in the outer thigh of the pig hind limb (biceps femoris and rectus femoris). These sites were chosen because they offer a large, thick region (4 - 6 cm) of muscle for HIFU exposures. To maintain a smooth layer on the muscle surface for coupling the HIFU transducer water cone, the muscle surface was exposed with a scalpel. This reduced the occurrence of bubbles trapped at the HIFU tissue interface. In addition, the US path to the HIFU focus was made consistent by removing the skin and underlying fat that are variable in depth along the muscle. HIFU exposures were done at 2 cm intervals along the muscles at a depth of 2 cm. After the experiments, the animals were euthanized with an overdose of the anesthetic mixture, followed by 20 mL KCl saturated saline.

HIFU, US imaging, and Cavitation Detection System

A single-element 1.1 MHz concave air-backed HIFU transducer (focal depth of 6.3 cm and f-number of 0.9; Sonic Concepts, Woodinville, WA) was driven at the frequency of its 3rd harmonic (3.32 MHz). The focus had a full-width half-maximum (FWHM) beam width and length of 0.45 mm and 4 mm, respectively, measured using a calibrated PVDF needle hydrophone (NTR Systems, Seattle, WA). A radiation force balance technique was used to determine the acoustic power output (Christensen 1988). In all experiments, the duty cycle of HIFU was 80% at a pulse-repetition-frequency of 6.26 Hz and total exposure time of 10 s. The transducer was manufactured with a 2 cm-wide hole at its center for placing a cavitation detection transducer coaxial to the HIFU path (Figure 3-6). A custom-built polycarbonate cone filled with degassed water and covered at the tip with a single-layered cellophane membrane was placed over the face of the HIFU transducer. This was used to couple the HIFU and cavitation detection transducer to the tissue and to set the HIFU transducer focus to a depth of 2 cm within the muscle. A B-mode diagnostic imaging probe was placed so that its imaging plane intersected the HIFU axis along its length, such that the HIFU focus was within the imaging plane (Figure 3-6). A broadband frequency (5-9 MHz) curved array probe (C9-5; Advanced Technology Laboratories, ATL, Bothell, WA) was selected for imaging because of its small footprint (1.9 cm diameter). US images were collected with an HDI-1000 US imaging system (ATL) and mini-DV video recorder (GL2, Canon, Lake Success, NY). It was possible to perform both cavitation detection and imaging of the HIFU focal region simultaneously with this configuration.

Synchronization of the HIFU system with the US imager was performed using a method and equipment previously reported by our group (Vaezy et al. 2001). The excitation pulse of the 64th element of the imaging probe was used to synchronize the HIFU pulse with the US imager. The excitation pulse was converted into a TTL-high pulse using three pulse generators in series (Model 4001, Global Specialties, New Haven, CT) (Figure 3-7). The TTL-high pulse was used to externally gate a frequency generator (33120A, Hewlett Packard, Palo Alto, CA). The passage of the signal from the frequency generator to a power amplifier (set to 55 dB gain; 150A100B Amplifier Research, Souderton, PA) was gated to a specific duration by a computer-controlled custom-built relay board. This set the total HIFU exposure to 10 s at an 80% duty cycle, and synchronized the HIFU exposure with the collection of the cavitation RF signal on a digital oscilloscope. The amplified signal was sent to a custom-built electrical matching network

(matched to a 50-Ω load) and then to the HIFU transducer. Throughout this experiment the time difference between any two pulses was 160 ms (Figure 3-8) as set by the US image system when the following parameters were used: mechanical index (MI) of 1.0 and US imaging depth of 6.9 cm. During HIFU excitation, interference from the US emitted by the HIFU source was seen as bands in the B-mode US image, illustrated as gray regions in the image plane in Figure 3-6.

The cavitation detection system, used for ACD and PCD consisted of a broadband single-element cavitation detection transducer (bandwidth of 0.5-5.5 MHz; V382, Panametrics, Waltham, MA) and a pulser/receiver (5072PR, Panametrics). The received RF waveforms during ACD and PCD were collected by a digital oscilloscope (9350AL, LeCroy, Chestnut Ridge, NY) and transferred for storage and processing to a personal computer (PC) via a GPIB interface using the Scope Explorer® program (LeCroy).
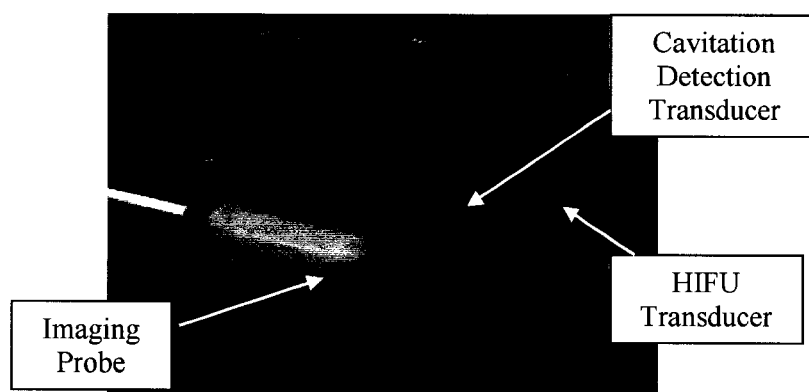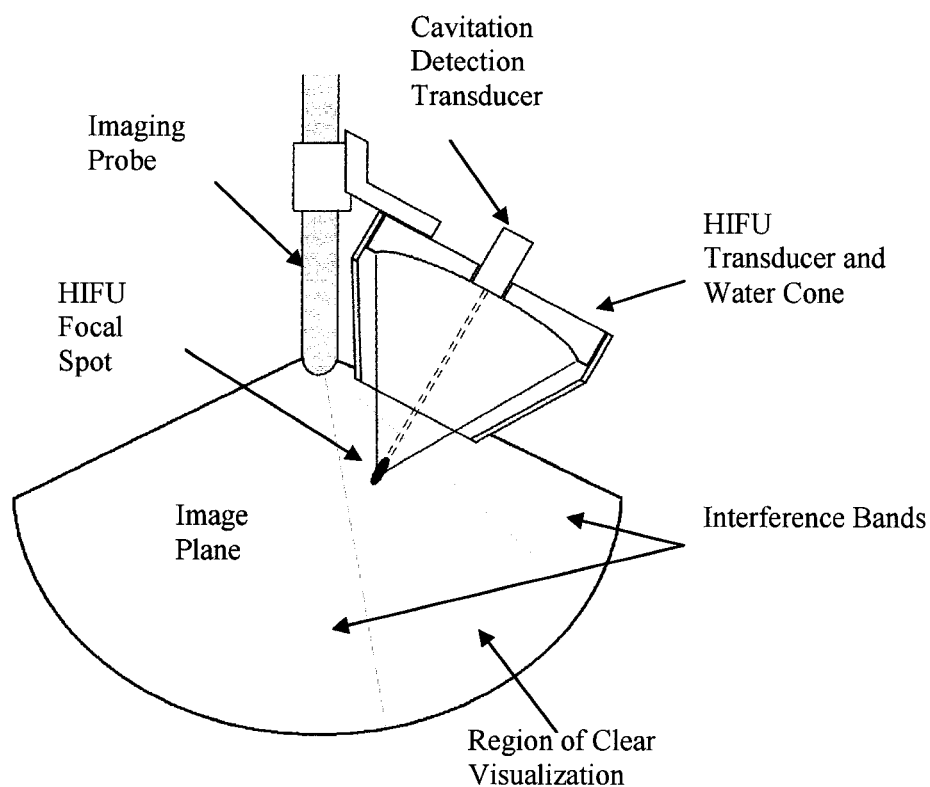
Figure 3-6: Schematic diagram and photograph of the integrated HIFU, imaging and cavitation detection system. Note the interrogation path (dotted line) of the ACD transducer that is coaxial to the HIFU focal spot. The light gray areas within the imaging plane represent the interference bands that occur during HIFU exposure.
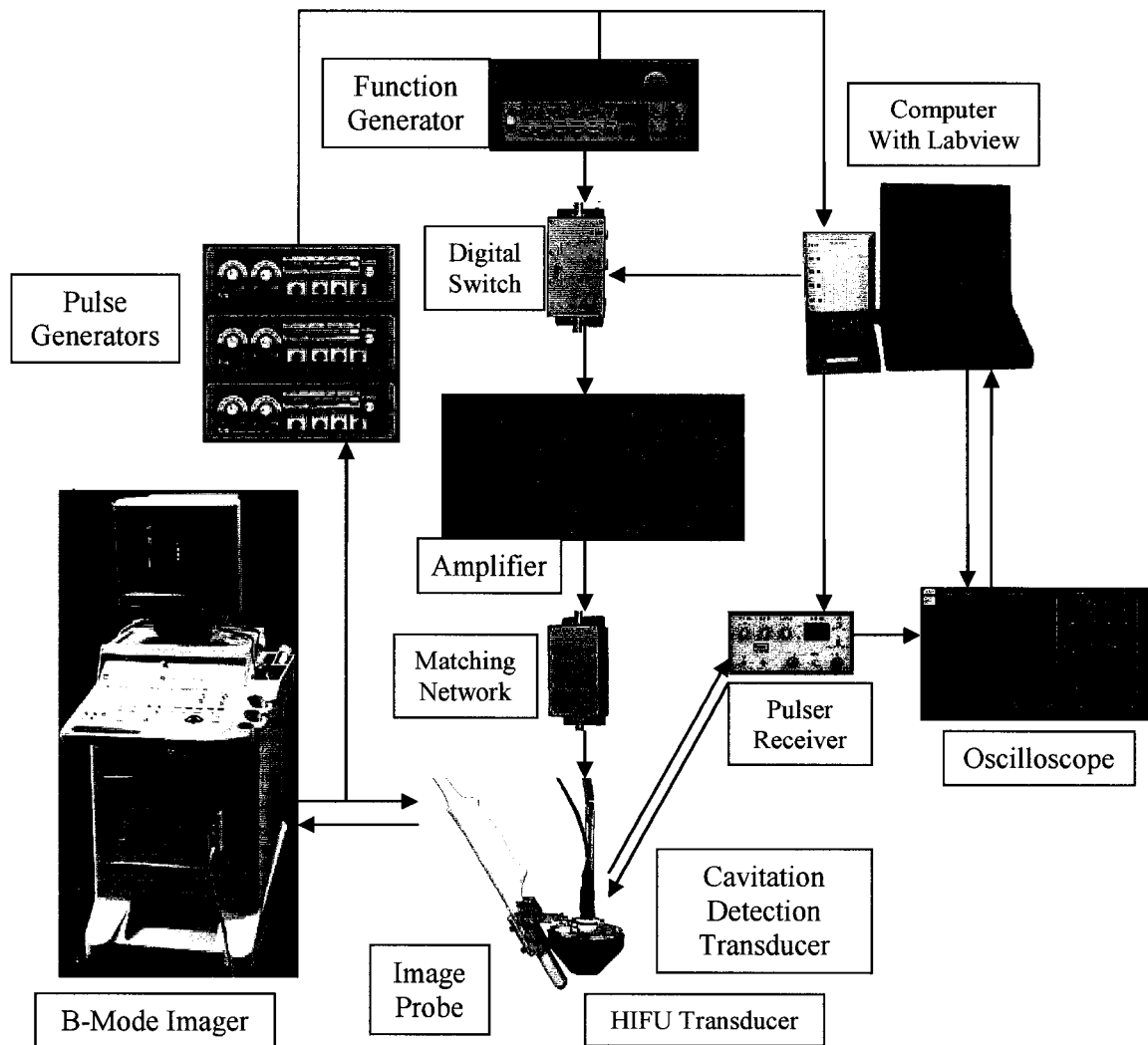
Figure 3-7: Schematic of the electronic system of the integrated HIFU, US imaging and cavitation detection system. The whole system was synchronized by the excitation pulse collected from the 64th element of the imaging probe.

Active Cavitation Detection and Analysis

Since the location (with respect to time of flight of the US signal) and time of occurrence of cavitation can be resolved by ACD (Roy et al. 1990), ACD was used to determine when cavitation was first observed after the HIFU pulse to which it was created in, and the location of cavitation associated with the tissue interface (when present) and the HIFU focus of our system by the time of flight of the return signal. Synchronization of the ACD excitation pulse, used for interrogating the HIFU focus, with the HIFU trigger pulse was performed using a laptop PC running a custom LabView® program (National Instruments, Austin, TX). The LabView program received the HIFU trigger pulse and sent a single-cycle trigger pulse to the pulser/receiver 1.0 ms after the end of each HIFU pulse (Figure 3-8d.1). Collection of the RF waveforms from the pulser/receiver was done with the oscilloscope in sequence mode. The oscilloscope was externally triggered with the HIFU trigger pulse (Figure 3-8a), delayed internally to 1 ms after the end of each HIFU pulse, and set to collect the signal for 200 μs per pulse (25 to 50-MHz sampling frequency; Figure 3-8d.2). The RF signal was collected from the pulser/receiver for 1 s prior to, 10 s during, and 6 s after each HIFU exposure for a total of 82 pulses (6.26 pulses/s).
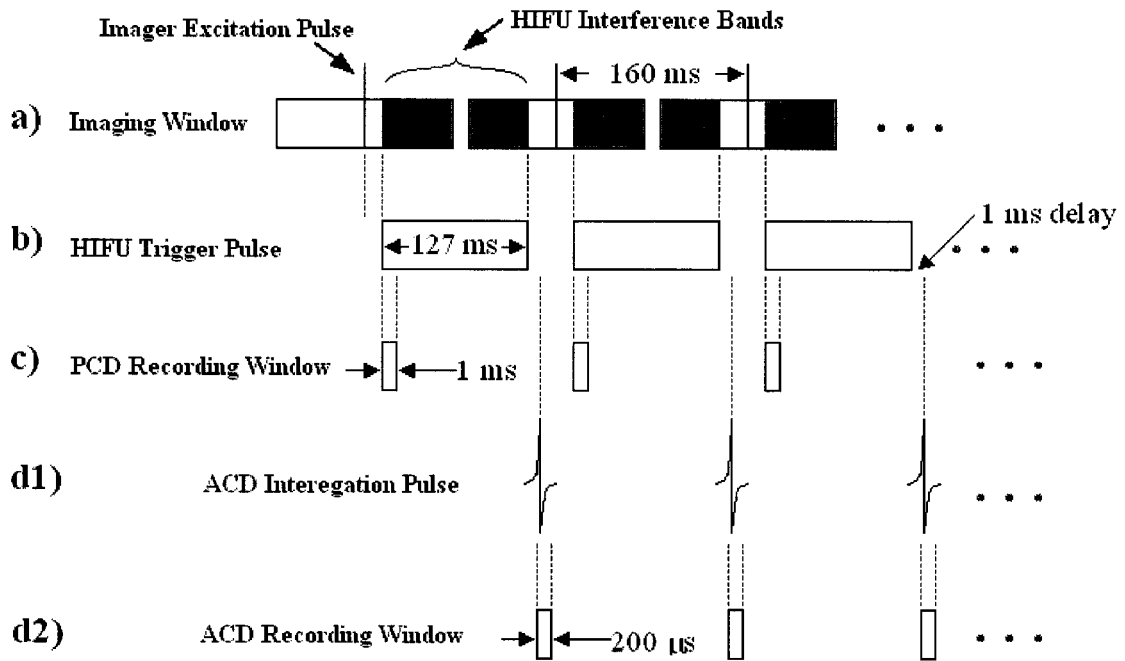
Figure 3-8: The timing sequence of the synchronization of US imaging (a), HIFU (b), PCD (c) and ACD (d1,2). During HIFU exposures clear visualization of the HIFU treatment site occurred between the interference bands in the US image (depicted as gray regions in (a)). ACD was conducted 1 ms after the end of the HIFU pulse for 200 μs (c) or PCD was conducted during the first 1 ms of the HIFU trigger pulse (d1 and d2).

The time of flight to and from the HIFU focus was calculated as 75 μs based on a path through degassed water of 4.3 cm and pig muscle of 2 cm as per our setup (Christensen 1988). The maximal peak-to-peak amplitude (max V_{pp}) was calculated for each sequence of the collected RF waveform for a window of 65 to 85 μs after each interrogation pulse (Figure 3-9). The window size was experimentally determined to include the variations in the formation of the lesion and its growth towards the transducer during exposures. Measurement of the max V_{pp} was performed with a custom-made algorithm written in Matlab (Mathworks, Natick, MA). The onset time of cavitation at the HIFU focus was defined as the time of the first HIFU pulse in which the max V_{pp} of the RF signal was greater than three standard deviations (SD) above the mean background signal measured for 1 s prior to each HIFU exposure.
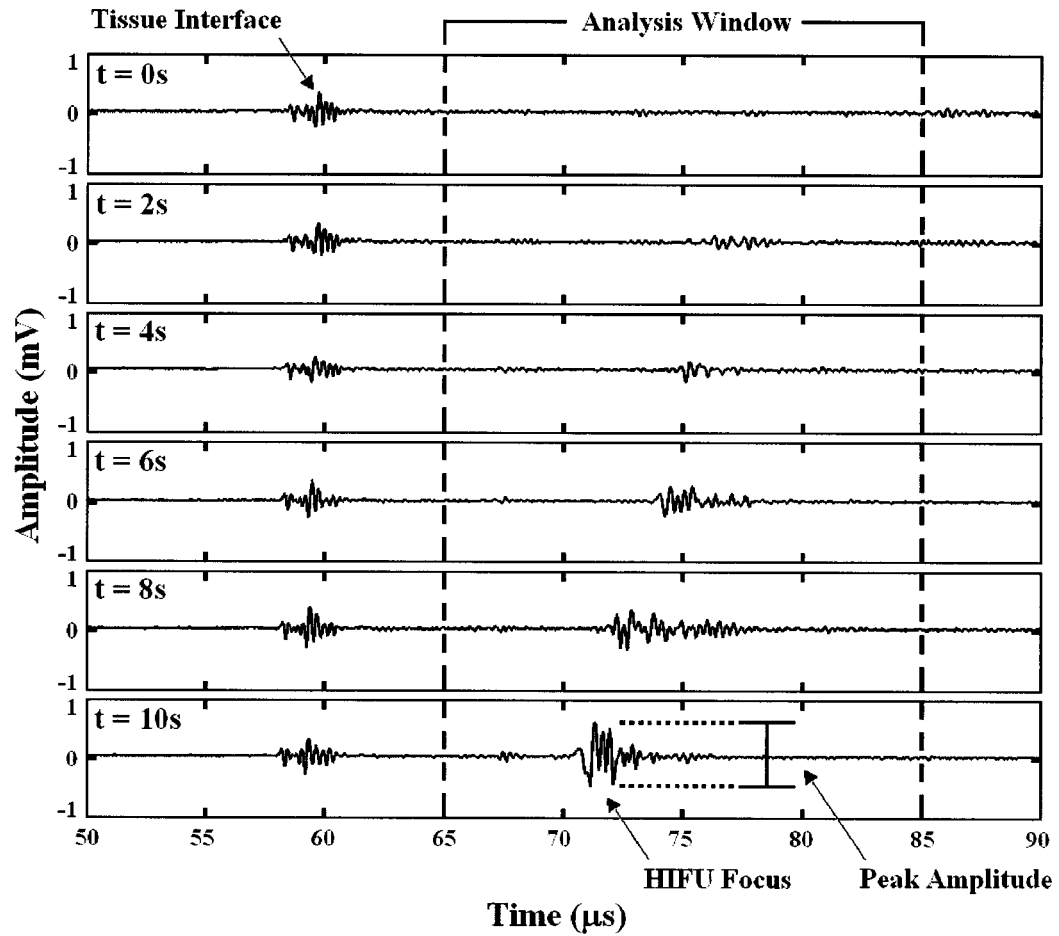
Figure 3-9: Series of time evolution plots at 0, 2, 4, 6, 8 and 10 s into a 10 s HIFU exposure at an intensity of 1710 W/cm^2 of the RF signal collected during ACD. The plots show the time of flight of the amplitude of the backscatter of the ACD RF signal returning from the tissue interface and HIFU treatment site (focus). Backscatter arising from cavitation at the treatment site can be observed, by a reduction in the time of flight, moving towards the tissue interface (at 60 µs) and HIFU source as the length of exposure increases from 0 s (top plot) to 10 s (bottom plot). The level of cavitation was measured as the peak-to-peak amplitude (horizontal dotted lines at t = 10 s) of the return signal for each pulse during a time window of 65 to 90 µs (represented by the region between the vertical dashed lines).

Passive Cavitation Detection for Inertial and Stable Cavitation

Passive cavitation detection consisted of measuring the levels of broadband noise (between 0.5-1.5 MHz) and subharmonic noise (at half of the fundamental frequency, 1.66 MHz) from Fourier spectra of the collected RF signal. Broadband noise and subharmonic noise were used as indicators of inertial (IC) and stable (SC) cavitation, respectively. The broadband noise was measured at 0.5 – 1.5 MHz where the signal to noise ratio was optimal. This was because the sensitivity of the cavitation detection transducer was optimal and because higher harmonics attenuate rapidly in tissue resulting in a reduction in signal amplitude at higher frequencies. The cavitation detection system described above was used with the following parameters: The RF signal was collected for the first 1 ms of each HIFU pulse due to a limitation in the memory capacity of the oscilloscope. The oscilloscope was set to 0 ms time delay, 1000 µs window (25 to 50-MHz sampling frequency), and for collection of 79 HIFU pulses.

Spectral analysis was performed with a custom-made Matlab algorithm that used a series of discrete Fourier Transforms over the length of the raw RF signal of each pulse (Chen et al. 2003). Each Fourier Transform was repeated across the entire signal for a 20 µs window that overlapped the previous window by 19 µs. The level of inertial cavitation was determined by calculating the root mean square (RMS) amplitude of the broadband noise for each spectrum over the frequency range of 0.5 to 1.5 MHz using a method similar to Chen et al. (2003). The maximal calculated RMS amplitude of the broadband noise and maximal subharmonic amplitude for each pulse were plotted as a function of the start time of each HIFU pulse. The amplitude of the IC and SC activities were normalized to 0-1.

The onset time of a significant level of IC at the HIFU focus was defined as the time of the first HIFU pulse in which the maximal amplitude of the broadband noise was greater than 3 SD ($p <$ 0.005) above the mean broadband noise measured during recordings of acoustic emissions prior to each HIFU exposure.

Ultrasound Image Analysis

Movies collected from the US imager were digitized using Adobe Premiere® Pro 7.0 (Adobe, San Jose, CA). A representative video frame from a HIFU exposure is shown in Figure 3-5a.

Interference bands on the US images (Figure 3-5) resulting from the noise generated during HIFU exposures were used for synchronization of the cavitation data with the US movies. The onset time of the hyperechoic region in the US images was determined as the difference in time between the start of the HIFU exposure and the appearance of a clinically useful hyperechoic region in the US image. For this study, a clinically useful hyperechoic region at the HIFU focus was defined as a region that was large enough (> 75 pixels) and had a distinct increase in the grayscale intensity (>12.5% above background levels) that it was easily observable by the HIFU operator.
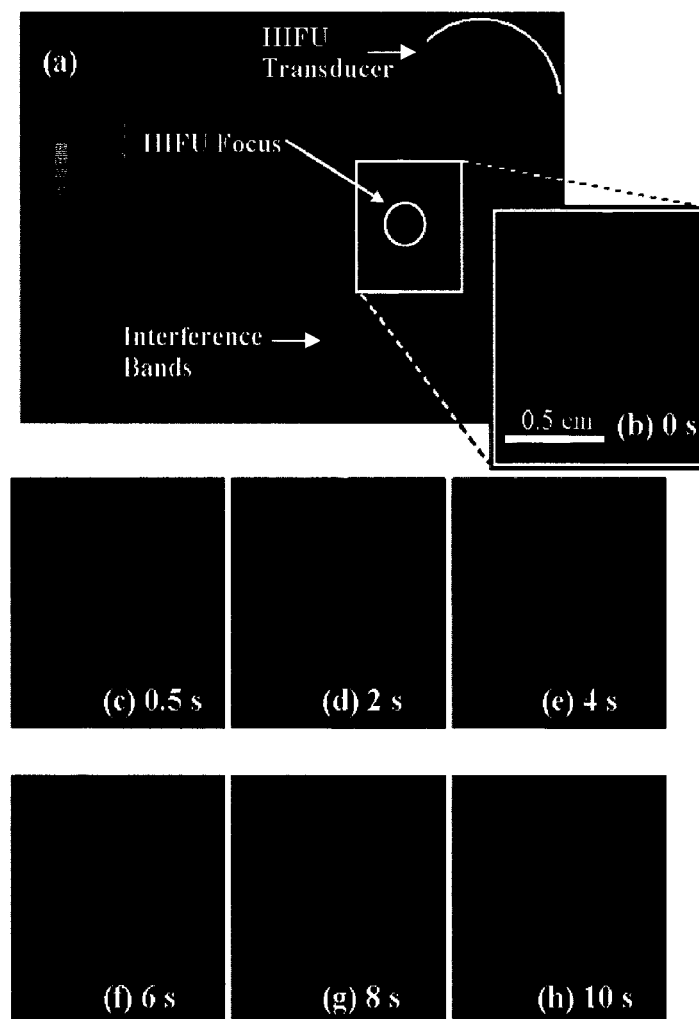
Figure 3-10: **Time evolution of a hyperechoic region within US images at the start (a) of a 10 s HIFU exposure at 1710 W/cm², with an expanded view of the region of the HIFU focus**

(b-h). A bright hyperechoic region appeared in the US image at 0.5 s into the exposure. In subsequent video frames at 2 s intervals (d through h), the hyperechoic region is seen growing and migrating towards the HIFU transducer (depicted in the upper right of (a); not to scale). Images (b) through (h) are of the same scale.

Statistical Analysis

A total of 195 HIFU exposures were performed. A total of 24 exposures were excluded from analysis for the following reasons: the close proximity of the HIFU focus to bone or other highly scattering objects; improper coupling of the HIFU transducer to the tissue; muscle twitching as a result of HIFU treatment; and the presence of air bubbles in the water filled HIFU coupling cone post-exposure. The goodness-of-fit of best-fit linear law was determined using the correlation coefficient (R^2-value) for comparison of the time of onset of cavitation and the time of appearance of a hyperechoic region.

A modified Z-score test using the median of absolute deviation above the mean was used to determine if the difference in time between the onset of cavitation and a hyperechoic region for all samples fit the sample population. Four outlier forty five samples were removed from the IC sample population for the intensity of 1280 W/cm² during PCD based on z-scores greater than 3.5.

3.2.2.   RESULTS

Table 3-1 reports the average HIFU exposure times to visualize a bright hyperechoic region (column 4) and the average times to detect cavitation (column 5) at the HIFU focus. No visualization was achieved for HIFU intensities below 850 W/cm². The percentage of trials with visualization of a hyperechoic region increased as the HIFU intensity increased (Table 3-1, column 3). The average HIFU exposure time needed to visualize a hyperechoic region and to detect cavitation was inversely related to *in situ* HIFU intensities. The average time for producing a hyperechoic region was less than 1 second at a HIFU intensity of 1710 W/cm² (Table 3-1, column 4). During ACD, the appearance time of a hyperechoic region preceded on average the onset time of cavitation at 1280 and 1710 W/cm², while the inverse was observed for 850 W/cm². During PCD, the average onset of cavitation preceded the average appearance time of a hyperechoic region at all intensities at which cavitation occurred.

Table 3-1: Percentage of HIFU exposure trials resulting in the US visualization of a hyperechoic region (column 3) and mean HIFU exposure time until visualization (column 4) and cavitation (column 5) occurred.

In Situ HIFU Intensity (W/cm²)	Number of HIFU Trials	Percentage of Successful Visualizations (%)	Mean ± SD of Exposure Time for Visualization (sec)	Mean ± SD of Exposure Time for Cavitation (sec)
ACD:				
220	13	0	--	--
490	16	0	--	--
850	24	45.8	3.89 ± 2.73	2.92 ± 2.70
1280	19	100	2.09 ± 2.02	2.56 ± 1.89
1710	19	100	1.22 ± 1.89	1.63 ± 1.80
PCD:				**Inertial Cavitation**
220	11	0	--	--
490	15	0	--	--
850	18	16.7	2.56 ± 1.04	1.61 ± 1.56
1280	22	81.8	2.30 ± 2.37	1.11 ± 1.11
1710	16	100	0.89 ± 1.29	0.49 ± 1.14

Figure 3-9 shows time series for a single 10 s HIFU exposure at 1710 W/cm² of the RF signal collected during ACD. The increase in amplitude of the RF signal between 70 μs and 80 μs correlated with the formation of a hyperechoic region at the HIFU focus located at a depth of 2 cm in muscle. The hyperechoic region and the increase in the RF signal amplitude from the cavitation detector first appeared at 0.5 s into the exposure. As the length of the HIFU exposure increased, the amplitude of the RF signal was observed growing and migrating towards the HIFU source (seen as a reduction in the time-of-flight between the cavitation detector and HIFU focus). Figure 3-10 shows the corresponding hyperechoic region in the US image for the raw RF signal shown in Figure 3-9. The original US image is shown in Fig. 4a with the region around the HIFU focus enlarged in Figure 3-5b-h. Figure 3-5c shows the HIFU focus at the start (0 s) of the exposure and prior to the visualization of a hyperechoic region. The hyperechoic region was observed appearing at 0.5 s (Figure 3-5c), and then growing.

Figure 3-11 shows typical time evolutions of the cavitation activity, as measured by ACD, at the HIFU focus for *in situ* intensities of 850, 1280, and 1710 W/cm^2. The time evolution of the cavitation is shown for both HIFU exposures without (Figure 3-11a.1) and with the appearance of a hyperechoic region for the intensity of 850 W/cm^2 (Figure 3-11a.2). An overall increase in the level of cavitation was observed after the appearance of a hyperechoic region (Figure 3-11), although an erratic change with respect to rise and fall in amplitude of the cavitation level occurred. A similar pattern of change in the area of the hyperechoic region (Figure 3-5) within the US image was observed, with the area changing erratically as it increased in size. After the end of each HIFU exposure, the level of cavitation and the size of the hyperechoic region no longer changed in an erratic manner and were observed to gradually return to background levels.

Figure 3-12 shows the time evolution of the cavitation activity at the HIFU focal zone for each *in situ* intensity, as measured by ACD. An increase in the average level of cavitation and a decrease in the average onset time of cavitation was observed with the increase in HIFU intensity.

Figure 3-13 shows a plot of the time to visualize the appearance of a hyperechoic region at the HIFU focus as a function of the onset time of cavitation activity at the HIFU focus, as measured by ACD. The dashed line represents unity between the two events. Data points below the line are a result of the hyperechoic region appearing prior to the onset of cavitation. Points above the line are a result of the onset of cavitation occurring prior to the appearance of the hyperechoic region. The occurrence of the two events appeared linear with R^2-values greater than 0.45, 0.82, and 0.86 for HIFU intensities of 850, 1280, and 1710 W/cm^2, respectively.

Figure 3-14 shows representative plots of typical Fourier spectra of the RF signal from HIFU pulses prior to (Figure 3-14a) and after (Figure 3-14b, c) the appearance of a hyperechoic region as observed by PCD. An increase in the level of broadband noise (interpreted as inertial cavitation) was observed during the appearance of a hyperechoic region (b). A threshold value of 1280 W/cm^2 was observed for the appearance of subharmonic noise (interpreted as stable cavitation). In addition, subharmonic noise was only present sporadically throughout some of the HIFU exposures and without correlation to the onset of a hyperechoic region. An example spectrum of a pulse that had subharmonic noise present is shown in Figure 3-14c. The

appearance of a second harmonic at 6.6 MHz was also observed after broadband and subharmonic noise was detected (Figure 3-14b, c).

Figure 3-15 shows a typical time evolution of IC activity, as measured by broadband noise during PCD, at *in situ* intensities of 850, 1280, and 1710 W/cm^2. Typically, an increase in the level of IC activity immediately preceded the appearance of a hyperechoic region (arrows in Figure 3-15a-c). The level of IC activity was seen returning to zero at the completion of each 10 s HIFU exposure.

Figure 3-16 shows a plot of the time to visualize the onset of a hyperechoic region at the HIFU focus, as a function of the onset time of IC activity at the HIFU focus as measured by PCD. The data appeared linear with R^2-values greater than 0.99 and 0.80 for HIFU intensities of 1280 and 1710 W/cm^2, respectively. However, in the majority of trials, IC was present prior to the onset of the hyperechoic region, represented in Figure 3-16 as data points above the dashed unity line. There were too few HIFU trials (n=3) resulting in a hyperechoic region at the intensity of 850 W/cm^2 to draw a conclusion regarding the correlation between the onset of IC and that of the hyperechoic region at this intensity. A strong correlation between the onset of IC and that of the hyperechoic region was observed at the intensities of 1280 W/cm^2 and 1710 W/cm^2 was observed.
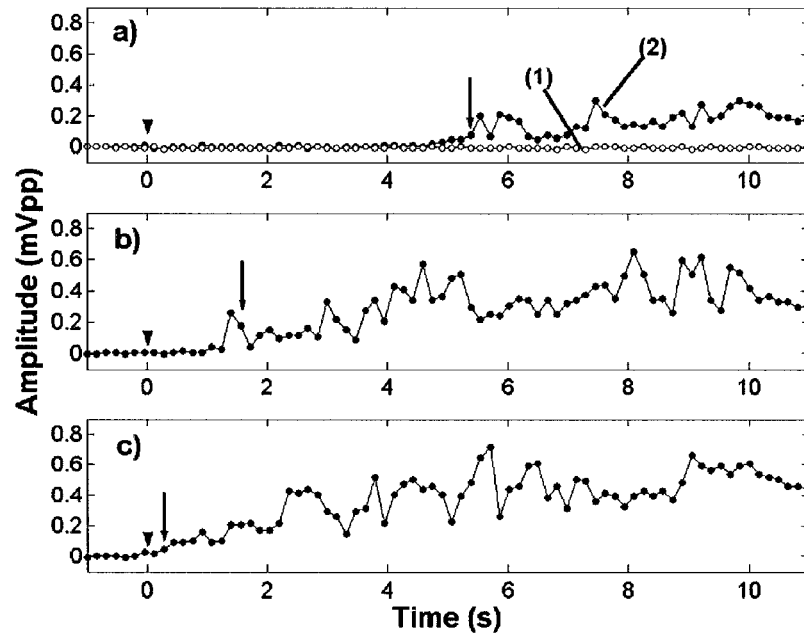
Figure 3-11: Evolution of the cavitation activity (max V_{pp}) as a function of time for the ACD signal corresponding to the HIFU focal zone during *in vivo* exposures of 10 s at (a) 850, (b) 1280 and (c) 1710 W/cm^2. Arrows indicate the onset time for the visualization of a hyperechoic region. Arrowheads indicate the start time of each HIFU exposure. The typical time evolution of the cavitation during HIFU exposures at 850 W/cm^2 without (1) and with (2) the appearance of a hyperechoic region are shown in (a).
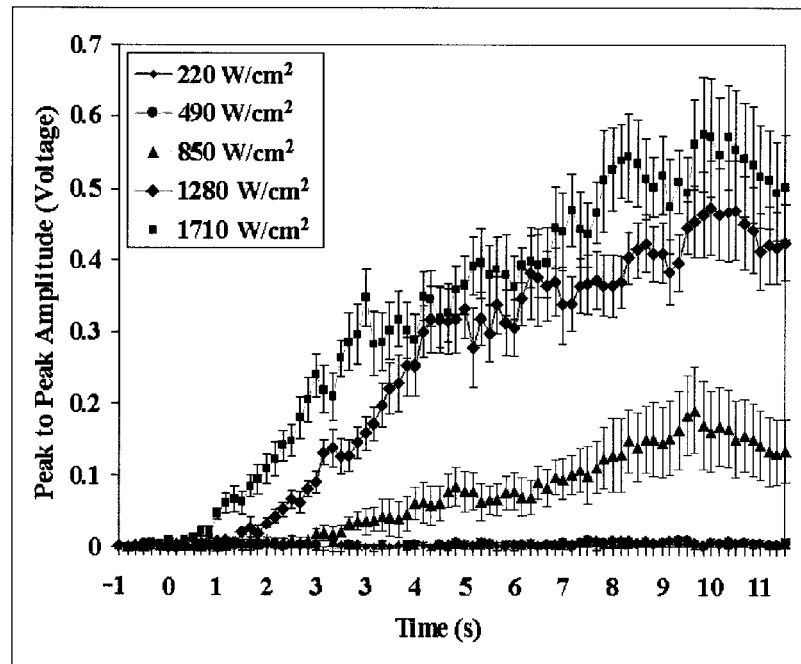
Figure 3-12: Time evolution of the average maximum peak-to-peak amplitude (volts) ±SEM as a function of time for the ACD signal corresponding to the HIFU focal zone. HIFU exposures were performed at (◆) 220, (●) 490, (▲) 850, (◆) 1280 and (■) 1710 W/cm^2 (I_{SPTA}) from 0 to 10 s.
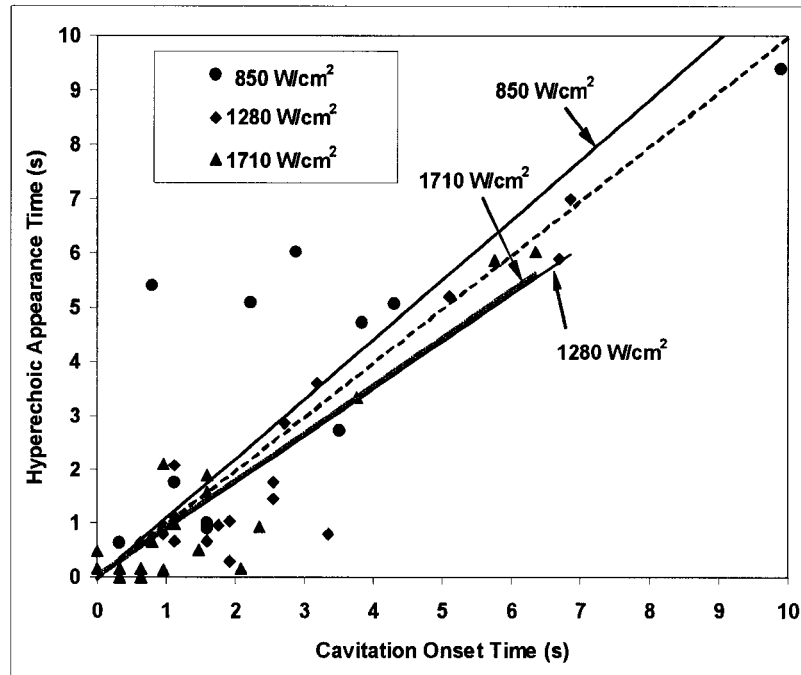
Figure 3-13: Appearance time of a hyperechoic spot in an ultrasound image verses the onset time of cavitation as measured by ACD from the HIFU focal zone during ablation *in vivo* for 10 seconds at (●) 850, (♦) 1280 and (▲) 1710 W/cm². The best-fit linear line for each intensity is shown and the associated linear correlation (R^2) for the intensities of 850, 1280 and 1710 W/cm² are 0.45, 0.82 and 0.86, respectively. The dashed line represents unity between the two onset times.
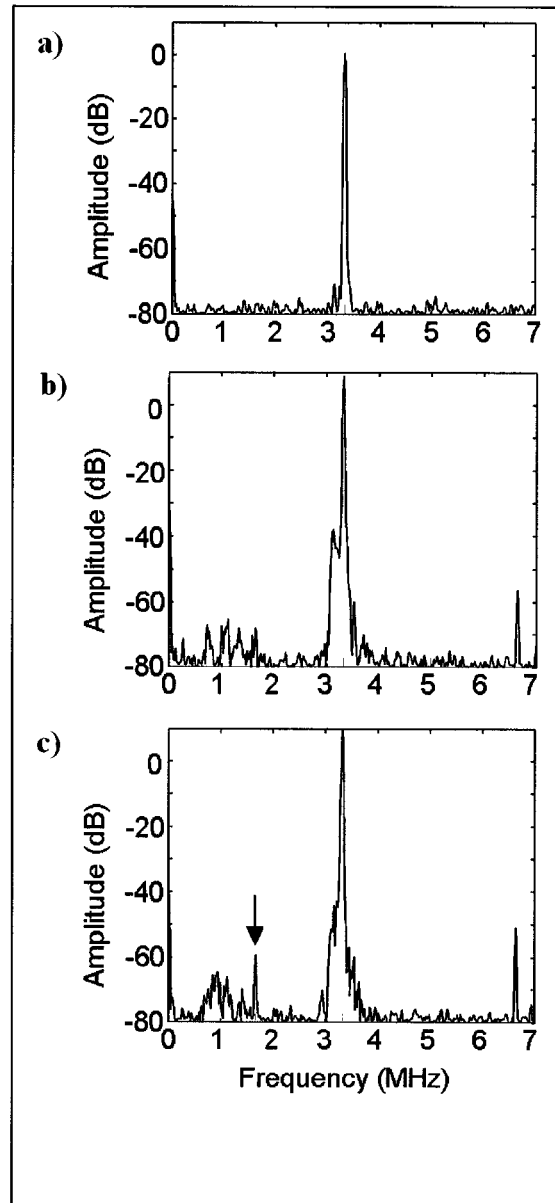
Figure 3-14: Representative plots of typical Fourier spectra from pulses prior to (a) and during (b, c) the appearance of a hyperechoic region in the US image for a HIFU exposure at 1280 W/cm^2. The background level of noise can be seen in the top plot (a) for a HIFU pulse. The spectrum in the middle plot (b) shows an increase in the broadband noise after appearance of a hyperechoic region at 5.6 s into the HIFU exposure. The bottom plot (c) shows an increase in both the broadband and subharmonic noise at 4 s after appearance of the hyperechoic region. The appearance of a second harmonic at 6.6 MHz can also be seen (b, arrow in c).
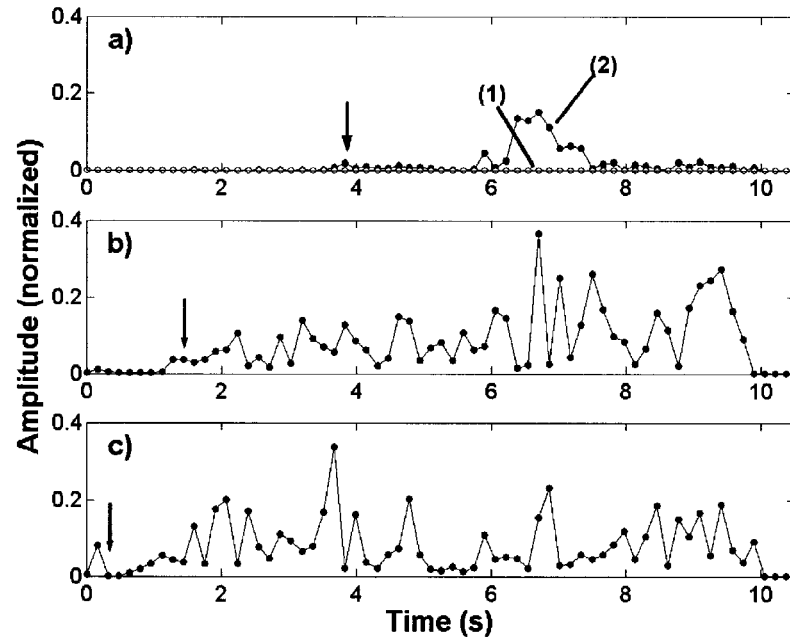
Figure 3-15: Typical time evolutions of the inertial cavitation levels for *in vivo* HIFU exposures of 10 s at (a) 850, (b) 1280 and (c) 1710 W/cm^2. Arrows indicate the onset time for the US visualization of a hyperechoic region. The typical time evolution of the inertial cavitation without (1) and with (2) the appearance of a hyperechoic region during HIFU exposures at 850 W/cm^2 are shown in (a). Amplitudes were normalized from 0 to 1.
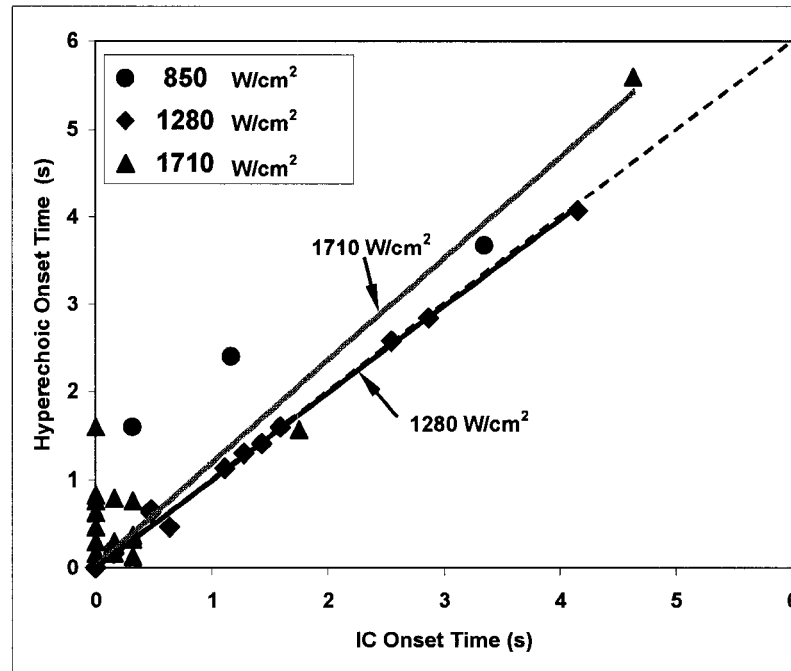
Figure 3-16: Plot of the appearance time of a hyperechoic region in an US image compared to the onset time of IC as measured by PCD from the HIFU focal zone during treatment *in vivo* for 10 seconds at (●) 850, (◆) 1280 and (▲) 1710 W/cm^2. The best-fit linear line for each intensity is shown. The associated linear correlations (R^2) for the intensities of 1280 and 1710 W/cm^2 are 0.99 and 0.80, respectively. Since only three HIFU exposures at 850 W/cm^2 resulted in a hyperechoic region, the linear regression was not performed at this intensity. The dashed line represents unity between the two onset times.

3.2.3. DISCUSSION AND CONCLUSION

The results from this study provide evidence that bubbles are present at the site of HIFU treatment around the time of appearance of a hyperechoic region in a diagnostic B-mode US image. A significant increase in the detected level of the backscatter RF signal during ACD and the broadband noise of the RF signal during PCD correlated with the appearance of a hyperechoic region at the HIFU focus.

The appearance time of a hyperechoic region in the US image decreased with the increase in HIFU intensity during both active and passive cavitation detection (Table 3-1). Others have reported similar results (Chan et al. 2002; Vaezy et al. 2001). In our study, a threshold HIFU intensity of 850 W/cm^2 at 3.32 MHz was found for the generation of a hyperechoic region, with the earliest appearance occurring at 0.6 s into the HIFU exposure. Prior studies have reported the threshold HIFU intensity for the appearance of a hyperechoic region within 1 s at 970 W/cm^2 *in vivo* in pig liver (Vaezy et al. 2001), and within 5 s at 760 W/cm^2 *in vitro* in turkey breast (Chan et al. 2002) (both studies used 3.5 MHz HIFU frequency). The lower intensity threshold observed *in vitro* is most likely due to a lack of perfusion (Arefiev et al. 1998) and/or the presence of gases in the tissue due to decay (Bush et al. 1993). The difference in threshold between pig muscle and liver *in vivo* may be due to differences in morphology, such as the perfusion rates, and therefore a difference in the rates of thermal deposition in tissue (Pennes 1948). Additionally, since the production of cavitation is reported to occur more readily in the fluids of blood vessels than in the surrounding tissues (NCRP 2002), cavitation may occur more readily in the highly vascularized liver than in the muscle.

The hyperechoic region in the US image and the ACD RF signal associated with the HIFU focus, were observed growing and migrating towards the HIFU transducer. The migration of the hyperechoic region towards the HIFU source has previously been reported and correlated with both cavitation and boiling, and the appearance of "tadpole-shaped" lesions in tissues and gels (Bailey et al. 2001; Chan et al. 2002; Vaezy et al. 2001). The appearance of the hyperechoic region in the US image was, on average earlier than the onset of cavitation detected by ACD. This was most likely a result of the unfocused ACD transducer being less sensitive than the US

imaging probe. A focused cavitation detection transducer is expected to improve the sensitivity of ACD and may make it a more sensitive method at detecting cavitation then US imaging.

ACD was unable to determine if bubbles at the HIFU focus were the result of cavitation alone and/or the result of boiling. Therefore PCD was performed to determine if inertial and/or stable cavitation contributed to the appearance of the hyperechoic region. The onset time of IC was found to correlate with the appearance of a hyperechoic region at HIFU intensities of 1280 and 1710 W/cm^2. A correlation could not be determined for the intensity of 850 W/cm^2, because only 3 of 18 exposures resulted in a hyperechoic region at this intensity.

In the majority of trials resulting in the appearance of a hyperechoic region, inertial cavitation was observed during or prior to the onset of the hyperechoic region. The appearance of a hyperechoic region in the US image was therefore due to scattering by the gas and/or vapor bubbles produced at the HIFU focus during cavitation. This confirms the results observed by Hynynen (1991) and Coleman et al. (1996) in which the presence of cavitation was observed in a few samples after the appearance of a hyperechoic region during HIFU and lithotripsy treatments, respectively. Furthermore, the observation of cavitation prior to the appearance of a hyperechoic region is an indication that the passive cavitation detector provided a more sensitive measure of the presence of cavitating bubbles than the US imager.

When using the appearance of a hyperechoic region to determine whether cavitation is present during HIFU therapy, it is important to be aware of the possibility of the appearance of a hyperechoic region occurring well after cavitation. During 5 out of 22 HIFU exposures at an intensity of 1280 W/cm^2, the appearance of a hyperechoic region occurred over 2.5 seconds after that of cavitation. Since the US imager and HIFU transducer alignment was not altered throughout this study, it is most likely due to a difference that existed between the path that the sound traveled from the HIFU focus to the PCD transducer and to the US imaging probe. Therefore, over treatment of tissue due to the presence of cavitation at the HIFU focus may occur prior to the detection of bubbles as a hyperechoic region in the US image.

In our study, stable cavitation was observed at and above the HIFU intensity threshold of 1280 W/cm^2 and was characterized by strong erratic (transient in time and amplitude) emissions of subharmonic noise. However, subharmonic noise was measured within only a few HIFU pulses of a few exposures. The intensity threshold of 2,000 – 3,000 W/cm^2 has previously been reported for the production of strong erratic emissions of subharmonic noise in rabbit brain *in vivo* at frequencies of 1 - 1.7 MHz (Vykhodtseva et al. 1995).

The detection of cavitation during HIFU therapy is important because if cavitation is present, lesions tend to form unpredictably with the majority of damage occurring closer to the HIFU source (Bailey et al. 2001; Chen et al. 2003; Malcolm and ter Haar 1996; Meaney et al. 2000; Watkin et al. 1996). In addition, pitting and tearing of tissue has been shown to result from cavitation at the HIFU focus (Clarke and ter Haar 1997; Vaezy et al. 2001). Therefore, treatment parameters below that of the cavitation threshold are usually used to produce controlled coagulative necrotic lesions (Hynynen 1991; Malcolm and ter Haar 1996). Necrosis at the HIFU focus and damage to adjacent tissues result in part from occluded blood vessels at the focus, and therefore a loss of blood perfusion to the treated and adjacent tissues (Chen et al. 1999). Since the threshold for cavitation is reported to occur more readily in the fluids of vessels than in the surrounding tissues (NCRP 2002), methods for detecting and avoiding vessels during treatment is necessary. Future studies are needed to determine the HIFU parameters for avoiding cavitation during HIFU treatments, or for the production of cavitation without tissue damage for locating the true HIFU focus prior to treatment.

Since this study has shown that cavitation is involved in the appearance of a hyperechoic region in a diagnostic B-mode US image, it may be feasible to use the appearance of a hyperechoic region to determine if cavitation is occurring during HIFU therapy. Before such a method should be used in therapeutic applications, the sensitivity of the US imager for detecting cavitation needs to be well characterized to ensure a clinically relevant threshold for the detection of cavitation. Alternatively, an active or passive cavitation detector may be easier to integrate with the HIFU transducer and may be a more sensitive method than US imaging for the detection of cavitation once fully developed. This study shows the feasibility of using either an active or passive cavitation detector integrated with a HIFU transducer for the detection of cavitation at the focus during HIFU therapy. In this particular study the passive cavitation detector was more sensitive

then the active cavitation detector method. Further optimization of both methods is needed to determine which one would work better in the clinical setting.

In conclusion, the evidence presented here leads us to believe that cavitation is involved in the formation of a hyperechoic region. This study both extends and confirms the findings of other investigators (Coleman et al. 1996; Fry et al. 1995; Hynynen 1991; Vaezy et al. 2001) that cavitation is involved in the visualization of HIFU induced lesions by diagnostic US imaging.

4. *IN VIVO* THERMAL MEASUREMENTS

To gain an understanding of the thermal and/or mechanical mechanisms that resulted in the formation of bubbles at the HIFU focus during the appearance of a hyperechoic region, the study described in Section 3.2 was repeated in pig muscle *in vivo* with a thermocouple at the HIFU focus for measuring the tissue temperature. The goal of this study was to gain an understanding of the relationship between the temperature at the HIFU focus and (1) the onset of cavitation, and (2) the appearance of a hyperechoic region resulting from HIFU sonication in an US image. This involved the following steps:

1. **Device Development and Characterization:** Fine wire thermocouples for measuring the temperature at the HIFU focus were incorporated into the integrated US imaging, HIFU, and cavitation detection system developed in Chapter 3. The system was characterized *in vitro* in a gel tissue phantom.

2. *In Vivo* **Thermal Measurements:** *In vivo* studies, in a pig model, were conducted to determine the relationship between the temperature increase at the HIFU focus and (1) the onset of cavitation by PCD and (2) the appearance of a hyperechoic region.

4.1. PRELIMINARY STUDIES

4.1.1. DEVELOPMENT OF A THERMAL MEASUREMENT SYSTEM

A system was developed to simultaneously measure the temperature and collect the PCD RF signal and US image from the HIFU focus during sonication. All four components of the system were synchronized using the method described in Section 3.2.1. After development, the system was characterized *in vitro,* in a gel tissue phantom prior, to use *in vivo* in pig muscle.

Data Acquisition and HIFU Excitation

The temperature measurement unit consisted of an E-type grounded thermocouple (0.254 mm diameter; Model EMQSS-010, Omega, Stamford, CN, USA) attached to a laptop PC via a shielded connector box (SCB-68, National Instruments Corp.) and data acquisition board (DAQCard-AI-16XE-50, National Instruments Corp.). The captured raw voltage was collected at 30 ms intervals from the thermocouple, converted to temperature (°C), and stored on the laptop PC by a custom LabView program (National Instruments Corp.). Excitation of the HIFU transducer, collection of the raw RF signal from the passive cavitation detector, and collection of the US images were conducted using the method described in Section 3.2. Synchronization of the excitation of the HIFU transducer with the temperature collected from the thermocouple and the PCD signal was done with the custom LabView program (Appendix A).

Thermocouple Guide

Prior published studies using thermocouples *in vivo* have used a hypodermic needle to place the tip of a thermocouple at the HIFU focal depth (Hynynen 1991; Malcolm and ter Haar 1996). Once at depth, the needle is removed and the HIFU focus is aligned with the thermocouple tip by moving the HIFU source while sonicating at intensities below that for producing irreversible tissue changes until a maximum temperature rise is observed (Clarke and ter Haar 1997; Hynynen 1991; Malcolm and ter Haar 1996). To reduce the amount of time to locate the thermocouple tip within the HIFU focus and to improve the reproducibility, a thermocouple guide was developed for insertion of the thermocouple into tissue approximately at the HIFU focus during the studies presented within this chapter.

The thermocouple guide (Figure 4-1) was designed for attachment to the US system used during the *in vivo* cavitation detection study discussed in Chapter 3. The guide consists of an arm mounted on the side of the HIFU transducer for guiding a hypodermic needle (22 gauge, 8.89 cm long), inserted through a hole in the tip of the arm, to within 3 mm of the HIFU focus. During *in vivo* and *in vitro* experiments, the needle was filled with degassed water prior to insertion into the tissue to reduce the chance of introducing bubbles into the tissue. By keeping the needle tip 3mm away from the HIFU focus, the amount of tissue damage and the probability of introducing bubbles within the focus was reduced. After the needle was inserted into the tissue, a

thermocouple was pushed through the needle and past the needle tip into the HIFU focus. The needle was then removed while the thermocouple remained in the tissue. Confirmation of the location of the thermocouple tip within the focus was done by moving the HIFU transducer while sonicating at a low intensity. The thermocouple tip was considered to be within the HIFU focus when the HIFU transducer was in a position that resulted in a maximum temperature rise. This method both reduced the time needed for locating the thermocouple tip with respect to the focus and reduced the variation in the angle of the thermocouple to the HIFU axis.
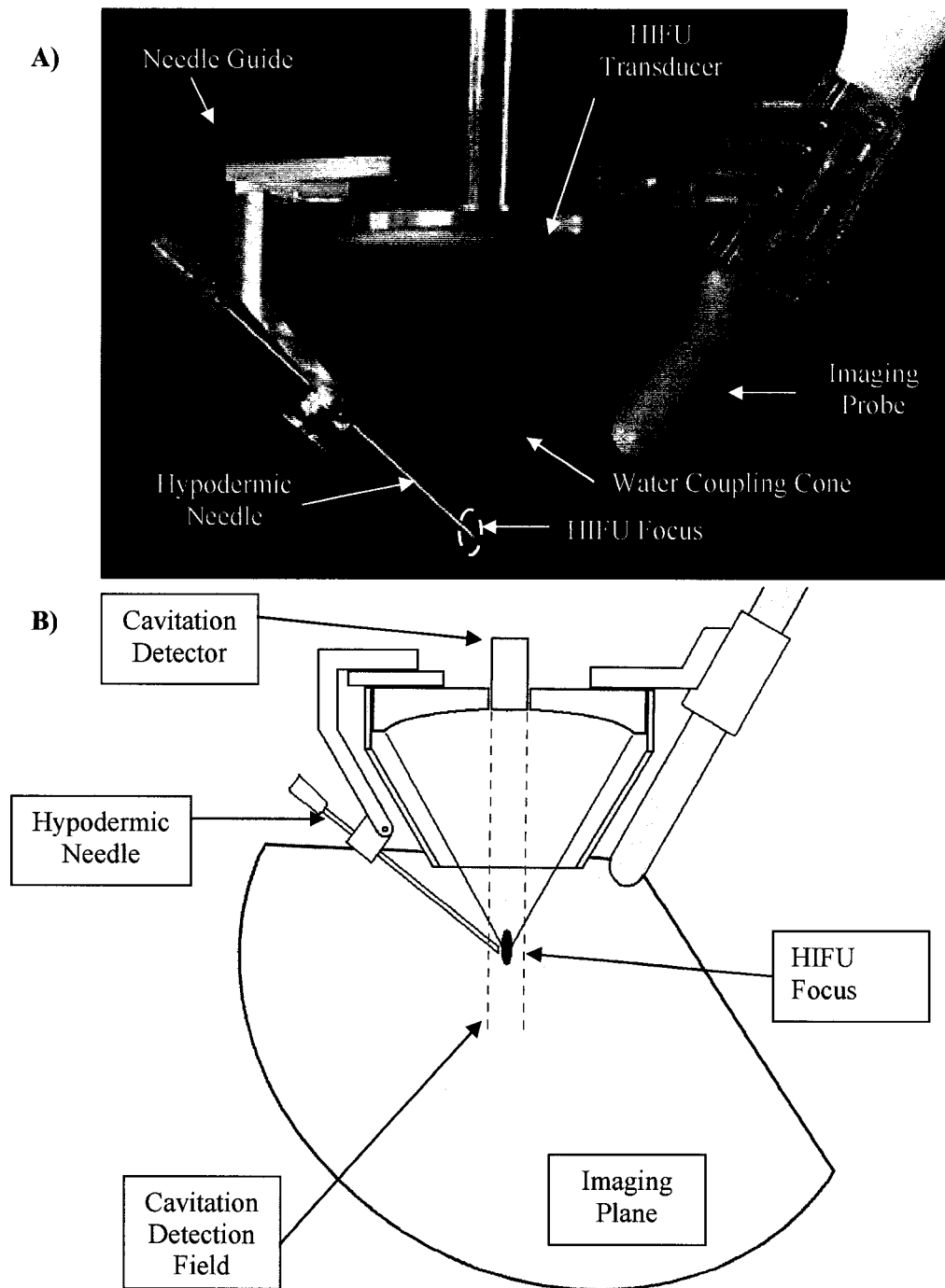
Figure 4-1: Photograph (A) and schematic (B) of the needle guide attached to the US-guided HIFU transducer. The needle can be seen extending into the HIFU focus (not to scale). The schematic (B) illustrates the US fields of the HIFU transducer, cavitation detector and US probe.

The use of Thermocouples in an US Field: Measurement Errors

There are four measurement artifacts associated with the use of a thermocouple in an US field that will lead to errors in determining the absolute temperature at the HIFU focus. As extensively reviewed in, and reported by Hynynen and Edwards (1989), the errors associated with using a thermocouple to measure the temperature in an US field are as follows:

(1) The use of highly absorbing materials around the thermocouple (such as insulation), results in increased temperatures at the thermocouple as opposed to the surrounding media. This is avoided in our setup since a metal thermocouple was used.

(2) Differences in the angle of the probe to the axis of the US source results in a difference in the rise in temperature of the probe from 0.2-3 °C for a change in angle from −10 to -90°. Because the thermocouple was inserted into the tissue using a guide with a set angle to the HIFU axis, the angle of the thermocouple with respect to the US axis remained consistent in the setup used within this thesis. Therefore, the error due to a difference between the angle of the thermocouple and HIFU axis remained constant in all my experiments.

(3) Distortion of the US beam by the thermocouple can result from the US wave scattering and reflecting from the probe. Hynynen and Edwards (1989) concluded that a probe smaller than $\lambda^{1/2}/5$ in diameter should not result in distortion effects. For our experimental setup (3.3 MHz), this would result in a probe smaller than 0.132 mm in diameter, which is smaller than the thermocouple used in these experiments (d = 0.254 mm). However, based on beam plots of distortion of the ultrasound field by different sized thermocouples Hynynen and Edwards (1989) also concluded that at an operating frequency of 3 MHz, the diameter should be smaller than 0.35 mm to eliminate most distortion effects. Therefore, the diameter of the thermocouple used was acceptable.

(4) The fourth measurement error is induced by US and is associated with heating due to viscous shearing, resulting from the relative motion of the surrounding medium with respect to the fine wire thermocouple (Hynynen and Edwards 1989). This artifact can be distinguished from normal temperature changes in the surrounding medium as a rapid small rise (0.5-3 degrees) and decline in the measured temperature at the start and completion, respectively, of the US exposure (Hynynen and Edwards 1989; Waterman and Leeper 1990) as illustrated in Figure 4-2. In the studies presented in this chapter, the measured temperature is not considered an absolute value, but rather accurate within 4°C.
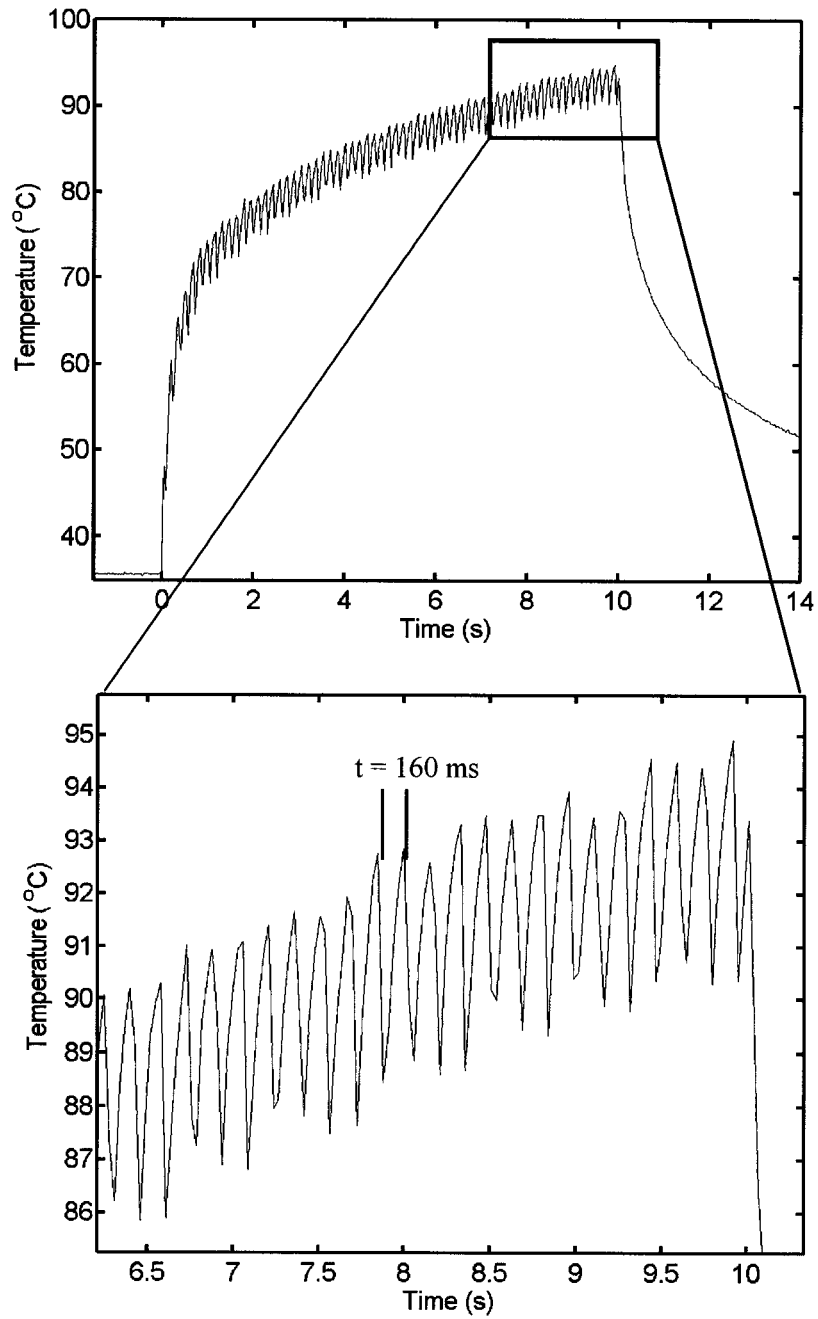
Figure 4-2: Plots of the temperature change at the HIFU focus during an *in vivo* sonication at 220 W/cm² for 10 sec. The rapid rise and fall of the temperature at the focus is correlated with the on and off time of each HIFU pulse (6.26 Hz), respectively.

In addition to the problems inherent to using a thermocouple in an US field, the use of thermocouples is an invasive method for measuring the temperature in tissue (Childs et al. 2000). Direct insertion of the thermocouple into muscle results in tissue damage and the possible introduction of cavitation nuclei in the form of gas bubbles or particles with gas trapped within them. To reduce the extent of damage, the hypodermic needle, used to guide the thermocouple towards the focus in the studies presented in this thesis, was not inserted directly into the tissue at the HIFU focus. By using this insertion method, the extent of tissue damage at the HIFU focus was reduced to that produced by the thermocouple alone. This procedure also helped to eliminate the introduction of bubbles and dirt into the HIFU focal volume by the hypodermic needle. For reducing the probability of dirt being introduced into the tissue, both the thermocouple and hypodermic needle were cleaned with rubbing alcohol followed by degassed saline prior to insertion into the tissue (Clark and ter Haar 1997; Hynynen 1991).

4.1.2.   IN VITRO CHARACTERIZATION OF THERMAL AND CAVITATION MEASUREMENT SYSTEM

In vitro experiments in a gel phantom were done to evaluate the thermocouple and US system and to gain an understanding of the change in thermal and cavitation behavior occurring at the HIFU focus during the appearance of a hyperechoic region.

Materials and Methods

A series of 50 HIFU exposures were done in a gel phantom consisting of 5% bovine-serum albumin (BSA) in 7% polyacrylamide. The US and thermal measurement system described in Section 4.1.1 (Figure 4-3) was used. The thermocouple was inserted into the tissue phantom and located in the HIFU focus using the method described previously (Section 4.1.1). HIFU was pulsed at an 80% duty cycle and PRF of 6.27 Hz at *in situ* intensities in polyacrylamide gel that were found to be both below and above that needed to produce a hyperechoic region (480 – 2500 W/cm^2). The RF signal from the passive cavitation detector was collected for the first 1 ms of each HIFU pulse and the US image of the lesion was recorded on a mini-DV recorder. Analysis of the PCD RF signal and US images were done using the method outlined in Section 3.2.1.
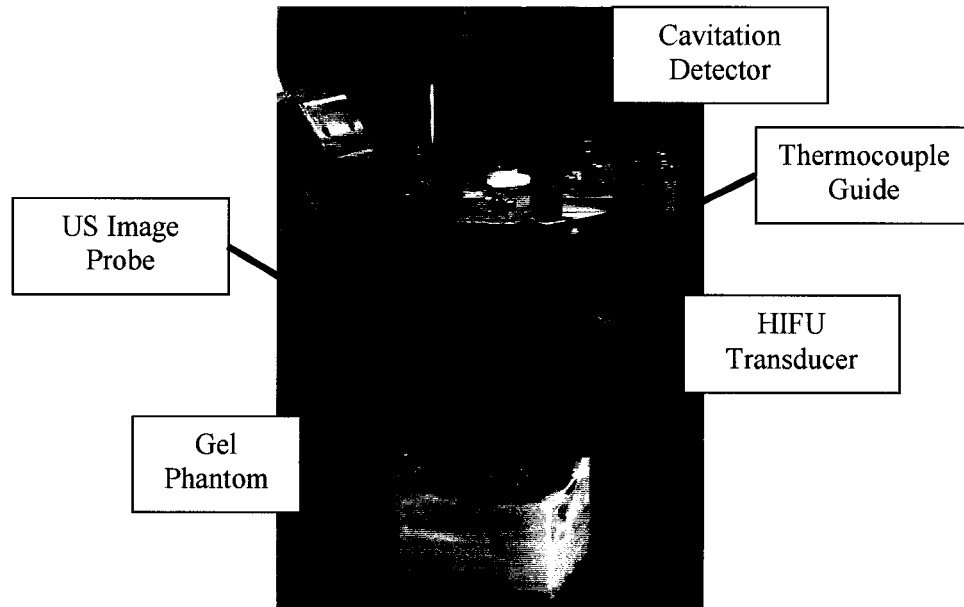
Figure 4-3: Photograph of the *in vitro* setup used for measuring temperature changes and cavitation levels during the appearance of a hyperechoic region in a gel phantom.

Results

Figure 4-4 shows the temperature and level of cavitation measured at the focus during 10 s HIFU exposures at (A) 480, (B) 690, and (C, D) 1070 W/cm^2 in which a hyperechoic region did not occur (A, B) and did occur (C, D). The appearance of a hyperechoic region typically occurred at 1070 W/cm^2 and above. Examples of cavitation-induced heating are illustrated in Figure 4-4C and D, for HIFU exposures at an intensity of 1070 W/cm^2. In Figure 4-4C, an increase in the level of cavitation (2.88 s; red line) preceded the rapid change in the rate of temperature rise (3.17 s; blue line). This sudden deviation in the rate of heating was associated with bubble-enhanced heating due to cavitation by two HIFU pulses. For this sample the appearance of a hyperechoic region in the US image (black arrow) occurred at 3.2 s into the HIFU exposure. In Figure 4-4D, cavitation occurred at the start of the first HIFU pulse (0 s) and a rapid 67°C rise in temperature occurred within 0.03 s, reaching a peak of 90°C at 0.2 s after the start of the HIFU exposure. The appearance of a hyperechoic region occurred 0.2 s into the HIFU exposure.
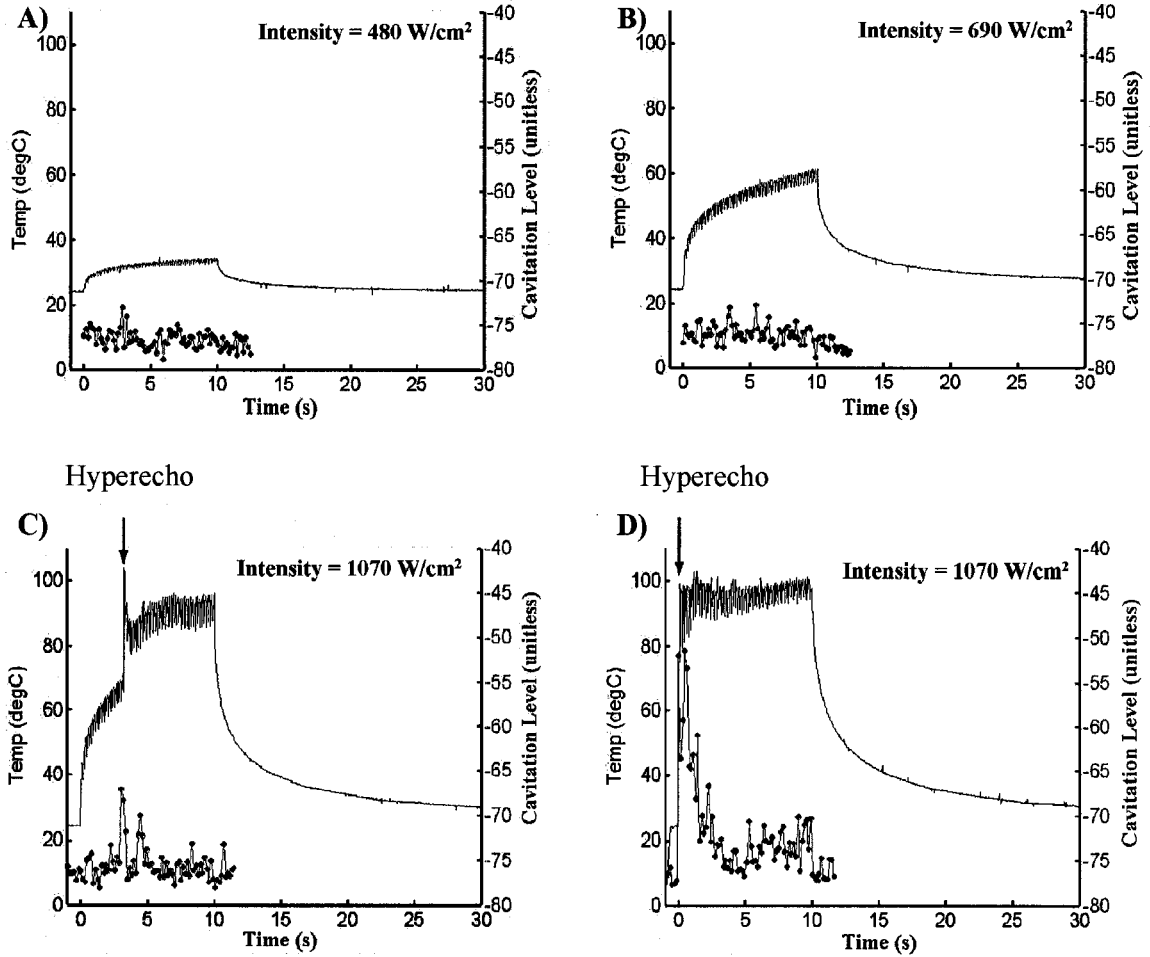
Figure 4-4: Plots of the temperature (blue line) and level of inertial cavitation (red line), in the absence (a, b) and during the appearance (c, d) of a hyperechoic region in polyacrylamide gel during 10 s HIFU exposures. The appearance time of the hyperechoic region is indicated by arrows in (c) and (d). Intensities are reported as *in situ* intensities in polyacrylamide gel. A rapid change in the rate of temperature increase is observed in (c) after the observation of inertial cavitation. A rapid rise in temperature to the boiling temperature of water and the appearance of a hyperechoic region are observed immediately at the start of the HIFU exposure in (d) along with the onset of cavitation.

4.1.3. SUMMARY AND CONCLUSION

Measurements of the temperature at the HIFU focus in polyacrylamide gel during sonications showed that the temperature rose dramatically during or after the onset of cavitation and the appearance of a hyperechoic region. Prior research has shown that cavitation results in a rapid rise in temperature at the HIFU focus, referred to as a "bubble-enhanced" heating effect (Holt and Roy 2001; Hynynen 1991). Further discussion of this phenomenon will be presented at the end of the *in vivo* thermal behavior study described in Section 4.2.

4.2. *IN VIVO* THERMAL AND CAVITATION BEHAVIOR OF A HYPERECHOIC REGION

A set of measurements of the change in temperature, cavitation activity (by PCD), and echogenicity in an US image were conducted *in vivo* at the HIFU focus in the thigh muscles of pigs at *in situ* HIFU intensities of 220 to 1710 W/cm^2. This set of measurements was done to gain an understanding of the temperature at the HIFU focus during the appearance of a hyperechoic region and the onset of cavitation.

4.2.1. MATERIALS AND METHODS

Animal Model

The thigh muscles (biceps femoris and rectus femoris) of 2 juvenile pigs were prepared using the same methods described in Section 3.2.1. Briefly, after the animals were anesthetized, the skin and underlying fat were removed from the muscle surfaces with a scalpel prior to coupling the HIFU transducer to the muscle. HIFU exposures were done for 10 s at a focal depth of 2 cm and at 2 cm intervals along the exposed muscle.

Data Collection and Processing

After the US imager and HIFU transducer had been coupled to the muscle surface and held in place by a custom built xyz-positioning system (Figure 4-5), a thermocouple was located at the HIFU focus. A 22 gauge 8.89 cm long spinal needle filled with degassed saline was inserted through a bubble of degassed saline on the muscle surface and into the tissue within 3 mm of the HIFU focus using a needle guide mounted to the HIFU transducer (Figure 4-1). A thermocouple was inserted into the site of the HIFU focus using the method described in Section 4.1.1. The location of the thermocouple tip within the HIFU focus was confirmed by exposing the tissue to HIFU at an intensity of 22 W/cm^2 for durations of 0.2 s, with a 0.5 s cooling period between exposures, and scanning the HIFU transducer with a mechanical xyz-positioning system (Figure 4-5) until a maximum temperature of 42°C was measured at the thermocouple tip. Since this procedure took 5-20 s to accomplish, no alterations in the properties of the tissue were anticipated to occur at this thermal dose (42°C for up to 20 s). After locating the tip, the HIFU focus was moved 1 mm away from the thermocouple tip while the tissue was allowed to return to body temperature. This was followed by HIFU exposures at *in situ* intensities from 220 to 1710 W/cm^2 for 10 s (80% DC). The thermocouple voltage was collected at 33.3 samples/s and stored on a laptop PC running a custom LabView (National Instruments Corp) program via a data acquisition card (DAQCard-AI-16XE-50, National Instruments Corp.).

The protocol for measurement of the RF signal and the appearance of the hyperechoic region in the US image at the HIFU focus was the same as that described for the *in vivo* cavitation detection experiment described in Chapter 3 with the following additions. The HIFU focus was monitored for changes in tissue temperature and US image echogenicity for 1 s prior to and throughout each HIFU exposure, and until the temperature had returned to the normal body temperature. Cavitation activity was monitored for the first 1 ms of each HIFU pulse (127 ms) using the method described in Section 3.2.1. Spectral analysis of the raw signal detected by the cavitation detector, the time of onset of cavitation, and the appearance time of the hyperechoic region were calculated by the same methods described in Section 3.2.1.

A sudden rapid rise in temperature of 10 - 40°C during US sonification has been reported to result from bubble enhanced heating, due to cavitation, in tissue-mimicking phantoms *in vitro* and rabbit and dog thigh muscle *in vivo* (Holt and Roy 2001; Hynynen 1991; Sokka et al. 2002;

Umemura et al. 2002). Therefore, to distinguish between direct heating of tissue by HIFU and bubble-enhanced heating at the HIFU focus, the temperature measured at the HIFU focus with a thermocouple was compared to a well established model of tissue heating by an US source (Clarke and ter Haar 1997; Holt and Roy 2001). The time of onset of a rapid rise in temperature was determined as the time at which the rate of the measured temperature rise deviated by greater then 130% from the theoretical predicted rate of temperature rise based on the following calculation of the expected temperature T for a thermocouple in the HIFU focus during sonication (Clarke and ter Haar 1997; Holt and Roy 2001):

$$T = \frac{2\alpha I_0}{\rho_0 C_0} e^{-r^2/a^2} \frac{a^2}{4\kappa_0} \ln\left[1 + \frac{4\kappa_0 t}{a^2}\right] \qquad (1)$$

were I_0 is the spatial-peak temporal-average acoustic intensity (I_{SPTA}) at the focus, $\kappa_0 = k/C_0$ is the thermal diffusivity of muscle, ρ_0 is the density of muscle, C_0 is the specific heat of muscle, k is the thermal conductivity of muscle, r is the distance between the thermocouple tip and the HIFU axis, a is the effective Gaussian radius of the HIFU focus, and α is the absorption coefficient of muscle. Table 4-1 gives the physical values of muscle used for modeling the temperature at the site of the thermocouple tip. The time onset of a rapid change in the temperature rise was measured and correlated with the onset time of cavitation and the appearance time of a hyperechoic region.

Table 4-1: Material properties of muscle.

	Density ρ_0 (g/ml)	Sound speed C (m/s)	Attenuation α (Np/cm/MHz)	Thermal conductivity k (W/cm °C)	Specific heat C_0 (J/kg °C)
Water	1.00[†]	1500[†]	0.025[#]	0.006[#]	4.18[#]
Muscle	1.07[†]	1566[†]	0.15[†]	0.0048[*]	3.59[*]

[*] (Gonzalez-Alonso et al. 2000)
[†] (Christensen 1988)
[#] (Holt and Roy 2001)
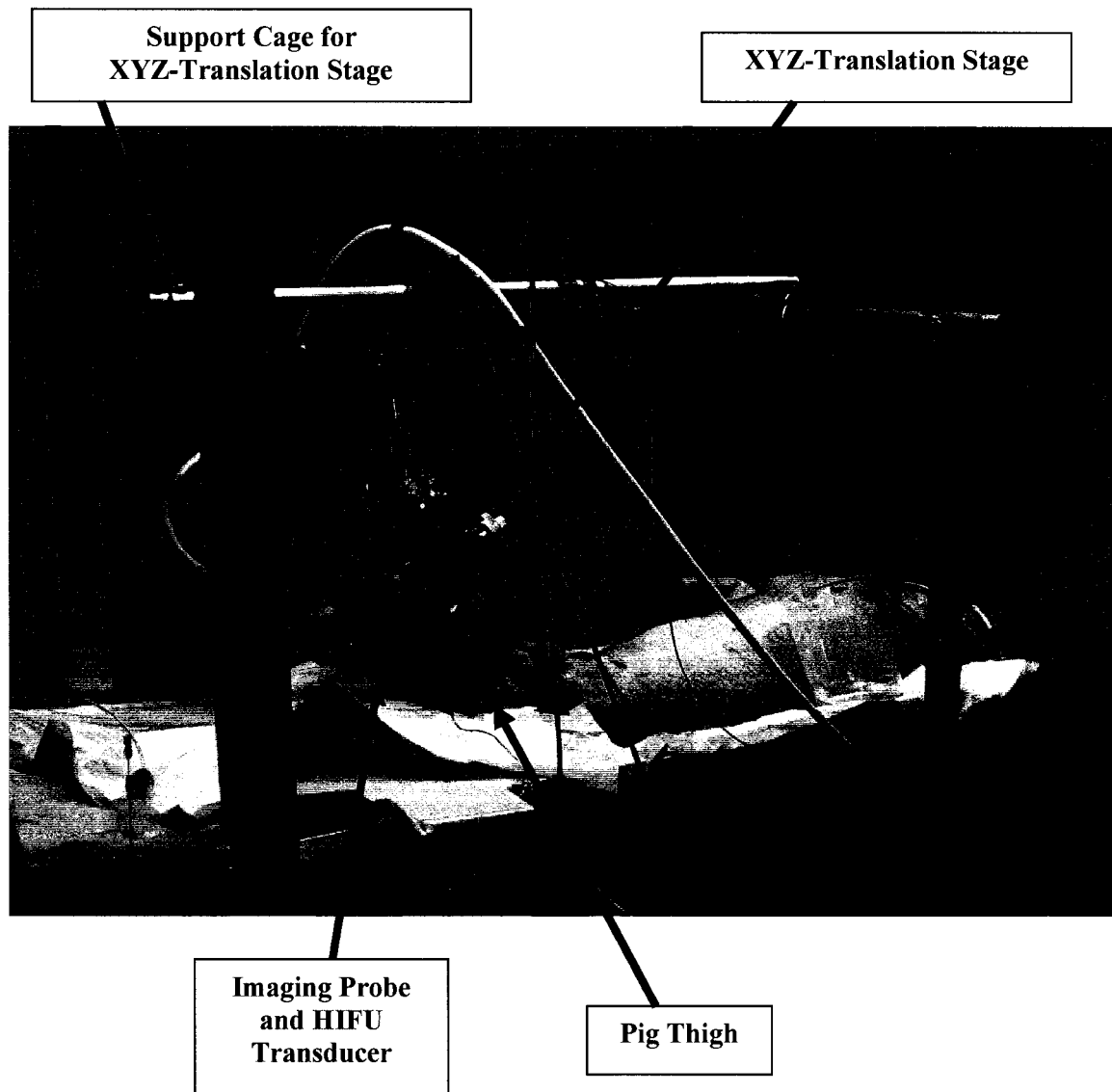
Figure 4-5: Photograph of the position system used during thermal measurements in pig muscle *in vivo*. The US system included an US imager, HIFU transducer, cavitation detection transducer, and a thermocouple. The US system was suspended above the pig and placed in position by an xyz-translation stage attached to a sturdy cage.

4.2.2. **RESULTS**

A total of 48 HIFU exposures were performed during which the tissue temperature was measured using a thermocouple placed at or near the HIFU focus. The level of broadband noise, an indicator of inertial cavitation, and echogenicity in an US image from the HIFU focal site were measured. Of the 48 HIFU exposures, 15 were excluded due to motion of the thermocouple tip with respect to the HIFU focus. The motion of the thermocouple tip was due to either animal respiration or due to muscle twitching in response to HIFU exposure, problems inherent to the *in vivo* animal model used.

Of the 32 HIFU exposures analyzed, the results were divided into 3 main and 1 sub category based upon how the measured temperature deviated from the predicted temperature and on the appearance time of a hyperechoic region with respect to the time to which the temperature deviated from predicted values. The categories, which include "Model Predicted", "Boiling", "Bubble-Enhanced Heating" and "High Predicted", are listed in Table 4-2 along with the number of HIFU exposures at each intensity.

The first category, "Model Predicted", included 14 HIFU exposures for which the measured temperature did not deviate significantly from the predicted temperature at the HIFU focus (Table 4-2 column 2). Of these exposures, 9 did not result in the production of a hyperechoic region. Figure 4-6 shows a typical plot of the temperature and the IC (broadband noise) at the HIFU focus during and after a HIFU application *in vivo*, in pig muscle, in which a hyperechoic region did not appear and the rate of change of measured temperature followed predicted values. The HIFU exposure was for 10 s at an *in situ* intensity of 220 W/cm^2 and 80% duty cycle. A maximum temperature of 95 °C was reached at the end of the HIFU exposure and the level of IC did not increase significantly above background levels.

Within the "Model Predicted" category, a subcategory referred to as "Boiling" included 5 exposures that resulted in the appearance of a hyperechoic region and the onset of cavitation within 0.4 s of the measured and predicted temperature rising above 100 °C (Table 4-2 column 3). These exposures appeared to result in "boiling" at the focus that in turn resulted in the onset of cavitation and the appearance of a hyperechoic region. Figure 4-7 is an example of the time

evolution of change in the measured and predicted temperature, the level of cavitation and the echogenic area in an US image of a "boiling" induced hyperechoic region.

Table 4-2: The number of HIFU exposures in each thermal category for each HIFU intensity. The "Model Predicted" category (column 2) includes HIFU exposures in which the temperature followed a predicted rate of heating. This category includes a subcategory of HIFU exposures, labeled Boiling (column 3), in which the temperature rise exceed 100°C followed by the appearance of a hyperechoic region and cavitation. The third category, "Bubble-Enhanced Heating" (column 4), includes exposures in which a hyperechoic region appeared prior to or during a significant deviation in the rate of the measured temperatures from the predicted temperature rise. The final category, "High Predicted" (column 5), includes HIFU exposures in which the measured and predicted temperature exceeded 100°C, and the appearance of a hyperechoic region occurred to rapidly to differentiate between boiling and bubble-enhanced heating.

Intensity (W/cm^2)	Model Predicted	Boiling	Bubble-Enhanced Heating	High Predicted
220	6		1	
490	7	4	2	
850	1	1	6	1
1280			2	2
1710			1	4
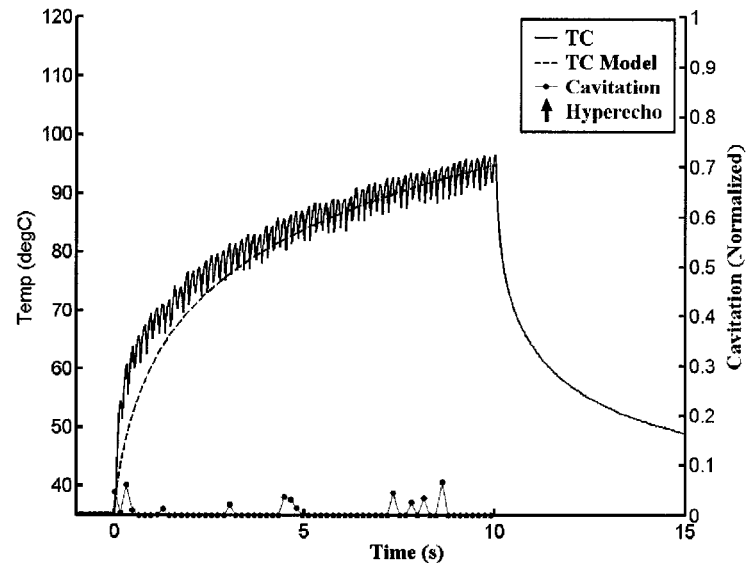
Figure 4-6: Typical plot of the time evolution of the temperature and cavitation (broadband noise) at the HIFU focus, and the pixel area of the hyperechoic region in an US image during and after a HIFU application of 220 W/cm^2 for 10 sec *in vivo* in pig muscle. A hyperechoic region did not appear during this HIFU exposure and the measured temperature (TC) followed the predicted temperature (TC Model).
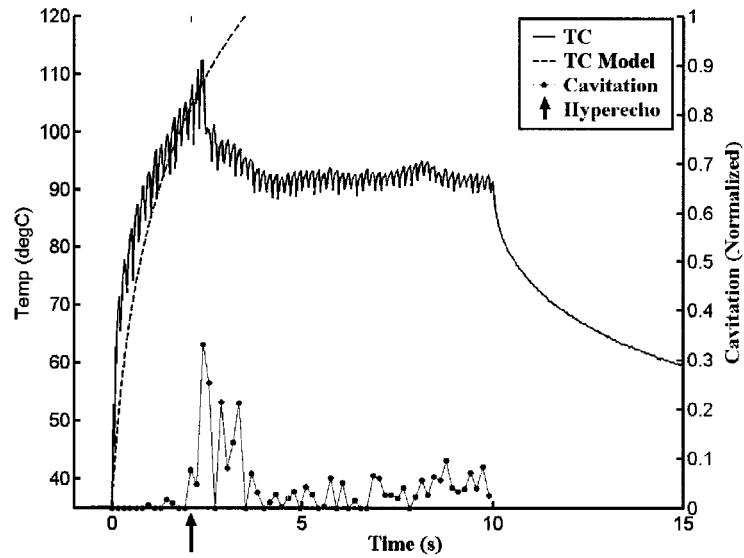
Figure 4-7: Time evolution plot of the temperature measured (TC) and predicted (TC Model) for a thermocouple at the HIFU focus during an exposure at 490 W/cm^2 for 10 s *in vivo* in pig muscle in which it appears as if boiling resulted in the production of a hyperechoic region. After the measured tissue temperature at the focus exceeded 100 °C at 1.59 s in the HIFU exposure, the initial onset of cavitation (broadband noise) and the appearance of a hyperechoic region (green arrow) were observed at 1.92 and 2.07 s respectively.

The second category, "Bubble-Enhanced Heating" included samples in which the onset of cavitation and/or the appearance of a hyperechoic region resulted in a rapid increase in the rate of the measured temperature rise. Prior studies refer to this phenomenon as bubble-enhanced heating (Clarke and ter Haar 1997; Holt and Roy 2001; Hynynen 1991). In this study, 12 HIFU exposures (Table 4-2 column 4) resulted in a distinct deviation of the measured rate of change in temperature from the predicted rate of change in temperature after the onset of cavitation and the appearance of a hyperechoic region. Figure 4-8 shows a plot in which a hyperechoic region appeared midway into the HIFU exposure followed by bubble-enhanced heating. The onset of cavitation occurred at 0.32 s after the start of HIFU. The temperature at the focus began to rise immediately and continued steadily until 1.15 s after the start of HIFU, when a rapid rise from 80°C to 115°C was observed. This followed the appearance of a hyperechoic region at 1.10 s. A significant decrease in the temperature is observed after ~3 s and is followed by a significant increase in temperature after 6 sec. The decrease in temperature correlated with the migration of the hyperechoic region away from the thermocouple tip and towards the HIFU transducer.

The final category, "High Predicted" (Table 4-2 column 5), includes 7 HIFU exposures in which the measured and predicted temperature exceeded 100°C, along with the appearance of a hyperechoic region, occurred to rapidly (< 0.3 s) to differentiate between boiling and bubble-enhanced heating. Because of the limitations of the measurement system used a conclusion could not be drawn as to whether the onset of cavitation and the appearance of a hyperechoic region occurred before or after the rapid rise in temperature of greater then 100°C. Figure 4-9 shows a typical plot of the temperature and IC at the HIFU focus and the appearance time of a hyperechoic region in an US image during and after a HIFU application in which a hyperechoic region occurred relatively early (0.167 s) in the HIFU exposure. The onset of cavitation and the rise in temperature above 100°C occurred almost immediately after the beginning of the HIFU application. The onset of cavitation occurred within the first 1 ms of the exposure and was followed by the appearance of a hyperechoic region at 0.167 s and a temperature rise above 100°C in 0.195 s. A significant decrease in the temperature was observed ~4 s after the start of HIFU and correlated to the enlargement and migration of the hyperechoic region away from the thermocouple tip and towards the HIFU transducer.
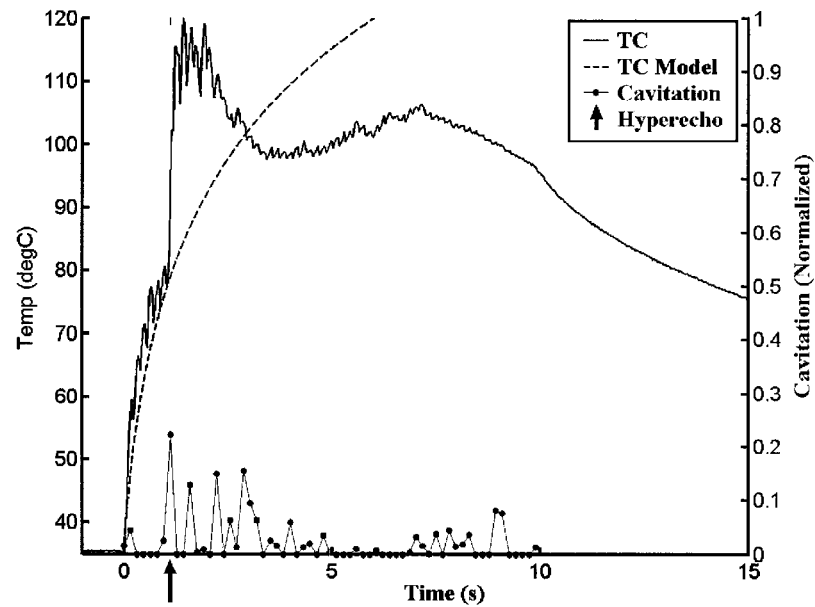
Figure 4-8: Time evolution plot of the temperature measured (TC) and predicted (TC Model) for a thermocouple 0.35 mm from the HIFU focus during an exposure at 850 W/cm^2 for 10 s *in vivo* in pig muscle. A rapid rise in temperature was measured after the appearance of a hyperechoic region (green arrow) and cavitation (broadband noise) was measured at the HIFU focus. The onset of cavitation and the appearance of a hyperechoic region occurred at 0.32 s and 1.10 s, respectively, after the start of HIFU. The temperature at the focus began to rise immediately and continued steadily until 1.15 s after the start of HIFU, when a rapid rise from 80°C to 115°C was observed. This followed the appearance of a hyperechoic region at 1.10 s. A significant decrease in the temperature is observed after ~3 s, most likely due to shadowing of the thermocouple tip by bubbles in the HIFU path. This was followed by a significant increase in temperature at 6 sec, presumably due to thermal diffusion from the region of tissue containing the bubble cloud that is associated with the hyperechoic region.
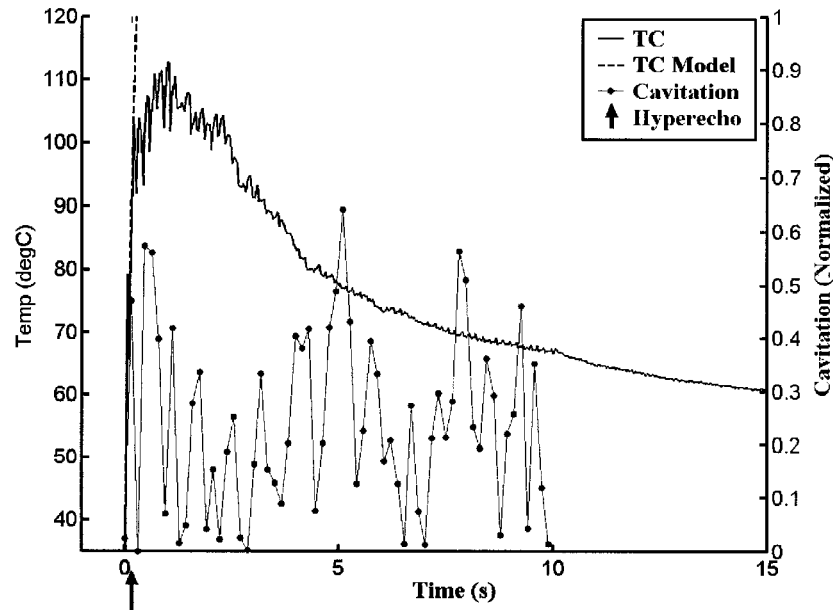
Figure 4-9: Typical time evolution plot of the measured temperature, predicted temperature, and IC at the HIFU focus during and after a HIFU exposure of 1280 W/cm² for 10 sec *in vivo* in pig muscle. The onset of cavitation and the rapid rise in temperature occurred immediately after the beginning of the HIFU exposure. This was followed by the appearance of a hyperechoic region (green arrow) at 0.167 s and the temperature reaching above 100°C at 0.195 s. The decrease in temperature after ~4 s is most likely due to shadowing of the thermocouple tip by bubbles in the HIFU path.

4.3. SUMMARY AND CONCLUSION

The results from this study, along with the results discussed during the cavitation study in Chapter 3, provide evidence that bubbles are present at the site of HIFU treatment during the appearance of a hyperechoic region in a diagnostic B-mode US image. The rate of temperature change measured at the HIFU focus followed predicted rates when cavitation and the appearance of a hyperechoic region were not observed. When the temperature rose in a predictable manner above 100°C, the onset of cavitation and the appearance of a hyperechoic region occurred within 0.4-0.7 s. The onset of cavitation and the appearance of a hyperechoic region were believed to occur after the temperature rose above 100°C, because the vapor pressure had increased in the tissue water to the point that vapor nuclei were produced. After this, the vapor nuclei may have filled with gas available in the surrounding tissue supersaturated due to heating and/or gas may have been drawn into the vapor nuclei by rectified diffusion (Crum et al. 1987).

Bubble-enhanced heating was observed in 12 samples as a significant increase in the detected level of cavitation and as an appearance of a hyperechoic region prior to a rapid increase in the rate of heating at the HIFU focus. A rapid rise in temperature in an ultrasound field due to bubble-enhanced heating, of up to 60°C within 1 s in vivo, has previously been reported in vitro (Holt and Roy 2001; Watmough et al. 1993), ex vivo (Clarke and ter Haar 1997) and in vivo (Hynynen 1991; Lele 1987; Sokka et al. 2002). A rapid change in the rate of heating was reported to occur either after the detection of cavitation, when bubbles were found by histology after sonication, or after bubbles were artificially injected into the sound path prior to sonication.

A significant decrease in temperature was typically observed after the hyperechoic region had enlarged and migrated towards the HIFU source. The decrease in temperature was most likely due to shadowing of the thermocouple tip by a bubble cloud proximal to the HIFU transducer, displayed as a hyperechoic region in the US image. Alternatively, the decrease in temperature may have been due to the insulation of the thermocouple by bubbles in contact with its tip. Clark and ter Haar (1997) have reported a similar barrier to the passage of HIFU, observed as a rapid drop in temperature and attributed to an increase in attenuation due to bubbles forming in the prefocal region of the HIFU transducer. In that study, bubbles were found in the tissue between the thermocouple tip and HIFU transducer after sonication.

The results of this study lead us to believe that the appearance of a hyperechoic region in an US image at the HIFU therapy site can occur as a result of HIFU induced cavitation alone and/or boiling induced cavitation. In addition, the results show that bubble-enhanced heating occurs after the production of a hyperechoic region. These results provide support for concern, that after the appearance of a hyperechoic region the temperature rapidly reaches levels well above predicted values and/or boiling has occurred. These results also demonstrate that the use of acoustic energy, defined as the US intensity multiplied by the duration of sonication and expressed in J/cm^2, is inadequate as a means for defining the HIFU dose when designing and discussing therapeutic regimes. Acoustic energy does not take into account additional heating due to thermal effects resulting from bubbles (cavitation) in the HIFU field, which have been observed to cause a rapid temperature rise known as bubble enhanced-heating.

5. HYPERECHOIC REGION FOR TARGETING: *IN VIVO* ASSESSMENT OF TISSUE DAMAGE

Even though the production of a hyperechoic region by HIFU has been shown to produce no short-term thermal damage in pig liver *in vivo* (Vaezy et al. 2001), it is important to assess long-term tissue damage resulting from the production of the hyperechoic region prior to using the hyperechoic region for targeting the HIFU treatment site. The goal of the studies in this chapter was to determine the short- and long-term (from 0 hr to 14 days) tissue damage associated with the production of a hyperechoic region adequate for targeting the HIFU treatment site. Completion of this aim involved:

1. **Development of a Device:** Development of an US image-guided HIFU device for the transcutaneous applications of HIFU in rabbit thigh muscles.

2. **Optimization of HIFU Parameters:** Optimization of the HIFU intensity values for the formation of a hyperechoic region within a relatively short (< 0.5 s) HIFU exposure in rabbit thigh muscle *in vivo*.

3. **Development of a Method for Transcutaneous HIFU:** Since this was a survival study, of up to 14 days post HIFU exposure, the skin on the animal was not removed to reduce, stress on the animal, surgical complications and the variability in the healing process between animals. Therefore, a method was developed transcutaneous application of HIFU in rabbit thighs in order to reducing skin burns resulting from the HIFU exposure.

4. **Optimization of Tissue Harvesting:** Optimization of a method for harvesting muscle samples for assessment of tissue damage. Because HIFU exposures were done transcutaneously and the tissue was collected from 0 hr − 14 days post HIFU exposure, a method for accurately locating the treated tissue was needed.

5. **Measurement of Temperature Changes:** Tissue temperature changes were measured during the appearance of a hyperechoic region within a relatively short HIFU exposure in rabbit thigh muscle *in vivo*.

6. **Short- and Long-Term Tissue Damage:** The short- and long-term tissue damage in rabbit thigh muscle *in vivo* induced by short transcutaneous HIFU exposures that produce a hyperechoic region were assessed. HIFU exposures were done for a single pulse of 31.25 ms at 4390 W/cm^2 and 62.5 ms at 3660 W/cm^2. Histological and morphological assessment of tissue damage was done at 0 hour, 4 hour, 2, 7 and 14 days post-HIFU exposure to determine the type of tissue damage resulting from the production of a hyperechoic region.

The studies described in this chapter were performed in the thigh muscles of New Zealand white rabbits, because, in addition to having thick muscles (1-3 cm in diameter) needed for our studies, this animal model is good for survival studies. Muscles were used in these studies because they are large and relatively homogenous in structure when compared to other soft tissue. In addition, muscles are constrained by their attachment to bone and the fascia that surrounds them, resulting in soft tissue that maintains its shape and location with respect to the animals skeleton which increases the probability of locating the HIFU treatment sites up to 14 days post treatment. Since ultrasound propagates differently across muscle fibers then along them, the orientation of the HIFU source was maintained perpendicular to the muscle fibers throughout the experiments. The HIFU focus was also oriented within the muscle in order to not involve the same muscle fiber (cell) in any two treatments. All procedures in this chapter were done in accordance with a protocol approved by the Animal Care Committee at the University of Washington and conducted according to the guidelines of the United States National Institutes of Health (NIH) for use of laboratory animals. Each animal was anesthetized with a 6:1 ratio of ketamine and xylaxine via an IV injection.

5.1.   PRELIMINARY STUDIES

5.1.1.   IMAGE-GUIDED   HIFU   DEVICE   FOR   TRANSCUTANEOUS APPLICATIONS

An image-guided HIFU device was designed for transcutaneous applications of HIFU in the rabbit thigh muscles. For this study, we switched to an air-backed spherical single-element HIFU transducer (3.2 MHz: Model SU-107, Sonic Concepts, Woodinville, WA) from the one used during the studies described in Chapter 4 and 5. The smaller footprint, overall size, and overall maneuverability of this transducer was more optimal for working with small animals such as the rabbit. The focus of the HIFU transducer had a full-width half-maximum (FWHM) beam length and width of 5.1 mm and 0.76 mm, respectively, measured using a calibrated PVDF needle hydrophone (NTR Systems, Seattle, WA). The volume of the ellipsoid-shaped focus was calculated to be 1.54 mm^3. A 14 mm thick polyacrylamide gel coupler (Prokop et al. 2003) was mounted on the face of the HIFU transducer for coupling the transducer to the rabbit thigh. The attenuation of the gel coupler was measured to be 0.059 Nepers/cm for the fundamental frequency of the HIFU transducer (3.2 MHz) using a standard acoustic transmission technique (Keshavarzi et al. 2001).

The HIFU transducer was coupled with either a curved transvaginal array (C9-5, Philips) or a curvilinear intraoperative imaging probe (CL10-5, Philips). A custom-built holder was designed in Solid Works and machined in the staff machine shop at the Applied Physics Laboratory, University of Washington, for attaching the C9-5 (Figure 5-1) imaging probe to the HIFU. An available holder was modified to work with the HIFU transducer and the CL10-5 imaging probe (Figure 5-2). The custom holders incorporated each US imaging probe with the HIFU transducer so that the US probe's imaging plane was coplanar to the HIFU axis and through the HIFU focus. The method and equipment described in Section 3.2.1 were used for excitation and synchronization of the HIFU transducer with the US imager (HDI-1000).

The two US-image guided HIFU devices incorporating the C9-5 curved array and CL10-5 curvilinear array imaging probes were compared to determine which system was better for coupling to the rabbit thigh and for the detection of the hyperechoic region. Using the method

outlined in Section 3.1.1, the axial resolution, lateral resolution, and the slice thickness of the C9-5 imaging probe were measured at the HIFU focal site to be 0.64, 1.26 and 15 mm, respectively. The axial and lateral resolution and the slice thickness of the CL10-5 imaging probe were measured at the HIFU focal site to be 0.43, 0.50 and 5 mm, respectively. Therefore, since both systems performed the same with respect to coupling to the rabbit thigh, the system incorporating the CL10-5 probe (Figure 5-2) was used during the survival study (Section 5.2) because it provided a better imaging quality.
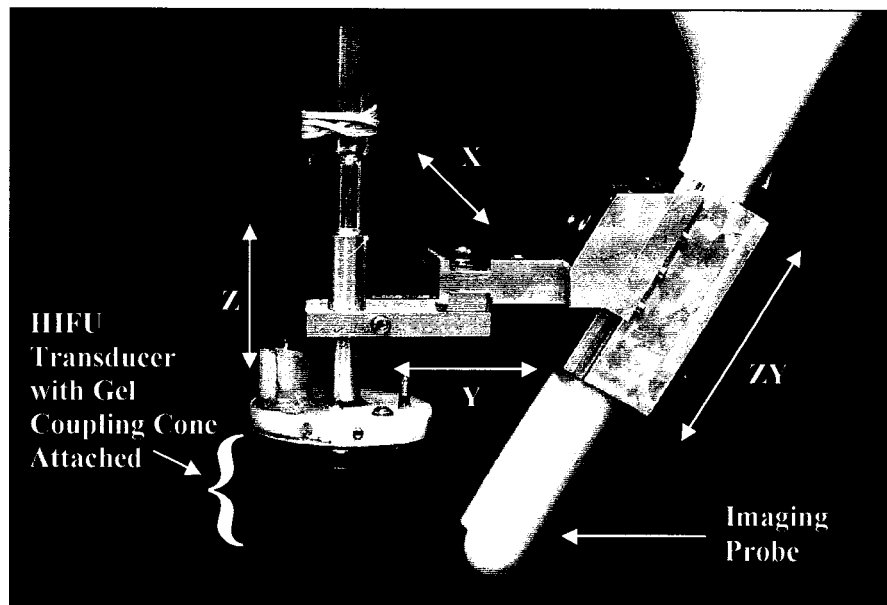
Figure 5-1: The C9-5 US image-guided HIFU device for transcutaneous HIFU applications. The device was designed so that the imaging probe could be moved in respect to the HIFU transducer for both, aligning the HIFU focus within the imaging plane and for improved coupling of both the HIFU and imaging probes to the contours of a rabbit's thigh.
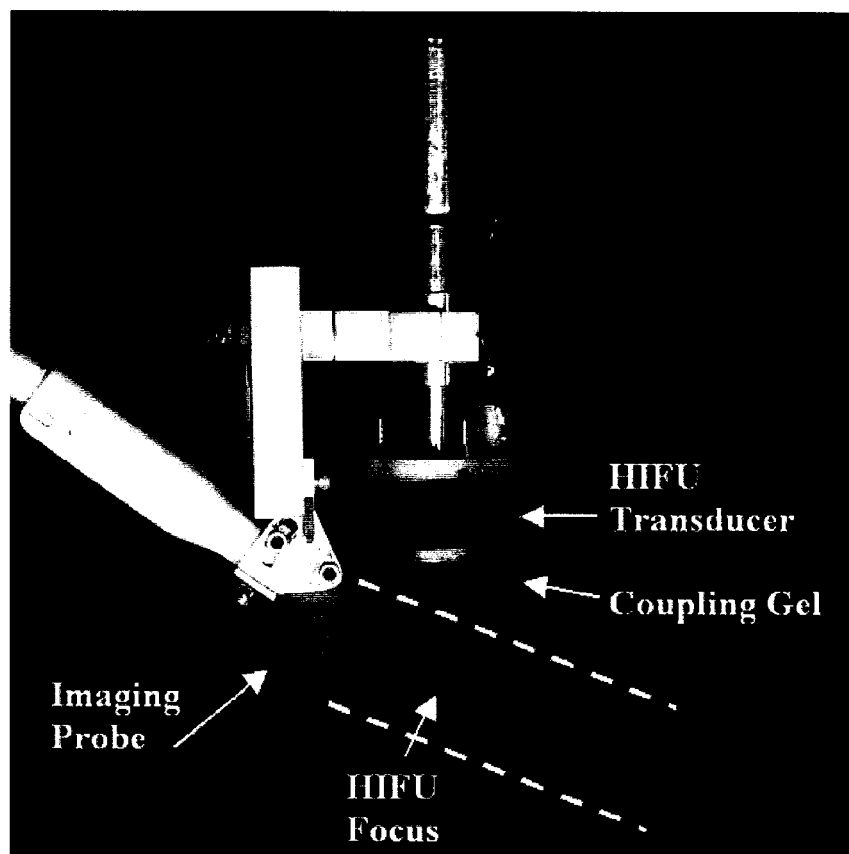
Figure 5-2: Photograph of the US image-guided HIFU device incorporating a CL10-5 curvilinear array imaging probe. The HIFU focus (red ellipse) is not to scale.

5.1.2. *DEVELOPMENT OF A METHOD FOR TRANSCUTANEOUS APPLICATION OF HIFU IN THE RABBIT THIGH*

Skin damage in the form of burns is a common problem associated with non-invasive HIFU therapy (Barkman et al. 1999; Wu et al. 2004). Once both of the US-image guided HIFU devices described above (Figure 5-1 and Figure 5-2) were completed, tests were performed *in vivo* in rabbits to develop a method for transcutaneous application of HIFU without producing skin damage at the tissue-HIFU interface. This study was originally needed because the HIFU parameters that were expected to be used during the survival study (described in greater detail in

Section 5.1.4) produced skin burns. A series of methods for preparing the skin prior to HIFU therapy were evaluated. After initially removing the hair on the rabbit's thigh with a standard electric hair clipper followed by 1-3 applications of hair removal cream (Nair, Church & Dwight Co., Inc, Princeton, NJ), each of the following methods were evaluated for coupling the HIFU transducer to the skin: (1) Coupling with degassed saline; (2) Coupling with US imaging gel; (3) Soaking the skin for up to 30 min in warm water; (4) repeating (1) and (2) after the skin, coated in water or rubbing alcohol, was rubbed with a plastic scrapper to remove gas bubbles; and (5) coating the skin and coupling gel with mineral oil. The first four methods resulted in severe skin burns, while the fifth method resulted in very few minor burns (approximately 1 out of 20 HIFU exposures at intensities (I_{SATA}) of 1500-2500 W/cm^2 for 1-5 s). Since the final protocol used in the survival study (Section 5.2) used HIFU exposure durations of 31.25 and 62.5 ms at *in situ* intensities (I_{SATP}) of 3660 and 4390 W/cm^2, respectively, which did not result in skin burns, degassed saline was used.

Figure 5-3: Skin damage resulting from transcutaneous Color Doppler guided femoral artery ablation with a 3.2 MHz HIFU transducer (1000 W/cm^2) shown in Figure 5-1. Two types of skin damage are shown. In the first (A) a skin burn resulted from improper coupling of the HIFU transducer to the skin. The second skin lesion (B), resulted from thermal damage with the growth of the HIFU lesion towards the skin from the HIFU focal point. Note the skin discoloration (gray) at the skin lesion in position (A) and the normal pink skin color at lesion site B.

5.1.3.   *OPTIMIZATION OF TISSUE HARVESTING*

The extent of damage at the HIFU focus, resulting from a hyperechoic region, was expected to be approximately the size of the focus (1.54 mm^3). Therefore, an accurate method for locating and harvesting tissue from the HIFU exposure site, up to 14 days post-HIFU application, was necessary. Two methods were used simultaneously for locating the HIFU exposure site within the thigh muscles of the rabbit: (1) stabilizing the leg and tracking the position of the HIFU focus with respect to the femur bone and (2) placing marker lesions in the muscle at specific locations.

For the first method, the leg was stabilized on a flat table and under a pair of optically transparent plastic plates mounted 35 cm above the leg (Figure 5-4). The plastic plates (5 cm apart) were used for recording the orientation of the HIFU transducer during each exposure. The plastic plates were marked such that laser beams passing through the plates would intersect with the greater trochanter (most outer part of the upper femur) and knee (Figure 5-4 b). This method allowed for the reorientation of the plates with the femur at the time of necropsy. The intersection of a laser beam from a laser mounted on the top of the HIFU transducer along the HIFU axis and the plastic plates was marked for later orientation of the HIFU axis with respect to the femur. Precise placement of the HIFU transducer was based on a horizontal xy-grid system with the x-axis along the axis of the femur (Figure 5-4c and Figure 5-5). The x-axis started at the greater trochanter and extended to the knee. By using these landmarks to orient the HIFU transducer, a series of lesion could be formed in a row parallel to the femur (x-axis) at a depth of 1.35 mm in a 3-6 cm thick section of the muscle tissue and located at a later time point, using a laser shun in the opposite direction through the markings on the plastic plates. To insure that muscle fibers did not extend through adjacent HIFU exposure and control tissue sites, exposures were performed out of axis with the muscle striation.

The second method incorporates the use of marker lesions placed in the muscle at either end of the row of HIFU exposure sites. This method was done in conjunction with the position tracking system for locating the HIFU treatment sites. Marker lesions, which were easily observable during tissue dissection, were produced at the same depth as the HIFU treatment sites. In prior studies by Dr. Vaezy's group, easily observable large lesions were produced within the tissue of
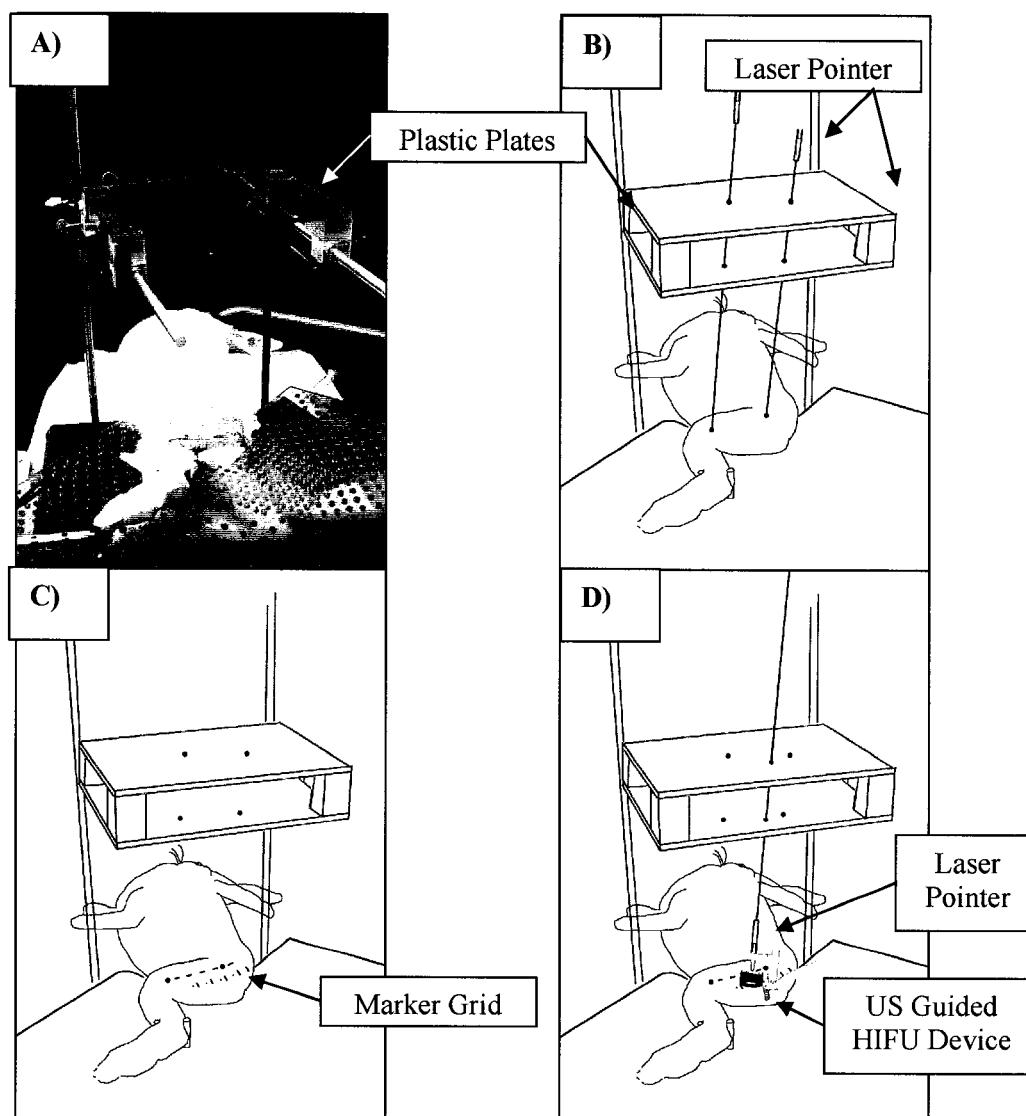
Figure 5-4: Photograph of the HIFU position tracking system. After placement of the rabbit on the table (A), the location of the hip and knee were marked on the skin. A laser was then aimed at the markings on the knee and hip (blue dots; B) and the intersection of the laser with the parallel plastic plates was marked (black dots; B). These two markers were used to reorient the plastic plates with the femur at the time of necropsy. The grid for positioning the HIFU transducer was then marked on the outer thigh (C). During each HIFU exposure a laser mounted atop the HIFU transducer was shone through the plastic plates and the intersection of the laser and plates was marked (D). During necropsy these markers were used to locate the HIFU focus by shining a laser through the marker points towards the rabbit thigh (in a similar process to A).

interest to mark the depth and location of lesions at the start and stop of each row. These marker lesions were successfully used to locate the HIFU treatment sites during necropsy.
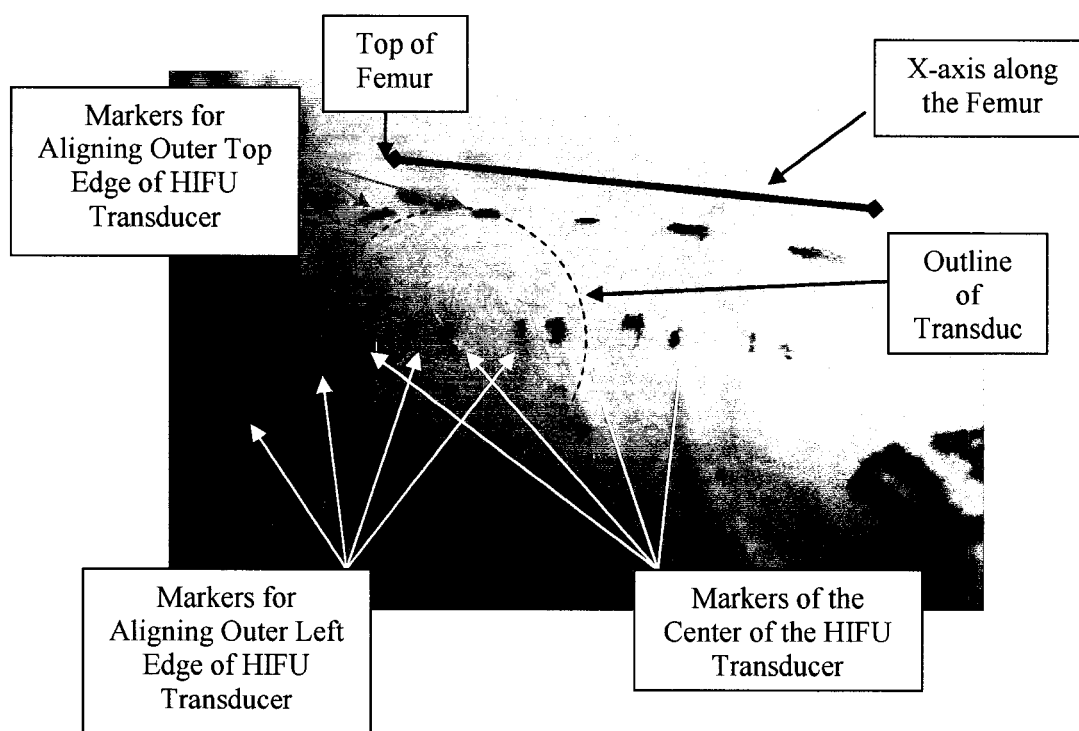
Figure 5-5: Photograph of shaved and marked rabbit thigh. The grid was used for orienting the outer edges of the transducer (green and yellow arrows) over leg preparation with grid.

At the time of tissue harvest, the animal was euthanized and the treated leg stabilized in the leg brace in the same position as used during treatment. The plastic marker plates were realigned with the femur using the landmarks at the distal and proximal ends of the bone. The skin was removed from the thigh and a series of hypodermic needles were then inserted into the muscle to mark each HIFU exposures site. To align each needle, the location and orientation of the HIFU axis was determined by aiming the laser pointer through the marker spots on the plastic plates and at the thigh muscle. The needles (1.35 cm in length) were then aligned parallel to, and 1 cm from, the HIFU axis and inserted into the tissue 1.35 cm deep. The needles were used for marking both the position and depth of the HIFU treatment site. Whole muscles were extracted from the rabbit thigh, and the outer side of the muscle was placed on a flat surface with the

needles facing up. The marker lesions were located to ensure proper placement of the needles. Square pieces of tissue ~1 cm on each side that contained the lesion were collected (Figure 5-6). This method was evaluated by relocating and harvesting the tissue that contained the lesions produced during the study described in Section 5.1.4.

Conclusion

There are no methods available for non-invasively marking the sites of HIFU sonication deep within muscle *in vivo* without affecting the morphology of the tissue. Therefore, if tissue damage does not result in a visibly detectable change in the tissue, the location of the treatment site may not be properly collected for histological analysis. Methods such as the ones described above are designed to improve the probability of relocating the treatment site up to 2 weeks post treatment. This was done by using a consistent placement of the HIFU treatment site with respect to a solid structure (the femur in this study), placing marker lesions, recording the orientation of the HIFU axis with respect to the femur, and collecting tissue samples larger then the treatment volume.
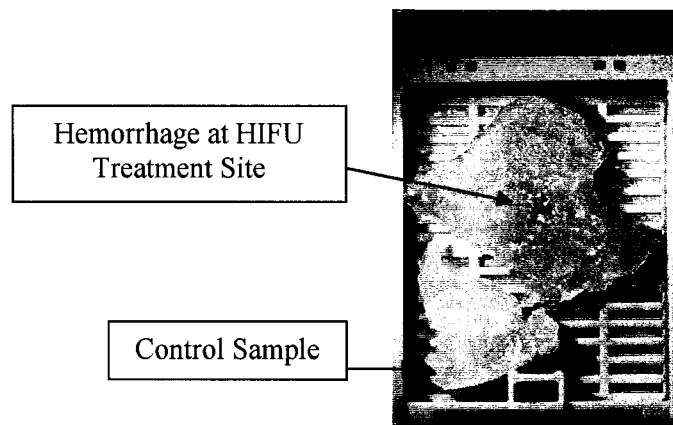
Figure 5-6: Photograph of a histology cassette containing samples of the HIFU treatment and control sites.

5.1.4. OPTIMIZATION OF HIFU ACOUSTIC PARAMETERS FOR THE PRODUCTION OF A HYPERECHOIC REGION

A series of 92 HIFU exposures were performed transcutaneously *in vivo* in the thigh muscles of both hind limbs of six rabbits to determine the minimum HIFU dose that would produce a hyperechoic region in an US image in > 90% of HIFU exposures.

Materials and Methods

The outer thigh muscles of 6 New Zealand white rabbits were used for optimization of the HIFU parameters (intensity, exposure duration, duty cycle, and pulse length) for the production of a hyperechoic region in the US image at the HIFU focus. The protocol described in Section 5.1.3 was used for preparating the animals and positioning the HIFU transducer on their outer thighs.

The initial HIFU parameters tested were based on the results of the *in vivo* cavitation and thermal studies, discussed in Chapter 3 and 4, regarding the time and percent of appearances of a hyperechoic region in the US image. The US system (Figure 5-2) incorporating the 3.2 MHz HIFU transducer and CL10-5 US imaging probe was used in this study. The initial HIFU parameters were set to a spatial average temporal peak intensity (I_{SATP}) between 1770 – 4390 W/cm^2, a duty cycle between 25 and 75% (pulse length of 31.25 – 93.75 ms), and a HIFU exposure duration of 0.5 s. The US image of each HIFU exposure was recorded and analyzed to determine the appearance time of the hyperechoic region at the HIFU focus. Review of the US images of the HIFU exposures reveled that the hyperecho at the HIFU focus was occurring within the first or second HIFU pulse (31.25 to 62.5 ms) at HIFU intensities at and above 2930 W/cm^2 in 75% of the HIFU exposures. Therefore, to minimize the overall HIFU dose while achieving a hyperechoic region, the HIFU exposure duration was set to a single pulse of either 31.25 or 62.5 ms at *in situ* (*in vivo*) intensities (I_{SATP}) of 2930-4390 W/cm^2. Synchronization of the HIFU excitation and US image collection was done using the method and equipment described in Section 3.2.1.

To optimize the detection of the hyperechoic region by the US imager, the end of the HIFU pulse was timed within 15 ms of the time at which the imaging probe interrogated the location of the HIFU focus (Figure 5-7). The 15 ms delay was determined by producing a hyperechoic region in a gel phantom (7% polyacrylamide and 5% BSA) with a single 31.25 ms HIFU pulse at an *in situ* (*in vivo*) intensity of 4390 W/cm^2. The interference bands produced by the HIFU transducer at an intensity of 200 W/cm^2 were then synchronized with the imager using the method outlined in Section 5.2. The HIFU focal depth was set to 1.45 cm into the muscle by a 1.4 cm coupling gel and 0.75 cm gel standoff (Figure 5-8). Throughout the experiment, the US imager (HDI-1000, ATL) was always set to a depth of 3.6 cm, MI of 0.5, and image persistence was turned off, resulting in 125 ms per an image frame. Rabbits were euthanized immediately after HIFU exposures, and gross histology was performed to determine the extent of damage associated with each set of HIFU parameters.
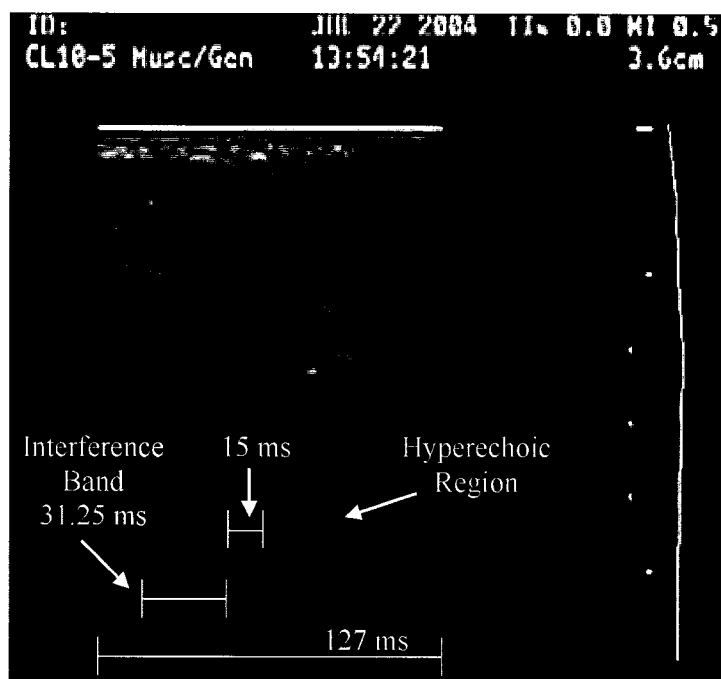
Figure 5-7: Image showing the synchronization of the HIFU pulse with the US imager. The HIFU pulse was timed to end within 15 ms of the time at which the HIFU focus was interrogated by the US imager. This was done in order to reduce the chance of overlap between the hyperechoic region and the HIFU interference bands while also reducing the time between the end of the HIFU pulse and the time the HIFU focus was interrogated by the US imager. The US imager (HDI-1000, ATL) was set to a depth of 3.6 cm, MI of 0.5, and the image persistence was turned off.
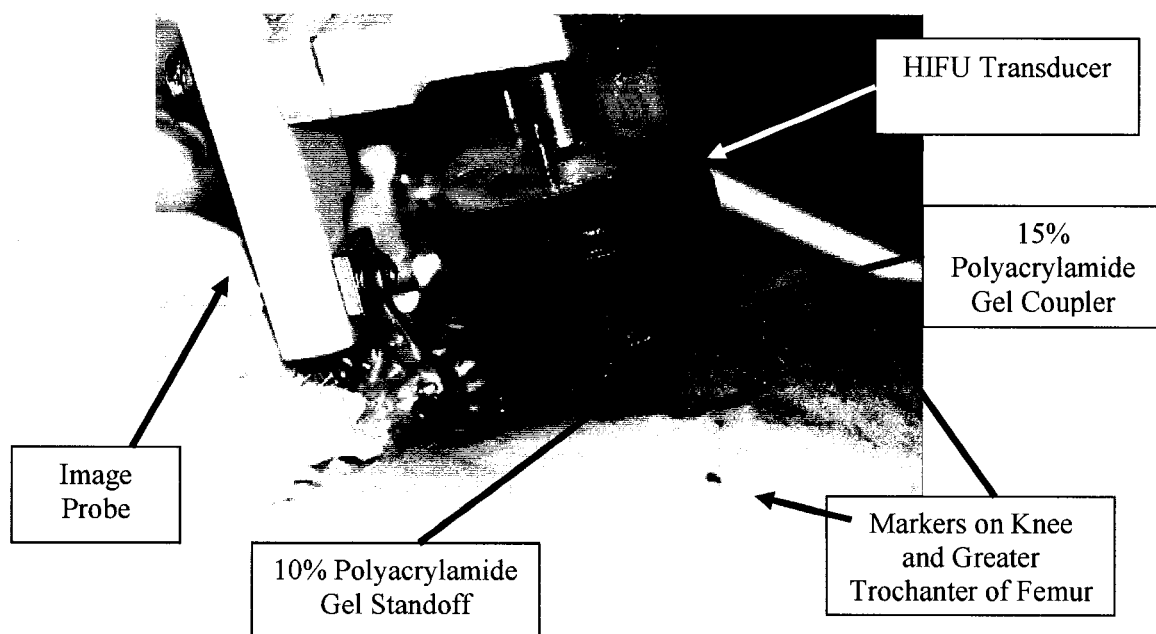
Figure 5-8: Photograph of the US image-guided HIFU system during transcutaneous applications in the rabbit thigh. The attenuation of the 10% standoff and 15% polyacrylamide gels was previously measured at 3.5 MHz to be 0.029 and 0.059 Nepers/cm, respectively (Prokop et al. 2003).

Results

Table 5-1 summarizes the results of the initial experiment in which HIFU exposures at intensities (I_{SATP}) of 1770 to 4390 W/cm^2 were done for a 0.5 s duration. Analysis of the appearance time of a hyperechoic region at the HIFU treatment site in the US image revealed that the hyperechoic region occurred within the first pulse of the HIFU exposure 75.7% of the time. Therefore, a second experiment was done in which only a single HIFU pulse was used to produce the hyperechoic region. Table 5-2 summarizes the results of the second experiment in which the HIFU exposure duration was reduced to a single pulse of either 31.25 ms or 62.5 ms. The number of exposures (Column 4), number of observed hyperechoic regions (Column 5), number of times the tissue moved as a result of the exposure (column 6), and percent of observed hyperechoic regions (column 7) are reported. The appearance of a hyperechoic region was not easily distinguished during HIFU sonications that resulted in muscle excitation and contraction which was observed as tissue motion by the naked eye and in the US image. In 90.9 % and 92.3 % of HIFU exposures at 4390 W/cm^2 for 31.25 ms and 3660 W/cm^2 for 62.5 ms, respectively, a hyperechoic region was observed at the HIFU focus. Therefore, these two parameters were chosen for use in the survival study.

Figure 5-9 shows a typical evolution of a hyperechoic region in which a hyperechoic region appeared during a HIFU exposure of 31.25 ms at an *in situ* intensity (I_{SATP}) of 4390 W/cm^2. The hyperechoic region was distinct, observable in real-time, and typically disappeared within 0.5 s. A similar hyperechoic region was observed for a HIFU exposure duration of 62.5 ms at an intensity (SATP) of 3660 W/cm^2.

Conclusion

In 90.9 % and 92.3 % of HIFU exposures at 4390 W/cm^2 for 31.25 ms and 3660 W/cm^2 for 62.5 ms, respectively, a hyperechoic region was observed at the HIFU focus. Therefore, these two parameters were chosen for use in the survival study (Section 5.2).

Table 5-1: HIFU parameters initially explored for the production of a hyperechoic region in an US image while minimizing tissue damage.

HIFU Exposure Duration (s)	I_{SATP} (W/cm^2)	Duty Cycle (%)	Pulse Length (ms)	Number of Exposures	Number of Observed Hyperechos	Tissue Motion	Percent Observed
0.5	4390	25	31.25	5	5	–	100
0.5	2930	50	62.5	1	1	–	100
0.5	3660	50	62.5	2	2	–	100
0.5	3810	50	62.5	1	1	1	100
0.5	3960	50	62.5	1	0	–	0
0.5	4100	50	62.5	3	1	–	33.3
0.5	4390	50	62.5	2	0	–	0
0.5	1770	75	93.8	2	0	–	0
0.5	2340	75	93.8	2	0	1	0
0.5	2780	75	93.8	1	0	1	0
0.5	2930	75	93.8	6	5	4	83.3
0.5	3220	75	93.8	9	6	3	66.7
0.5	3370	75	93.8	1	1	–	100
0.5	3660	75	93.8	5	3	–	60
0.5	3960	75	93.8	1	0	1	0

Table 5-2: Second set of HIFU parameters explored for the production of a hyperechoic region in an US image while minimizing tissue damage. Column 4 is the percent of the image frame that HIFU sonication was on for. This value is equivalent to the duty cycle in Table 5-1.

I_{SATP} (W/cm^2)	Duration (ms)	AE (J/cm^2)	% of Image Frame	Number of Exposures	Number of Observed Hyperechos	Tissue Motion	Percent Observed
3220	31.25	101	25	1	0	–	0.0
3660	31.25	114	25	2	1	–	50.0
4100	31.25	128	25	6	4	–	66.7
4390	**31.25**	**137**	**25**	**11**	**10**	**–**	**90.9**
2930	62.50	183	50	2	1	1	50.0
3220	62.50	202	50	13	8	–	61.5
3660	**62.50**	**256**	**50**	**13**	**12**	**–**	**92.3**
4390	62.50	274	50	2	2	–	100.0
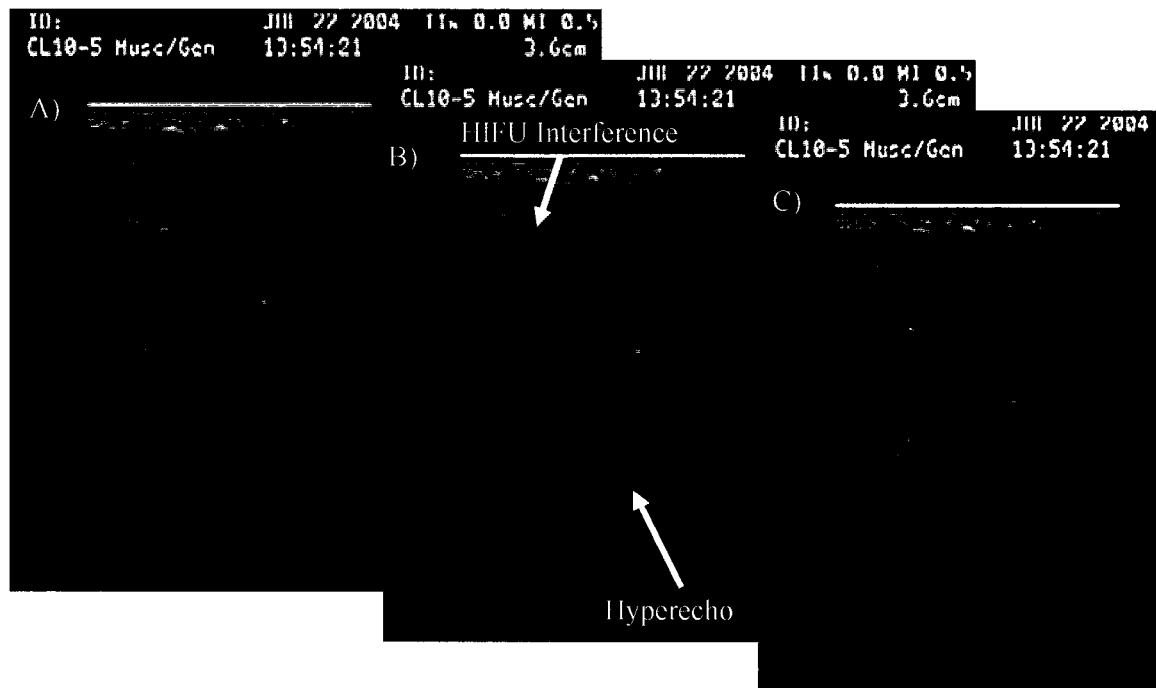
Figure 5-9: A series of US images of the treatment site one image frame (A) before, (B) during, and (C) after a 31.25 ms HIFU exposure at an intensity (I_{SATP}) of 4390 W/cm^2. The appearance of interference bands in 25% of the image frame and the appearance of a very short-lived hyperechoic region (< 127 ms) can be observed during the HIFU exposure (B). The US imager (HDI-1000) was set to a depth of 3.6 cm, MI of 0.5, toggle gain compensation (TGC) of 75% at the HIFU focus, and the image persistence feature was turned off.

5.1.5.   THERMAL MEASUREMENT OF THE TISSUE AT THE HYPERECHOIC REGION

The goal of this study was to measure the temperature rise occurring at the HIFU focus during the appearance of a hyperechoic region in an US image. This study was done to determine the temperature rise at the HIFU treatment site using the same HIFU parameters as those used during the short- and long-term tissue damage study to be described in Section 5.2.

Materials and Method

The thigh muscles (biceps femoris and rectus femoris) of a New Zealand white rabbit were exposed to HIFU transcutaneously at *in situ* intensities (I_{SATP}) of 3660 and 4390 W/cm^2 for 62.5 and 31.25 ms, respectively. The same protocol was used for preparing the animals and positioning the HIFU transducer on their outer thighs as described in Section 5.1.3. For this study, the system incorporating an air-backed spherical single-element HIFU transducer (3.2 MHz: Model SU-107, Sonic Concepts, Woodinville, WA) with a CL10-5 imaging probe (ATL) was used (Figure 5-2). Prior to each sonication, a 0.254 mm diameter E-type thermocouple (EMQSS-G-010, Omega) was inserted into the muscle using a 22-gauge hypodermic needle filled with degassed saline as described in Section 4.2.1. Once at the HIFU focal depth, the hypodermic needle was removed. The thermocouple was located within the HIFU focus by sonicating at a low intensity (25 W/cm^2) and short durations (0.2 s on, 0.5 s off) while moving the HIFU transducer along the surface of the rabbit thigh. The thermocouple was considered to be at the focus once a maximal temperature rise of 4°C was achieved. HIFU exposures at intensities (I_{SATP}) of 3660 and 4390 W/cm^2 for 62.5 and 31.25 ms, respectively, were performed after the tissue had returned to the normal body temperature of the rabbit. During each sonication, the US images were collected with a HDI-1000 US imaging system at 8 frames/s (Depth = 3.6 cm, MI = 0.5, Persistence = 0 and TGC = 75% at HIFU treatment depth) and a mini-DV video recorder at 29.7 frames/s (GL2, Canon, Lake Success, NY). The temperature was collected throughout each sonication (33.3 samples/s) and stored on a laptop PC running a custom LabView (National Instruments Corp) program via a data acquisition card (DAQCard-AI-16XE-50, National Instruments Corp.) as explained earlier in Section 4.2.1.

Results

A total of 4 measurements of the temperature at the HIFU focus were conducted during the appearance of a hyperechoic region in an US image resulting from the transcutaneous application of HIFU *in vivo* in rabbit thigh muscle. Figure 5-10 shows example plots of the temperature measured at the HIFU focus during transcutaneous HIFU applications in rabbit thigh muscle *in vivo* at a focal depth of 1.35 cm. A peak temperature of 43.4°C was measured during a HIFU exposure at an *in situ* intensity of 3660 W/cm^2 for 62.5 ms (A) and a peak temperature of 39.4°C was measured during a HIFU exposure at 4390 W/cm^2 for 31.25 ms (B). In both cases, the temperature dropped to half of the maximum achieved within 1 s and return to normal body temperature within 12-15 s.

5.1.6.   SUMMARY AND CONCLUSION

The maximum temperature reached at the HIFU focus was 43.4°C during a HIFU exposure at an *in situ* intensity (I_{SATP}) of 3660 W/cm^2 for 62.5 ms and 39.4°C during a HIFU exposure at 4390 W/cm^2 for 31.25 ms. For all HIFU exposures, the temperature decreased to half of the maximum achieved within 1 s and return to normal body temperature (37°C) within 12-15 s. Prior studies have shown that the temperature would need to be maintained for 30-60 min at 43°C for coagulative necrosis to occur (Diederich and Hynynen 1999). Therefore, thermal damage to the tissue at the HIFU focus is not expected to occur as a result of HIFU exposure with the parameters used in this study and in the survival study described in Section 5.2.
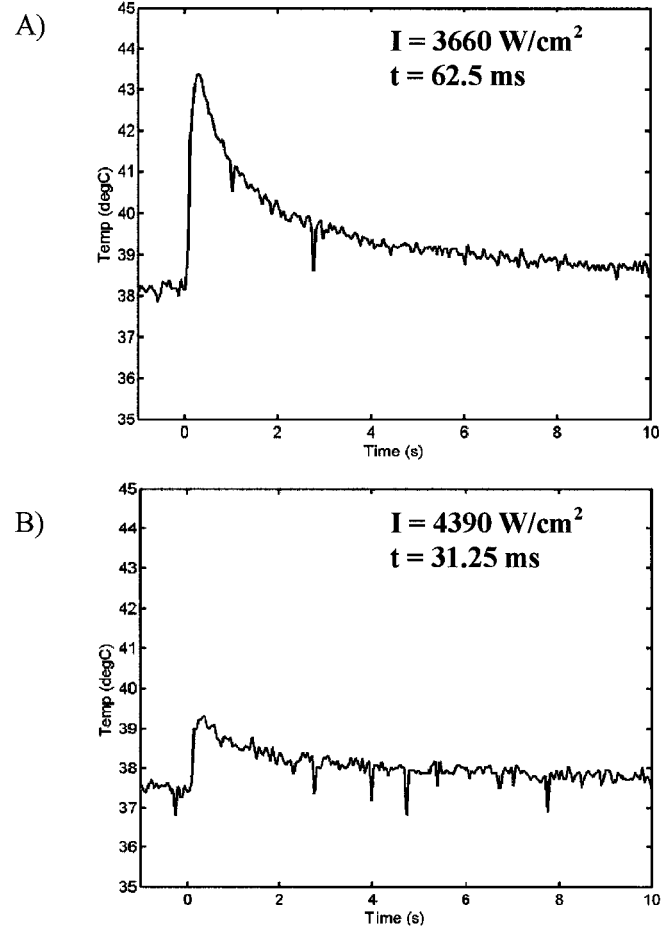
Figure 5-10: Plots of the temperature measured *in vivo* in rabbit thigh muscle at the HIFU focus during transcutaneous applications of HIFU at (A) 3660 W/cm^2 for 62.5 ms, and, (B) 4390 W/cm^2 for 31.25 ms at a focal depth of 1.35 cm.

5.2. DETERMINATION OF HISTOLOGICAL DAMAGE RESULTING FROM THE APPEARANCE OF A HYPERECHOIC REGION

The goal of this study was to determine the short- and long-term (up to 14 days) tissue damage associated with the production of a hyperechoic region adequate for targeting of the HIFU treatment site.

5.2.1. MATERIALS AND METHODS

Animal Model and Experimental Setup

Ten New Zealand white rabbits weighing 4.5-5.5 kg were anesthetized with a 6:1 ratio of ketamine and xylaxine (IV) and the hair was removed from their outer thighs. Hair was removed with a standard electric hair clipper followed by 1-3 applications of Nair hair removal cream. Remaining hair was removed by shaving with a razor blade. Each leg was stabilized on a custom plastic surgical table (Figure 5-4) and the skin over the treatment site marked with a grid oriented along the axis of the femur bone (Figure 5-5). The HIFU transducer was aligned with respect to the grid on the skin. HIFU exposures were done at *in situ* acoustic doses, defined as the intensity (W/cm^2) multiplied by the duration (s) of sonication, of 137 J/cm^2 (intensity (I_{SATP}) of 4390 W/cm^2 for 31.25 ms) and 229 J/cm^2 (3660 W/cm^2 for 62.5 ms). The position and orientation of the HIFU transducer with respect to the femur was recorded during each exposure on a custom position tracking device (Figure 5-4). The HIFU focal depth was set to 1.35 cm using a 1.4 cm thick coupling gel (15 % polyacrylamide) attached to the HIFU transducer and a 0.75 cm gel standoff (10 % polyacrylamide). The depth of the HIFU transducer was set to 1.35 cm in order to remain within the same muscle along the length of the rabbit thigh. HIFU exposures were done on both the front and back thigh muscles of both hind limbs in rows made up of four treatments each 1.5 cm apart. The lesions were located with respect to the femur using the laser guided method described in Section 5.1.3. Single marker lesions were also placed in line with the treatment lesions in each muscle for marking the depth and position of the line of treatment lesions for aiding in the collection of tissue samples during necropsy.

To optimize the detection of the hyperechoic region by the US imager, the HIFU excitation pulse was synchronized to end 10-15 ms prior to the time at which the region of muscle at the HIFU treatment site was to be interrogated by the US imaging probe (Figure 5-7). Therefore, there was a minimal delay of 10 ms after the conclusion of the HIFU pulse to the time the treatment site was imaged. US images were collected with an HDI-1000 US imaging system (Depth = 3.6 cm, MI = 0.5, Persistence = 0) and a mini-DV video recorder. Video footage collected from the US imager was digitized using Adobe Premiere® Pro 7.0 (Adobe, San Jose, CA) to determine if a distinct hyperechoic region appeared at the HIFU focus during each exposure.

Tissue Collection and Histological Assays

Histological and morphological assessment of damage at the HIFU treatment site was done 0 h, 4 h, 48 h, 7 days and 14 days post HIFU exposure. After euthanizing the rabbits with an IV injection of ketamine and xylaxine (6:1) the rabbit was placed with one of their legs mounted in the holder in the same position as it was during HIFU treatment. The skin of the outer thigh was removed and the position of the knee and the greater trochanter on the femur were marked. A laser beam directed through the plastic positioning plates and at the markers on the femur was then used to realign the plate with the rabbit leg (Figure 5-4). Using the laser to locate the HIFU treatment site, 22-gauge hypodermic needles were placed 1 cm away from the treatment site such that their tips were at the same depth as the lesion. The group of muscles in the front and back of the thigh were excised. Gross observation of the tissue was conducted and photographs of the treatment sites were taken. Slices of tissue containing the treatment site and control site (1 cm square by 0.4 cm thick) were collected and fixed in 10% formaldehyde. Fixed samples were imbedded in paraffin blocks, sectioned in 5 μm thick slices and stained with hematoxylin and eosin (H&E) for histological examination.

5.2.2. RESULTS

Appearance of Targeting Hyperechoic Region

Single HIFU exposures at *in situ* acoustic doses of 4390 W/cm^2 for 31.25 ms and 3660 W/cm^2 for 62.5 ms resulted in the formation of distinct hyperechoic region at the HIFU focus in an B-mode US image during 84.0% and 80.3% of the exposure, respectively (Table 5-3). The hyperechoic region typically disappeared within 0.2 s. When a hyperechoic region failed to appear in the US image, the coupling of the HIFU transducer to the rabbit thigh was evaluated. Improper coupling was found to be the major cause (17 of 26 exposures) of a lack of hyperechoic regions to appear. Other causes included muscle twitching in response to a HIFU exposure (4 of 26), poor image quality due to improper coupling of the imaging transducer to the rabbit thigh (3 of 26), and misplacement of the HIFU transducer partway over the underlying femur bone (2 of 26).

Table 5-3: **Percentage of targeting HIFU exposures that resulted in the US visualization of a hyperechoic region at the focus.**

HIFU Intensity (W/cm^2)	HIFU Duration (ms)	Number of HIFU Exposures	Number of Hyperechos	Percent Of Appearances
4390	31.25	71	57	80.3%
3660	62.5	75	63	84.0%

Analysis of Tissue Damage

Damage to the tissue at the HIFU focal site was observed in 25% and 40% of HIFU exposures at intensities of 4390 W/cm^2 for 31.25 ms and 3660 W/cm^2 for 62.5 ms, respectively, that resulted in the formation of a hyperechoic region in rabbit thigh muscle *in vivo* (Table 5-4 column 5). Tissue damage was not observed in any of the HIFU exposure that did not produce a hyperechoic region.

Table 5-4: **Percentage of targeting HIFU exposures that resulted in the US visualization of a hyperechoic region at the focus.**

HIFU Intensity (W/cm^2)	HIFU Duration (ms)	Number of Hyperechos	Number Resulting in Tissue Damage	Percent of Hyperechos Resulting in Damage
4390	31.25	57	23	40%
3660	62.5	63	16	25%

Table 5-5 lists the types of tissue damage observed by light microscopy with respect to the time at which the tissue sample was collected after each HIFU exposure. At each time point (0 h, 4 h, 2 days, 7 days, and 14 days), cellular damage was indistinguishable between samples treated at the different HIFU doses. Gross damage was presented by a blanched area of tissue and/or hemorrhage at 0 h (Figure 5-11 and Figure 5-13), 4 h (Figure 5-16) and 2 days (Figure 5-17) post treatment (Table 5-5). Gross damage was not observed 7 and 14 days post HIFU treatment.

Table 5-5: Tissue damage presented at time of necropsy.

	Post Treatment Time				
	0 h	4 h	2 d	7 d	14 d
Total Number of Samples with Damage	5	7	10	5	8
Gross Tissue Damage	3	7	10	0	0
Intracellular cavities	5	6	0	0	0
Hemorrhage	3	6	1	0	0
Loss of Stain Uptake		7	10	5	8
Sarcolemmal Collapse			6	5	8
Signs of Myocyte Regeneration			1	2	2
Mineralization, Granular Cytoplasm			4	3	2
Fibrosis / Scar Tissue					2
Extracellular Mineralization				1	3
Thrombosis Within Treatment Site					4
Thrombosis Outside of Treatment site					2

Tissue collected 0 and 4 h after the HIFU exposure exhibited cavitation-induced damage in the form of cavities and tearing of the intracellular structure of muscle cells at the HIFU focal site. Hemorrhage with extravasated erythrocytes was observed at both 0 h and 4 h post treatment. Figure 5-11 and Figure 5-12 show by gross morphology and light microscopy, respectively, the damage associated with a hyperechoic region after a HIFU exposure at an *in situ* intensity of 4390

W/cm^2 for 31.25 ms at 0 h. Voids in the cells and hemorrhage were visible in Figure 5-12.

Figure 5-13 shows gross macroscopic and light microscopy photographs of the damaged tissue observed 0 h post HIFU exposure at an intensity of 3360 W/cm^2 for 62.5 ms in which a hyperechoic region was observed. Blanching of the muscle fibers and hemorrhaging was observed at the time of necropsy, with intra- and extracellular cavities and extravasated erythrocytes observable by light microscopy. Figure 5-14 shows a light microscopy image of the damage at the HIFU focus after a single HIFU pulse of 31.25 ms at an *in situ* intensity of 4390 W/cm^2 that resulted in a hyperechoic region. Damaged cells at the treatment site had cavities ranging from 4 – 25 μm within the intracellular matrix that are magnified in Figure 5-15.
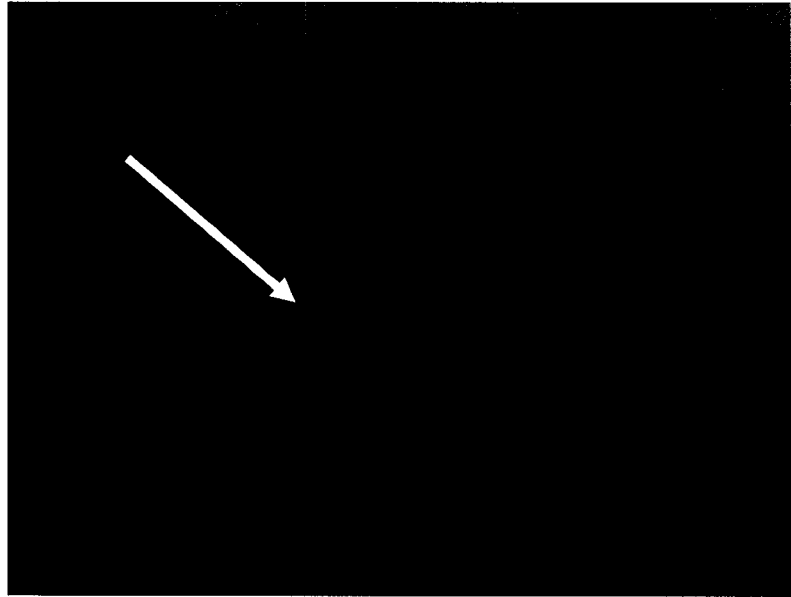
Figure 5-11: Photograph of the damage to muscle within 30 minutes of a HIFU exposure at 31.25 ms at an *in situ* intensity of 4390 W/cm^2. Damage is observed at both the surface of the muscle (black arrow) and deep within the muscle in the form of hemorrhage (petechiae; white arrow). The muscle surface was treated in this particular sample because the intervening muscle layer ended just proximal to the HIFU focus, with respect to the HIFU source. The black arrow also indicates the HIFU axis, which had passed through an adjacent muscle, before reaching the focus.
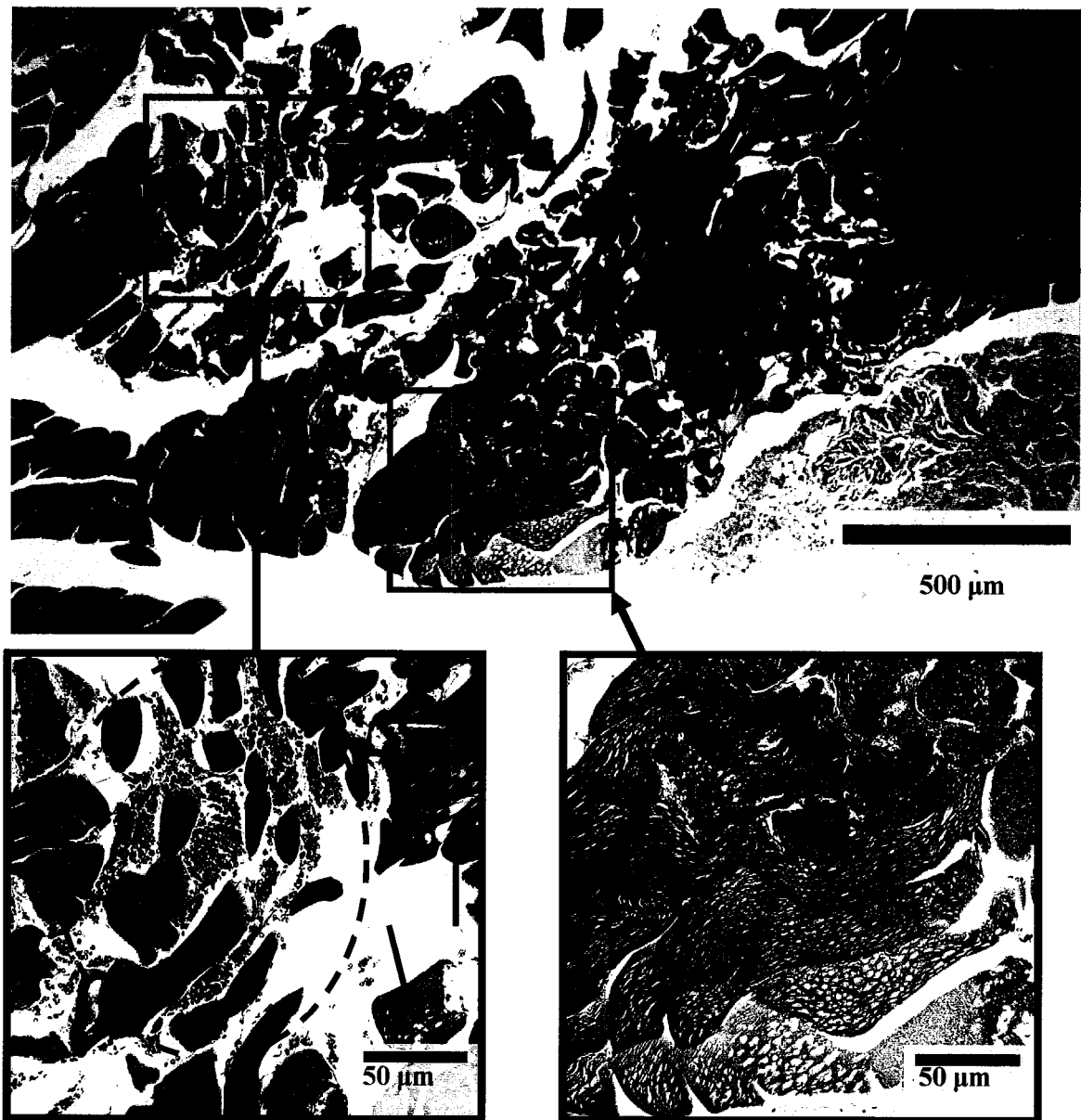
Figure 5-12: Light microscopy of the damaged tissue observed within 30 min of a HIFU exposure for 31.25 ms at an *in situ* intensity of 4390 W/cm^2. Blood cells are located between the muscle fibers as a result of hemorrhage at the distal end of the HIFU focus (blue dashed circle), with respect to the HIFU source. Damage, in the form of cavities in the intercellular compartment similar to those presented in Figure 5-14, was observed throughout the region of treated muscle (blue arrows and throughout the region in the green box). The region highlighted by the green box corresponds to the region highlighted by the black arrow in Figure 5-14. The region highlighted by the black box corresponds to the region highlighted by the white arrow in Figure 5-14. H&E 5x, 40x
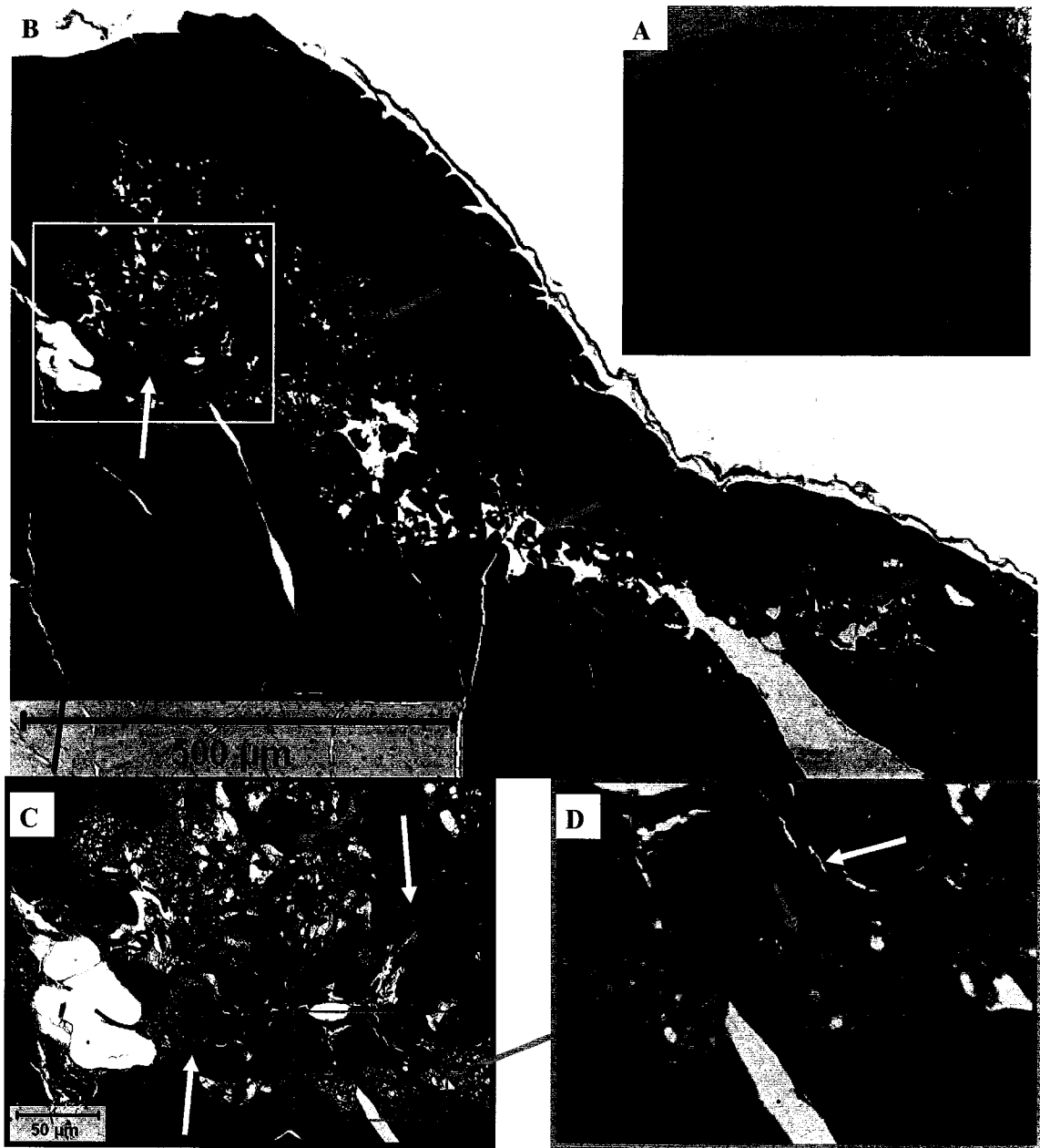
Figure 5-13: Gross macroscopic and light microscopy photographs of the damaged tissue observed within 30 min of a HIFU exposure at *in situ* intensity of 3360 W/cm^2 for 62.5 ms. Blanching of the muscle fibers and hemorrhaging was observed at time of necropsy (A: image in upper right corner). Extensive damage, in the form of intra- and extracellular cavities (blue arrows), was observed throughout the HIFU lesion site by light microscopy (B-D). Extensive hemorrhaging with erythrocytes located in the extracellular matrices (yellow arrows) was also observed. H&E 5x, 20x, 63x.
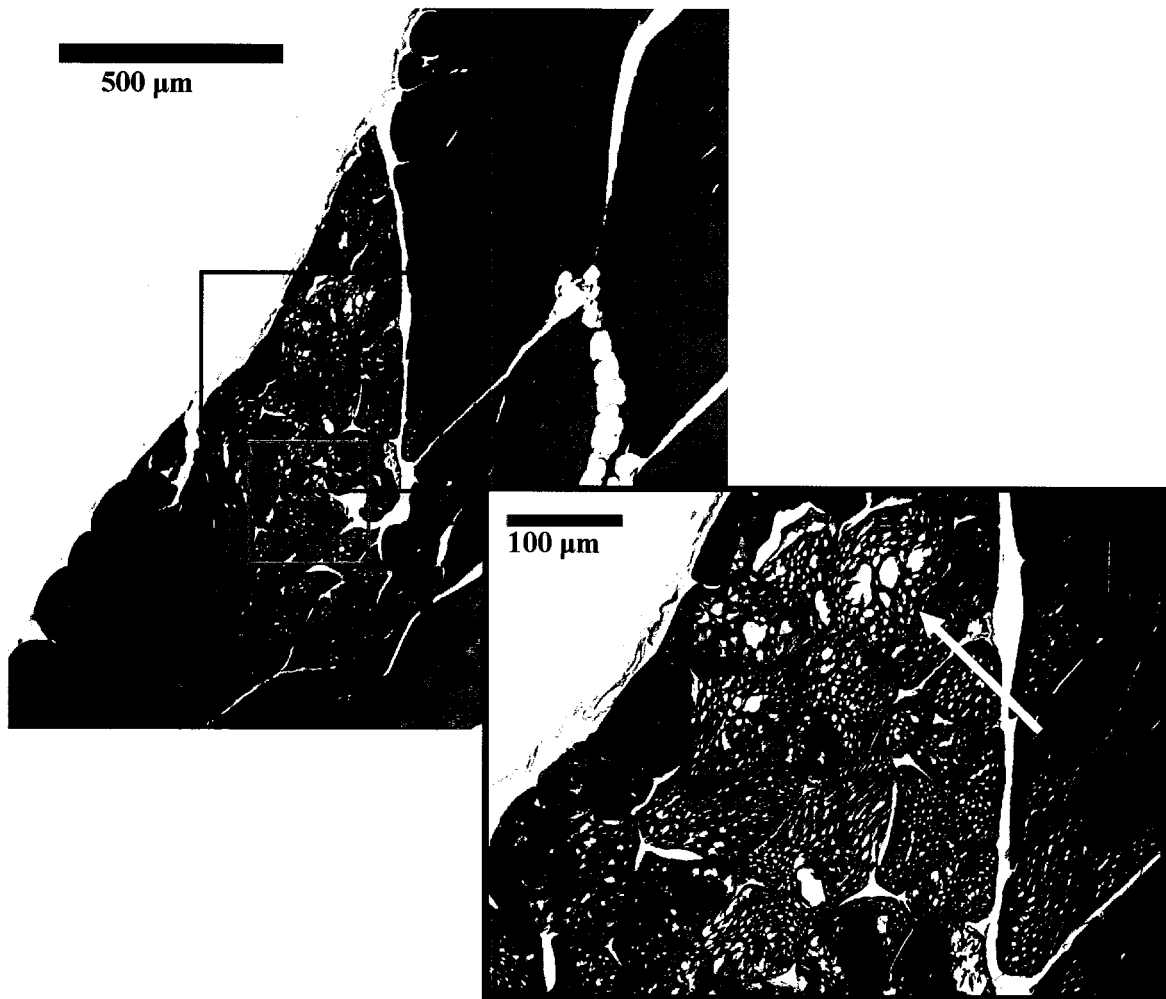
Figure 5-14: Light microscopy images of the damage at the HIFU focus in rabbit skeletal muscle (cross section) after a single HIFU pulse of 31.25 ms at an *in situ* intensity of 4390 W/cm^2. The green arrow represents the approximate orientation of the HIFU axis. Damaged cells at the treatment site presented with voids within the intracellular matrix and a dark staining, a sign of necrosis, when compared to cells outside of the HIFU target area (blue arrow). The voids in the cells ranged from 4 – 25 μm within the intracellular matrix (yellow arrow) and are magnified in Figure 5-15 (light blue box). H&E 5x, 20x
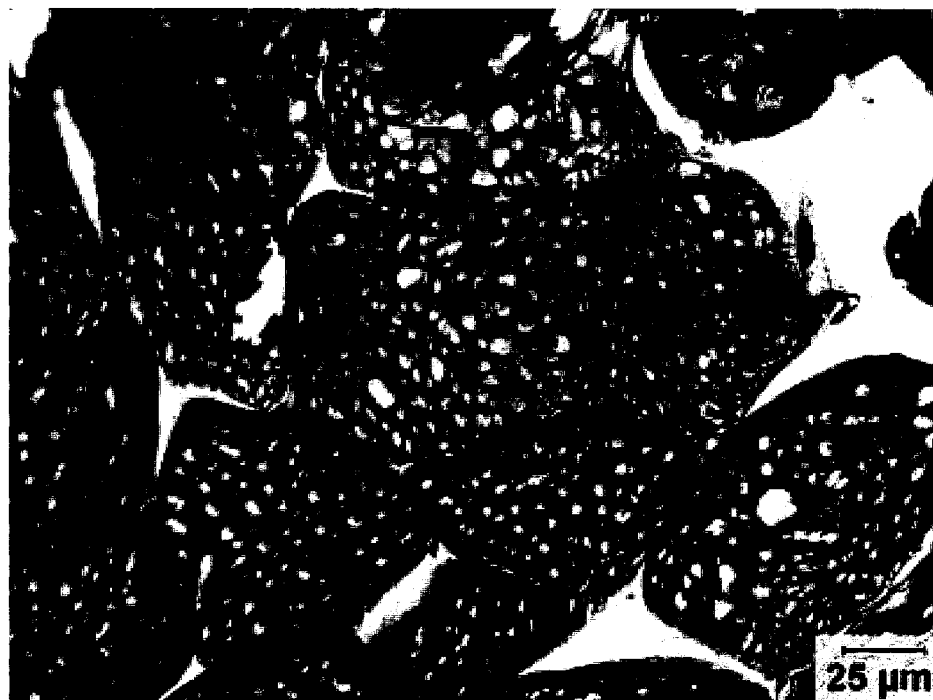
Figure 5-15: Light microscopy (40x H&E) of muscle cells at the HIFU focus within 30 min after a single HIFU pulse of 31.25 ms at an *in situ* intensity of 4390 W/cm^2 that resulted in a hyperechoic region in an US image.

Stain uptake was reduced in damaged cells, as compared to normal cells, in samples taken at 4 h, 2, 7 and 14 days treatment, a sign of cellular necrosis. Figure 5-16 shows a typical lesion 4 h post HIFU treatment in which a hyperechoic region was produced with a single HIFU pulse. Blanching of the tissue and hemorrhaging at the HIFU focal site were observable by the naked eye. Intra- and extra cellular damage and hemorrhages were observable by light microscopy. Undamaged cells were observed within the region of tissue damage.

By day 2-post treatment, muscle cells exhibited necrosis typical of myocytes undergoing a normal repair process (Kumar et al. 2004). Signs of necrosis like sarcolemmal collapse, granular cytoplasm due to mineralization, vacuolization (most likely due to necrosis and not cavitation), and infiltration of the extracellular matrix by leukocytes (specifically neutrophils) were observable by light microscopy. Segmental necrosis, in which a portion of the myocyte's length

has undergone destruction, was also observed on day 2 followed by myophagocytosis of the necrotic regions by macrophages on 7 and 14 d post treatment. Regenerative myocytes, indicated by internalized nuclei and prominent nucleoli, were observed on day 2, 7, and 14 in a total of 5 out of 23 samples.

Figure 5-17 shows gross tissue damage 2 days post HIFU treatment at an *in situ* intensity of 3660 W/cm^2 for 62.5 ms duration in which a hyperechoic region occurred in an US image. Although the focus is an ellipsoid with diameters of 5.1 mm, 0.76 mm, and 0.76 mm, tissue damage extended 0.5 cm to either side of the focus in 7 of 10 samples, because of the length of the muscle cells. Figure 5-18 shows a light microscopy image of the tissue damage on day 2 post HIFU exposure of 3660 W/cm^2 for 62.5 ms, in which a hyperechoic region was observed.

No tissue damage was observed by gross morphological assesment on day 7 and 14 post HIFU exposures that produced a hyperechoic region in an US image at the HIFU focus. Light microscopy 7 days post HIFU exposures in which a hyperechoic region occurred (Figure 5-19) showed necrotic muscle cells and infiltration of the exposure site by multinucleated macrophages. Tissue damage was not observed in samples in which a hyperechoic region did not occur.

Figure 5-20 shows typical damage 14 days after the appearance of a hyperechoic region at the site of HIFU treatment. Signs of normal wound healing were observed including: necrosis and absorption of the muscle cells (as indicated by shrinkage and discoloration of muscle cells); infiltration of macrophage cells; an increase in the amount of fibrosed (scar) tissue; and, extracellular mineralization. Thrombosed vessels were observed in and outside of the treatment site. Neovascular regeneration was observed within the lumen of a majority of thrombosed vessels.
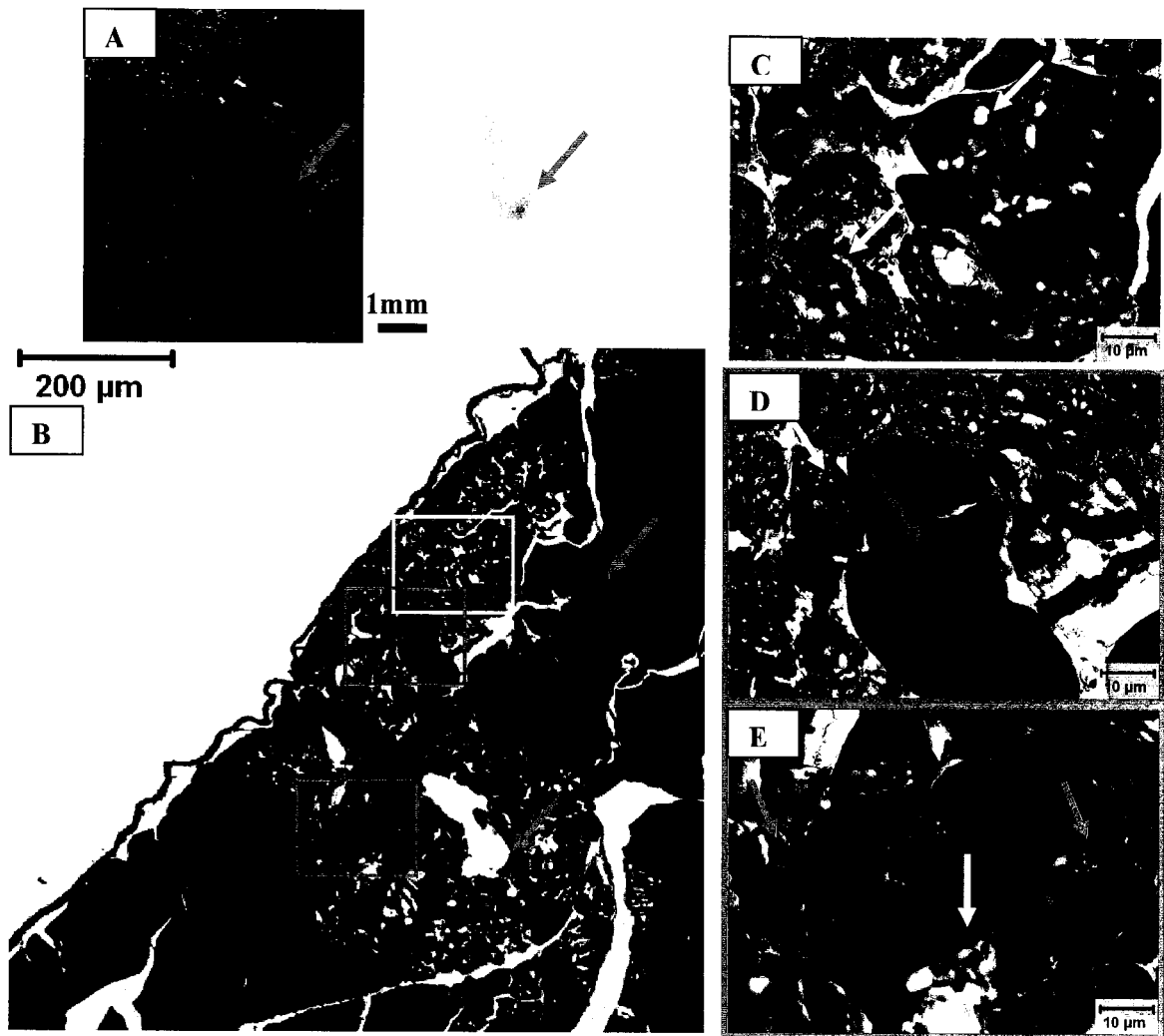
Figure 5-16: Macroscopic and light microscopy of tissue damage at a HIFU treatment site 4 h after a single HIFU pulse of 4390 W/cm^2 for 31.25 ms in which a hyperechoic region was produced. The top left image shows that blanching of the tissue and hemorrhaging (blue arrows) at the HIFU focal site were observable by the naked eye (images illuminated by direct lighting (A: left) and back lighting (A: right). Intra- and extra cellular cavities (yellow arrows) and hemorrhages (blue arrows) were observable by light microscopy. Undamaged cells (green arrow) were observed within the region of tissue damage. Photographs C, D, and E represent the areas in B with the same color as their boarders. H&E 5x (B), 40x (C – E).
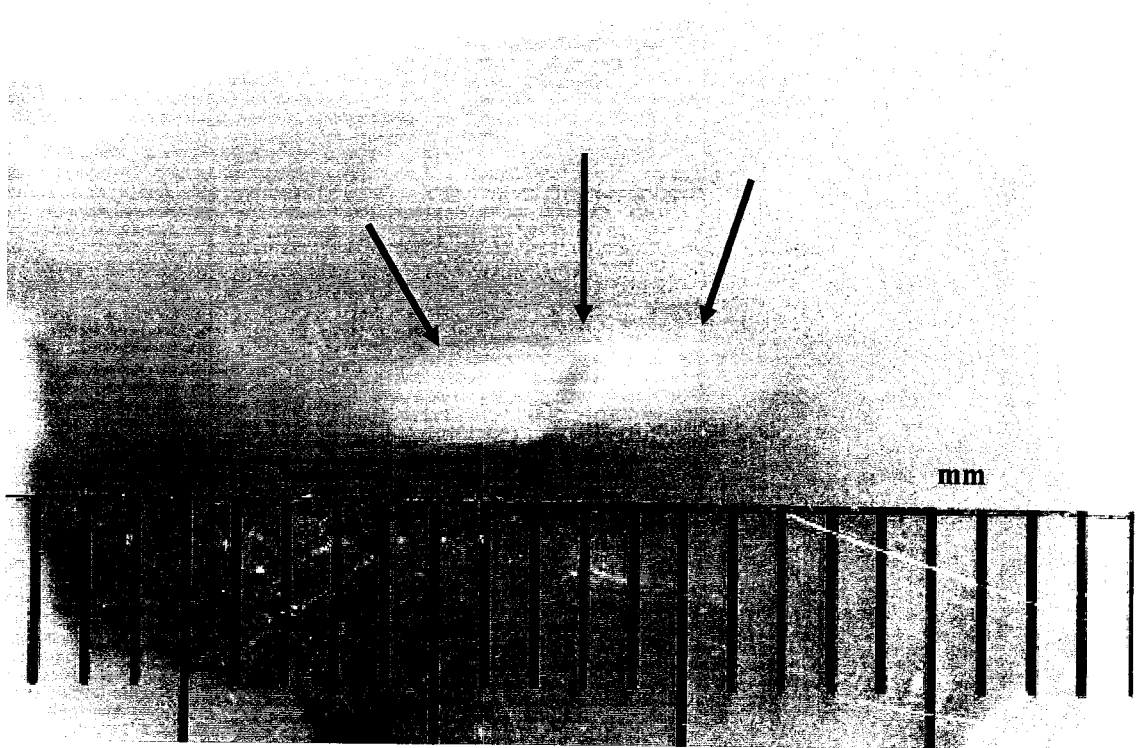
Figure 5-17: Photograph of damage in muscle at the HIFU treatment site 2 days post HIFU exposure of 3660 W/cm^2 for 62.5 ms. The HIFU focus was located at the center of the lesion (black arrow), but the damage extends ~0.5 cm to either side of the focus (blue arrows) due to the length of the damaged muscle cells.
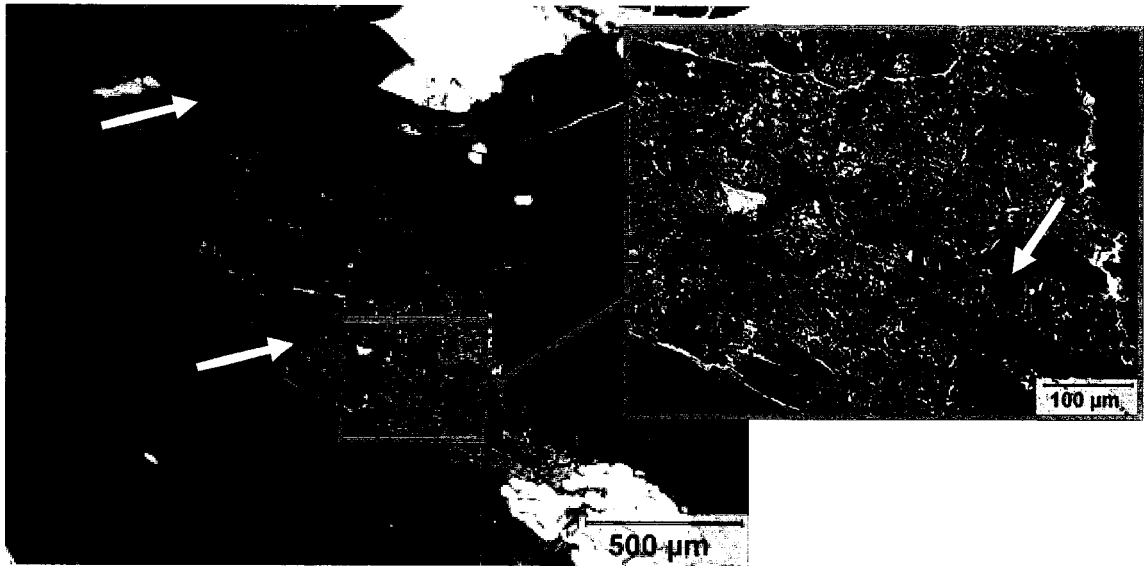
Figure 5-18: Light microscopy images of a lesion (Figure 5-17) in muscle 2 days after a HIFU exposure of 3660 W/cm^2 for 62.5 ms. Damaged muscle cells are indicated by a lighter color (blue arrows) than healthy viable cells. Regions infiltrated by macrophages, where cells are being absorbed, are indicated by yellow arrows. H&E stained 5x and 20x.
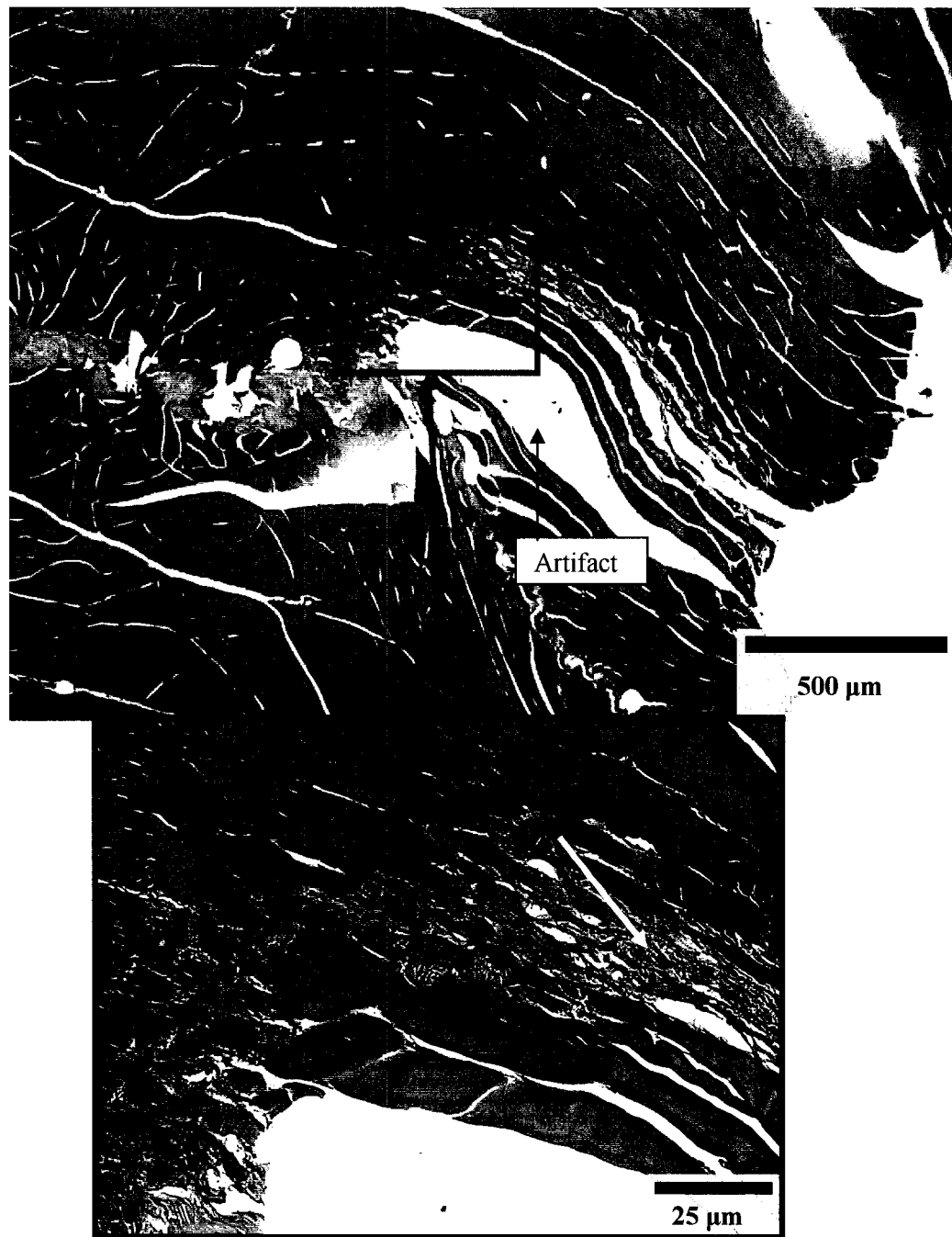
Figure 5-19: Light microscopy photographs of damage at the HIFU treatment site 7 days after a HIFU treatment of 4390 W/cm² for 31.25 ms. Necrosis and absorption of the muscle cells are indicated by shrinking and discoloration of muscle cells in addition to the infiltration of macrophage cells (blue arrow). Fibrosis and scar tissue were also observed (yellow arrow). H&E 5x, 20x
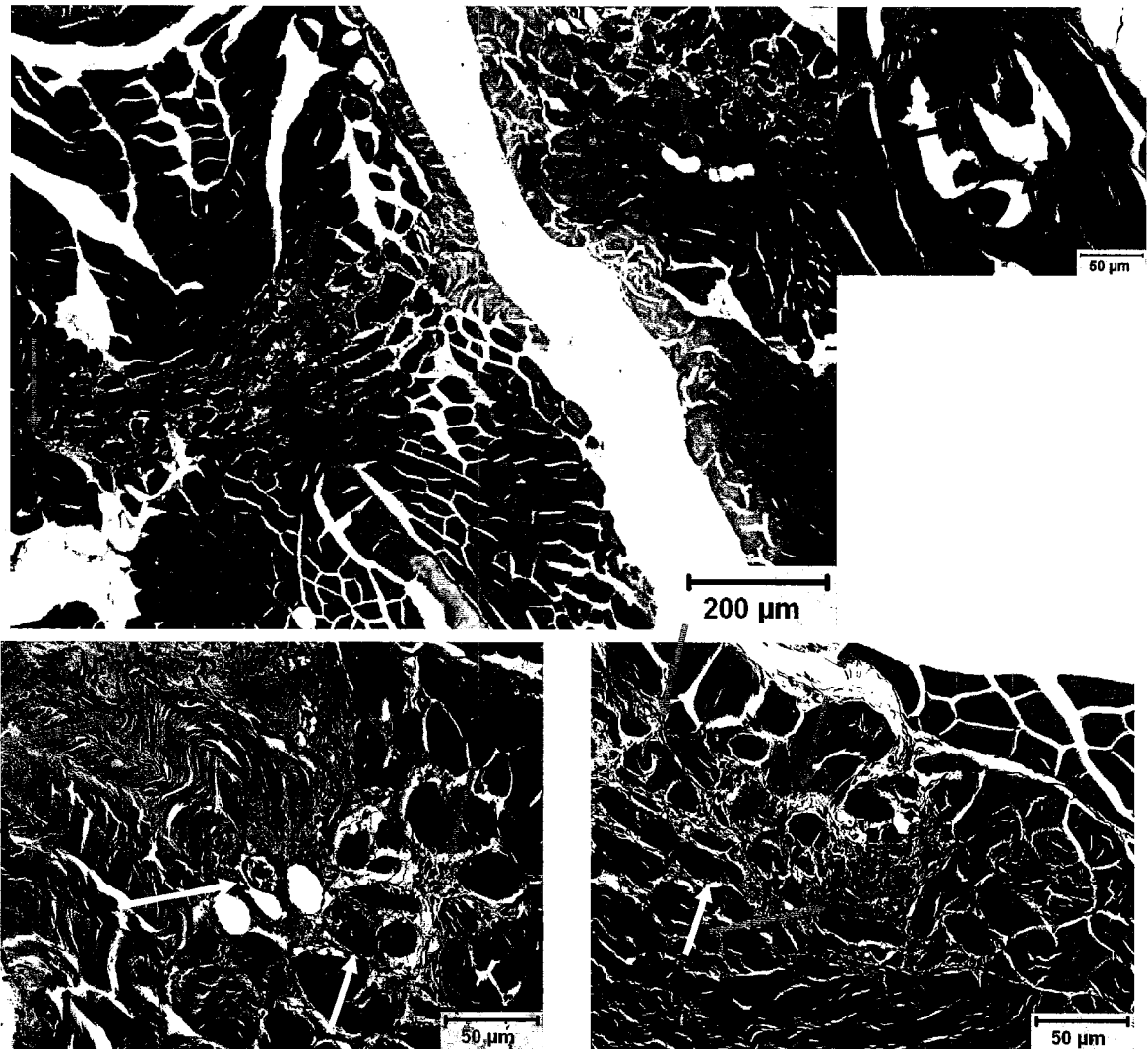
Figure 5-20: Light microscopy photographs of the HIFU focal site 14 days after a HIFU treatment of 3660 W/cm^2 for 62.5 ms showing typical muscle wound healing. Necrosis and absorption of the muscle cells are indicated by shrinkage and discoloration of the muscle cells and infiltration of macrophage cells (white arrow), fibrosis (green arrows), and extracellular mineralization (yellow arrow). An increased number of thrombotic vessels was observed (light blue arrows) along with neovascularization (photo in upper right corner). Neovascularization was observed by the presence of new vessels walls (dark blue arrows) within the original thrombosed vessels lumen.

5.3.   SUMMARY AND CONCLUSION

The production of a hyperechoic region by HIFU has been previously reported to produce no short-term thermal damage in pig liver *in vivo* by Vaezy et al. (2001). In the study reported here, short- and long-term damage was found in 39 of 120 HIFU exposures in rabbit skeletal muscle samples in which a hyperechoic region appeared in an US image of the HIFU treatment site. The measured tissue thermal dose (Section 5.1.3) was below that needed to produce cellular death by a purely thermal mechanism (Kennedy et al. 2003; ter Haar et al. 1988). Therefore, this study supports the previously reported findings of Vaezy et al. (2001) that a hyperechoic region can be produced without thermal damage *in vivo*.

The hyperechoic regions produced during this study were easily observable and therefore useful for determining the location of the HIFU treatment site prior to commencement of a therapeutic treatment regime. A hyperechoic region occurred in 82% of 146 HIFU exposures conducted and tissue damage was not observed when a hyperechoic region failed to appear. Improper coupling of the HIFU transducer to the rabbit thigh was found to be the major cause of failure to produce a hyperechoic region. Improper coupling of the imager and muscle twitching in response to the application of HIFU contributed to a minor degree to the failure to produce a region at the HIFU focus. Therefore, the absence of a hyperechoic region does not assure that cavitation and tissue damage did not occur. The inability to detect the appearance of a hyperechoic region needs to be taken into account when using the hyperechoic region for targeting. Over treatment and unwarranted damage may occur as a result of the need to apply multiple HIFU exposures after the initial exposure did not result in the visualization of a hyperechoic region.

Macroscopic and microscopic tissue damage was not observed in 81 of the HIFU exposures in which a hyperechoic region was observed. Therefore, the amount of cavitation at the HIFU treatment site necessary for the appearance of a hyperechoic region appears to not result in permanent tissue damage. A similar result has been reported for HIFU sonications in rabbit brains in which cavitation was detected by PCD (Vykhodtseva et al. 1995). In that study, sonications were done at 1.72 MHz with a spatial peak temporal peak intensity of 7000 W/cm^2 for single pulse durations of 0.01, 0.05, and 0.1 s durations. Tissue damage was not observed until the number of pulses was increased from to 2 or above, despite the observance of subharmonic noise (as an indicator of stable cavitation) within exposures of 1 HIFU pulse. This

leads us to believe that a HIFU exposure criterion can be developed for producing hyperechoic regions at the HIFU focus without short- or long-term tissue damage for the purpose of targeting the treatment site in an US image.

At 0 and 4 h post HIFU exposure, two main effects were observed at the HIFU treatment site: direct damage to the intra- and extracellular matrices in the form of cavities (4 – 25 μm in diameter) and hemorrhages resulting from vascular damage. The formation of cavities within the cellular matrix was indicative of cavitation and only occurred in tissue samples in which a hyperechoic region had been observed in an US image. The intracellular cavities observed shortly after HIFU treatment were extensive, very distinctive and appeared to be due to the presence of bubbles. A few studies have previously reported intra- and extracellular cavities in tissue treated by HIFU and were believed to be due to cavitation and/or boiling (Arefiev et al. 1998; Chen et al. 1993; Mesiwala et al. 2002; Righetti et al. 1999). The cavities reported in these studies ranged in diameter from a few microns to 0.2 mm. Other studies have reported tissue damage of a greater magnitude, including pitting, tearing, and hemorrhaging, used as indicators of acoustic cavitation (Chen et al. 1993; Chen et al. 1999) or in correlation with acoustic emissions indicative of cavitation (Vykhodtseva et al. 1995).

The largest extent of damage found was restricted to a flat disc shaped lesions 1 cm by 0.5 cm by 0.4 cm thick 2 days post HIFU treatment. Although damage extended outside of the focal volume it was mostly due to the length and shape of the muscle cells treated. Occlusion of blood vessels was observed at all time points. Thrombi located outside of the treatment area were only observed on day 14 post treatment, evidence that damage may have occurred outside of the treatment site in tissue feed by the occluded vessels.

Slightly more successful with fewer number resulting in damage.

For the two HIFU parameters (4390 W/cm^2 for 31.25 ms and 3660 W/cm^2 for 62.5 ms) used in this study, there was not a significant difference in the number of HIFU exposures that resulted in the appearance of a hyperechoic region. No tissue damage was observed for HIFU exposures in which a hyperechoic region did not occur. This is believed to be due to the absence of cavitation or levels below that necessary to produce a hyperechoic region. Of the HIFU exposures in which a hyperechoic region appeared, the intensity of 3660 W/cm^2 and duration of 62.5 ms resulted in fewer samples with tissue damage (25%) then exposures at the intensity of 4390 W/cm^2 and

duration of 31.25 ms (40%). The morphology of the tissue damage was not distinguishable between tissues treated at the two different sets of HIFU parameters. Two different sets of HIFU parameters were used in this study with the hopes of observing a difference in the number of HIFU exposures that would result in tissue damage in treatments when a hyperechoic region had appeared. The findings of this study indicate that there may be HIFU parameters that will result in the appearance of a hyperechoic region in the majority of HIFU exposures and without observable tissue damage. Since the measured thermal doses were below levels which produce thermal injury (Kennedy et al. 2003; ter Haar et al. 1988), the extent of damage was expected to be lower with the set of HIFU parameters that resulted in the lower amount and duration of cavitation. The extent of tissue damage would be expect to be different for the two sets of HIFU parameters used in this study if the amount of time that cavitation was occurring and the level of cavitation varied between them. In this study the level and duration of cavitation was not measured, therefore we had not anticipated which set of HIFU parameters would produce less damage.

Further dosimetry studies are needed to determine whether a hyperechoic region can be produced without short- and long-term tissue damage. In addition, studies are needed to determine how many HIFU exposures can be performed to create a hyperechoic region without causing clinically significant adverse effects in tissue. Cumulative effects of overlapping hyperechoic regions that would result from the need to accurately determine and adjust the location of the HIFU focus within tissue need to be addressed.

Although this study was aimed towards exploring the use of short high intensity HIFU doses for targeting of the treatment site, two findings have arisen from the results of the survival study: (1) tissue can be treated with a very short amount of time (30-60 ms) resulting in coagulative necrosis and tissue repair at the HIFU focus; and, (2) insight has been gained into the type of damage that can result from cavitation, observed by the appearance of a hyperechoic region in an US image, *in vivo* in muscle tissue.

6. SUMMARY AND CONCLUSION

This dissertation describes the investigations into the source of a hyperechoic region in a B-mode diagnostic ultrasound image during the visualization of HIFU therapy. The role of bubbles in the generation of a hyperechoic region and the mechanisms (thermal and/or mechanical) involved in their inception were studied, along with the short- and long-term damage associated with the production of a hyperechoic region primarily by acoustic cavitation.

The primary findings of the experimental research conducted are presented in the list below, followed by a more detailed discussion:

1. The appearance of a hyperechoic region in an US image of HIFU therapy was correlated with the onset of cavitation *in vivo*, thereby indicating that bubbles are involved in the appearance of a hyperechoic region (Chapter 3).

2. Measurements of the tissue temperature during the appearance of a hyperechoic region at the HIFU treatment site showed that: a) tissue temperatures above the boiling point of water (100°C) resulted in the production of acoustic cavitation and the appearance of a hyperechoic region, and b) acoustic mechanisms can produce a hyperechoic region, via cavitation, at temperatures well bellow the boiling point of water (Chapter 4).

3. Short HIFU pulses that result in the appearance of a hyperechoic region can be produced without significant temperature rises at the HIFU focus *in vivo*. This confirms the results of point 2.b above (Chapter 5.1).

4. Bubble-enhanced heating occurred *in vivo* at the HIFU focal site during the appearance of a hyperechoic region (Chapter 4).

5. The HIFU treatment site can be targeted using a hyperechoic region resulting from a very short HIFU pulse with minor tissue damage *in vivo* (Chapter 5.2).

6. The appearance of a hyperechoic region *in vivo* correlated with cavities in the intra- and extracellular matrices of muscle cells in the absence of significant heating (Chapter 5.2).

Through the synchronization of a HIFU therapeutic transducer with a cavitation detector and an US imager, the appearance of a hyperechoic region in the US image was correlated with the onset of cavitation during HIFU sonication of pig muscle *in vivo*. During this study, both active and passive cavitation detection methods were used to determine if bubbles were present at the HIFU focus. An increase in the amplitude of the raw RF signal during ACD and the broadband noise of the RF signals spectrum during PCD were interpreted as a direct result of bubbles in the sonication field.

To gain an understanding of what mechanism, thermal and/or mechanical, resulted in the formation of bubbles at the HIFU focus during the appearance of a hyperechoic region, the above study was repeated in pig muscle *in vivo* with a thermocouple at the HIFU focus for measuring the tissue temperature during the appearance of a hyperechoic region. During this study both mechanisms, thermal and mechanical, were found to be involved in the production of bubbles during the appearance of a hyperechoic region and the onset of cavitation as measured by PCD. During some HIFU exposures, the hyperechoic regions and cavitation were initially observed after the tissue temperature at the focus had increase in a predictable manner to above the boiling point of water (100°C). During other HIFU exposures, the hyperechoic region and cavitation were observed at temperatures well below 100°C. During these HIFU sonications, bubble-enhanced heating was also observed after the appearance of the hyperechoic region. This set of data gave rise to the conclusion that bubbles at the HIFU treatment site, which resulted in the appearance of hyperechoic region, could arise from either a thermal (i.e. boiling) and/or a mechanical mechanism (i.e. acoustically driven cavitation).

For purposes of using a hyperechoic region for targeting of the HIFU therapy site, a set of HIFU parameters were determined for the production of a hyperechoic region primarily by acoustic cavitation. This was done to reduce tissue damage associated with thermally induced coagulative necrosis that would occur from a thermally induced (i.e. boiling) hyperechoic region. Using these HIFU parameters, an *in vivo* study was conducted in rabbit thigh muscles to determine the extent of short- and long-term tissue damage that resulted from a hyperechoic region useful for targeting of the HIFU treatment site within an US image. At the HIFU acoustic doses of 4390 W/cm^2 for 31.25 ms and 3660 W/cm^2 for 61.25 ms at 3.2 MHz used in this study, a hyperechoic region was observed at the HIFU focus in 82% of 145 HIFU exposures. Tissue damage was not found by gross macroscopy or light microscopy in samples in which a hyperechoic region failed to occur.

When tissue damage was observed shortly after sonication (0 and 4 h), it was characterized by cells with a spongy appearing intracellular matrix that were filled with spherical shaped cavities of $4 - 25$ μm in diameter and by hemorrhaging. On days 2, 7 and 14 post HIFU treatment, wound healing and repair of tissue damage was observed to be progressing normally.

In conclusion, this set of studies have shown that: (1) bubbles are involved in the appearance of a hyperechoic region in a B-mode diagnostic US image at the site of HIFU therapy, (2) bubbles can be formed as a result of either a thermal (i.e. boiling) and/or a mechanical mechanism (i.e. acoustically driven cavitation), and (3) that it may be feasible to use a hyperechoic region within an US image for targeting of HIFU therapeutic sites.

6.1.   FUTURE RESEARCH DIRECTIONS

Dosimetry

To optimize the use of a hyperechoic region for locating the HIFU focal site in an US image prior to commencement of therapy, a thorough study needs to be conducted. During the study presented in Chapter 5, in which the short- and long-term tissue damage resulting from the production of a hyperechoic region was explored, a limited set of HIFU doses were used. In that study, tissue damage was observed in 39 of 145 HIFU exposures that produced a hyperechoic region. A set of studies is therefore needed to find more optimal HIFU doses for reproducible production of a hyperechoic region while eliminating tissue damage.

A second part of the dosimetry study needs to address the cumulative effect of a series of targeting hyperechoic regions that may be needed in the clinical setting to accurately place the HIFU focus within the desired treatment site. Of particular concern are the following: (1) cavitation nuclei remaining in the tissue from a prior targeting hyperechoic region may result in a higher overall dose of cavitation during subsequent overlapping targeting hyperechoic regions, (2) damage to tissue may result in a lower threshold for the production of cavitation during subsequent overlapping targeting hyperechoic regions and/or during therapy, resulting in an increased rate of tissue destruction. Concerns such as these will need to be adequately addressed by a dosimetry study.

Determination of the cavitation nucleation site *in vivo*

The short-term tissue damage observed in rabbit skeletal muscle after the production of hyperechoic regions *in vivo* was typified by spongy intracellular matrices. The spongy appearance was most likely due to micron sized cavities produced in the muscle fibers during sonication. Further study of this phenomenon is need in order to determine if indeed the cavities were due to cavitation nuclei (i.e. bubbles) and to determine the origin of such cavitation nuclei.

Real-Time Detection for Improved Visualization of Hyperechoic Regions

To improve upon the ability to visualize and locate the hyperechoic region within an ultrasound image, it will be important to automate a method for capturing and outlining the hyperechoic region. During the studies done to complete this thesis, the observation of a hyperechoic region was confirmed by analyzing video tape recordings of the US image after each experiment. Such a method would be too time consuming and therefore not feasible for routine use in the clinical setting. A real-time image processing method for detecting and outlining the location of the hyperechoic region within the US image is therefore needed.

Develop a Definition of HIFU Dose

The end result of defining and prescribing a dose regime for any particular therapy is to produce a fairly reproducible biological effect at the treatment site. Defining a HIFU dose is complicated since both cavitation and thermal damage can occur at the treatment site. Damage due to a purely thermal regime is well understood and thermal doses have been defined in terms of a temperature rise over a specified duration. Unless a method for monitoring the tissue temperature accurately and in real-time is developed, the thermal dose for any particular treatment site will not be predictable. This is because non-linear propagation of US waves, differences in perfusion rates, and bubble induced heating occur at the HIFU treatment site. Using the amount of cavitation as a dose criterion has its issues. First, cavitation is not truly quantifiable. Second, tissue temperature can achieve therapeutic levels without producing cavitation. Third, bubble-enhanced heating can occur after cavitation inception causing potential injury from both a mechanical and thermal

mechanisms that could be difficult to predict and quantify. The acoustic dose, in terms of J/cm^2, does not take into account increased absorption of acoustic energy due to non-linear propagation of US, cavitation, tissue perfusion, and thermal diffusion rates in tissue. Therefore acoustic dose does not appear to correlate directly with the type or amount of tissue damage resulting from HIFU. All of these issues will need to be accounted for when developing a definition of HIFU dose.

BIBLIOGRAPHY

Arefiev A, Prat F, Chapelon JY, Tavakkoli J and Cathignol D. Ultrasound-induced tissue ablation: studies on isolated, perfused porcine liver. Ultrasound Med Biol 1998;24:1033-1043

Bailey MR, Couret LN, Sapozhnikov OA, et al. Use of overpressure to assess the role of bubbles in focused ultrasound lesion shape in vitro. Ultrasound Med Biol 2001;27:695-708

Barkman CA, Almquist LO, Kirkhorn T and Holmer NG. Thermotherapy: feasibility study using a single focussed ultrasound transducer. 1999;15:63-76

Blana A, Walter B, Rogenhofer S and Wieland WF. High-intensity focused ultrasound for the treatment of localized prostate cancer: 5-year experience. 2004;63:297-300

Bohris C, Jenne JW, Rastert R, et al. MR monitoring of focused ultrasound surgery in a breast tissue model in vivo. Magn Reson Med 2001;19:167-175

Bush NL, Rivens I, ter Haar GR and Bamber JC. Acoustic properties of lesions generated with an ultrasound therapy system. Ultrasound Med Biol 1993;19:789-801

Chan AH, Fujimoto VY, Moore DE, Martin RW and Vaezy S. An image-guided high intensity focused ultrasound device for uterine fibroids treatment. Med Phys 2002;29:2611-2620

Chapelon JY, Ribault M, Birer A, et al. Treatment of localised prostate cancer with transrectal high intensity focused ultrasound. 1999;9:31-38

Chen L, Rivens I, ter Haar G, et al. Histological changes in rat liver tumours treated with high-intensity focused ultrasound. 1993;19:67-74

Chen L, ter Haar G, Robertson D, Bensted JPM and Hill CR. Histological study of normal and tumor-bearing liver treated with focused ultrasound. Ultrasound Med Biol 1999;25:847-856

Chen W-S, Brayman AA, Matula TJ, Crum LA and Miller MW. The pulse length-dependence of inertial cavitation dose and hemolysis. Ultrasound Med Biol 2003;29:739-748

Chen W-S, Lafon C, Matula TJ, Vaezy S and Crum LA. Mechanisms of lesion formation in high intensity focused ultrasound therapy. ARLO 2003;4:41-46

Christensen DA, 1988, Ultrasonic Bioinstrumentation: New York, Wiley.

Church CC. Spontaneous homogeneous nucleation, inertial cavitation and the safety of diagnostic ultrasound. Ultrasound Med Biol 2002;28:1349-1364

Clarke RL and ter Haar GR. Temperature rise recorded during lesion formation by high-intensity focused ultrasound. Ultrasound Med Biol 1997;23:299-306

Coleman AJ, M. JC and Saunders JE. Detection of acoustic emission from cavitation in tissue during clinical extracorporeal lithotripsy. Ultrasound Med Biol 1996;22:1079-1087

Crum LA, Daniels S, ter Haar GR and Dyson M. Ultrasonically induced gas bubble production in agar based gels: Part II. Theoretical analysis. 1987;13:541-554

Delon-Martin C, Vogt C, Chignier E, et al. Venous thrombosis generation by means of high-intensity focused ultrasound. Ultrasound Med Biol 1995;21:113-119

Diederich CJ and Hynynen K. Ultrasound technology for hyperthermia. Ultrasound Med Biol 1999;25:871-887

Elliott MR and Thrush AJ. Measurement of resolution in intravascular ultrasound images. 1996;17:259-265

Fry FJ, Kossoff G, Eggleton RC and Dunn F. Threshold ultrasonic dosages for structural changes in the mammalian brain. J Acoust Soc Am 1970;48:Suppl 2:1413+

Fry FJ, Sanghvi NT, Foster RS, Bihrle R and Hennige C. Ultrasound and microbubbles: their generation, detection and potential utilization in tissue and organ therapy--experimental. Ultrasound Med Biol 1995;21:1227-1237

Fry WJ, Barnard JW, Fry EJ, Krumins RF and Brennan JF. Ultrasonic lesions in the mammalian central nervous system. 1955;122:517-518

Fry WJ, Mosberg WH, Jr., Barnard JW and Fry FJ. Production of focal destructive lesions in the central nervous system with ultrasound. 1954;11:471-478

Gianfelice D, Khiat A, Boulanger Y, Amara M and Belblidia A. Feasibility of Magnetic Resonance Imaging-guided Focused Ultrasound Surgery as an Adjunct to Tamoxifen Therapy in High-risk Surgical Patients with Breast Carcinoma. J Vasc Interv Radiol 2003;14:1275 -1282

Gonzalez-Alonso J, Quistorff B, Krustrup P, Bangsbo J and Saltin B. Heat production in human skeletal muscle at the onset of intense dynamic exercise. 2000;524 Pt 2:603-615

Holt RG and Roy RA. Measurements of bubble-enhanced heating from focused, MHz-frequency ultrasound in a tissue-mimicking material. Ultrasound Med Biol 2001;27:1399-1412

Hynynen K. The threshold for thermally significant cavitation in dog's thigh muscle in vivo. Ultrasound Med Biol 1991;17:157-169

Hynynen K, Colucci V, Chung A and Jolesz F. Noninvasive arterial occlusion using MRI-guided focused ultrasound. Ultrasound Med Biol 1996;22:1071-1077

Hynynen K and Edwards DK. Temperature measurements during ultrasound hyperthermia. Med Phys 1989;16:618-626

Hynynen K, Pomeroy O, Smith DN, et al. MR Imaging-guided Focused Ultrasound Surgery of Fibroadenomas in the Breast: A Feasibility Study. Radiology 2001;219:176-185

Kennedy JE, ter Haar GR and Cranston D. High intensity focused ultrasound: surgery of the future? Br J Radiol 2003;76:590-599

Kennedy JE, Wu F, ter Haar GR, et al. High-intensity focused ultrasound for the treatment of liver tumours. 2004;42:931-935

Keshavarzi A, Vaezy S, Kaczkowski PJ, et al. Attenuation coefficient and sound speed in human myometrium and uterine fibroid tumors. J Ultrasound Med 2001;20:473-480

Kumar V, Abbas AK, Fausto N, Robbins SL and Cotran RS, 2004, Robbins and Cotran pathologic basis of disease: Philadelphia, Elsevier/Saunders, xv, 1525 p.

Leighton TG, 1994, The Acoustic Bubble: San Diego, USA, Academic Press. Inc., 613 p.

Lele PP, 1987, Effects of ultrasound on "solid" mammalian tisssues and tumors in-vivo, in MH Repacholi, M Grandolfo and A Rindi, eds., Ultrasound: Medical applications, biological effects and hazard potential.: New York, Plenum Publishin Corp., p. 275-306.

Malcolm AL and ter Haar GR. Ablation of tissue volumes using high intensity focused ultrasound. Ultrasound Med Biol 1996;22:659-669

Maris HJ and Quan X. Nucleation of bubbles in liquid helium at negative pressure. 1989;63:1078-1081

Martin RW, Vaezy S, Kaczkowski P, et al. Hemostasis of punctured vessels using Doppler-guided high-intensity ultrasound. Ultrasound Med Biol 1999;25:985-990

Meaney PM, Cahill MD and ter Haar GR. The intensity dependence of lesion position shift during focused ultrasound surgery. Ultrasound Med Biol 2000;26:441-450

Melodelima D, Lafon C, Prat F, et al. Transoesophageal ultrasound applicator for sector-based thermal ablation: first in vivo experiments. 2003;29:285-291

Mesiwala AH, Farrell L, Wenzel HJ, et al. High-intensity focused ultrasound selectively disrupts the blood-brain barrier in vivo. Ultrasound Med Biol 2002;28:389-400

Miller DL and Gies RA. The interaction of ultrasonic heating and cavitation in vascular bioeffects on mouse intestine. 1998;24:123-128

Miller DL and Song J. Tumor growth reduction and DNA transfer by cavitation-enhanced high-intensity focused ultrasound in vivo. Ultrasound Med Biol 2003;29:887-893

Mulcahy N and Franklin D. Panel Backs Novel Fibroid Treatment. 2004;37:1,4

NCRP, 2002, Exposure criteria for medical diagnostic ultrasound II, Criteria based on all known mechanisms: Bethesda, Md., NCRP.

Pennes HH. Analysis of tissue and arterial blood temperatures in the resting human forearm. J Appl Physiol 1948;1:93-122

Prokop AF, Vaezy S, Noble ML, et al. Polyacrylamide gel as an acoustic coupling medium for focused ultrasound therapy. Ultrasound Med Biol 2003;29:1351-1358

Righetti R, Kallel F, Stafford RJ, et al. Elastographic characterization of HIFU-induced lesions in canine livers. Ultrasound Med Biol 1999;25:1099-1113

Rowland I, Rivens I, Chen L, et al. MRI study of hepatic tumours following high intensity focused ultrasound surgery. Br J Radiol 1997;70:144-153

Roy RA, Madanshetty SI and Apfel RE. An acoustic backscattering technique for the detection of transient cavitation produced by microsecond pulses of ultrasound. J Acoust Soc Am 1990;87:2451-2458

Sanghvi NT, Foster RS, Bihrle R, et al. Noninvasive surgery of prostate tissue by high intensity focused ultrasound: an updated report. 1999;9:19-29

Sokka S, King R, McDonnald N and Hynynen K, 2002, Gas-bubble enhanced heating in rabbit thigh in vivo, Proceedings IEEE Ultrasonic Symposium, Volume 2, p. 1415-1418.

Tavakkoli J, Birer A, Arefiev A, et al. A piezocomposite shock wave generator with electronic focusing capability: application for producing cavitation-induced lesions in rabbit liver. Ultrasound Med Biol 1997;23:107-115

ter Haar G, Sinnett D and Rivens I. High intensity focused ultrasound--a surgical technique for the treatment of discrete liver tumours. Phys Med Biol 1989;34:1743-1750

ter Haar GT, Walling J, Loverock P and Townsend S. The effect of combined heat and ultrasound on multicellular tumour spheroids. 1988;53:813-827

Thuroff S, Chaussy C, Vallancien G, et al. High-intensity focused ultrasound and localized prostate cancer: efficacy results from the European multicentric study. 2003;17:673-677

Umemura S-i, Kawabata K-I, Sanghvi NT and Sasaki K, 2002, In vivo accleration of ultrasonic tissue heating, Proceedings IEEE Ultrasonic Symposium, Volume 2, p. 1415-1418.

Vaezy S, Martin R and Crum L. High intensity focused ultrasound: a method of hemostasis. Echocardiography 2001;18:309-315

Vaezy S, Martin R, Yaziji H, et al. Hemostasis of punctured blood vessels using high-intensity focused ultrasound. Ultrasound Med Biol 1998;24:903-910

Vaezy S, Shi X, Martin RW, et al. Real-time visualization of high-intensity focused ultrasound treatment using ultrasound imaging. Ultrasound Med Biol 2001;27:33-42

Van Leenders GJLH, Beerlage HP, Ruijter ET, de la Rosette JJMCH and van de Kaa CA. Histopathological changes associated with high intensity focused ultrasound (HIFU) treatment for localised adenocarcinoma of the prostate. J Clin Pathol 2000;53:391-394

Vykhodtseva N, Sorrentino V, Jolesz FA, Bronson RT and Hynynen K. MRI detection of the thermal effects of focused ultrasound on the brain. Ultrasound Med Biol 2000;26:871-880

Vykhodtseva NI, Hynynen K and Damianou C. Histologic effects of high intensity pulsed ultrasound exposure with subharmonic emission in rabbit brain in vivo. Ultrasound Med Biol 1995;21:969-979

Waterman FM and Leeper JB. Temperature artifacts produced by thermocouples used in conjunction with 1 and 3 MHz ultrasound. 1990;6:383-399

Watkin NA, ter Haar GR and Rivens I. The intensity dependence of the site of maximal energy deposition in focused ultrasound surgery. Ultrasound Med Biol 1996;22:483-491

Watmough DJ, Lakshmi R, Ghezzi F, et al. The effect of gas bubbles on the production of ultrasound hyperthermia at 0.75 MHz: a phantom study. Ultrasound Med Biol 1993;19:231-241

Wu F, Chen W-Z, Bai J, et al. Tumor vessel destruction resulting from high-intensity focused ultrasound in patients with solid malignancies. Ultrasound Med Biol 2002;28:535-542

Wu F, Wang ZB, Cao YD, et al. A randomised clinical trial of high-intensity focused ultrasound ablation for the treatment of patients with localised breast cancer. Br J Cancer 2003;89:2227-2233

Wu F, Wang Z-B, Chen W-Z, et al. Extracorporeal high intensity focused ultrasound ablation in the treatment of 1038 patients with solid carcinomas in China: an overview. 2004;11:149-154

Wu F, Wang Z-B, Jin C-B, et al. Circulating tumor cells in patients with solid malignancy treated by high-intensity focused ultrasound. 2004;30:511-517

APPENDIX A: LABVIEW CODE

LabView VI: HIFU_PCD_TC
Used for controlling HIFU, collection of PCD RF signal, and collection of thermocouple voltage changes
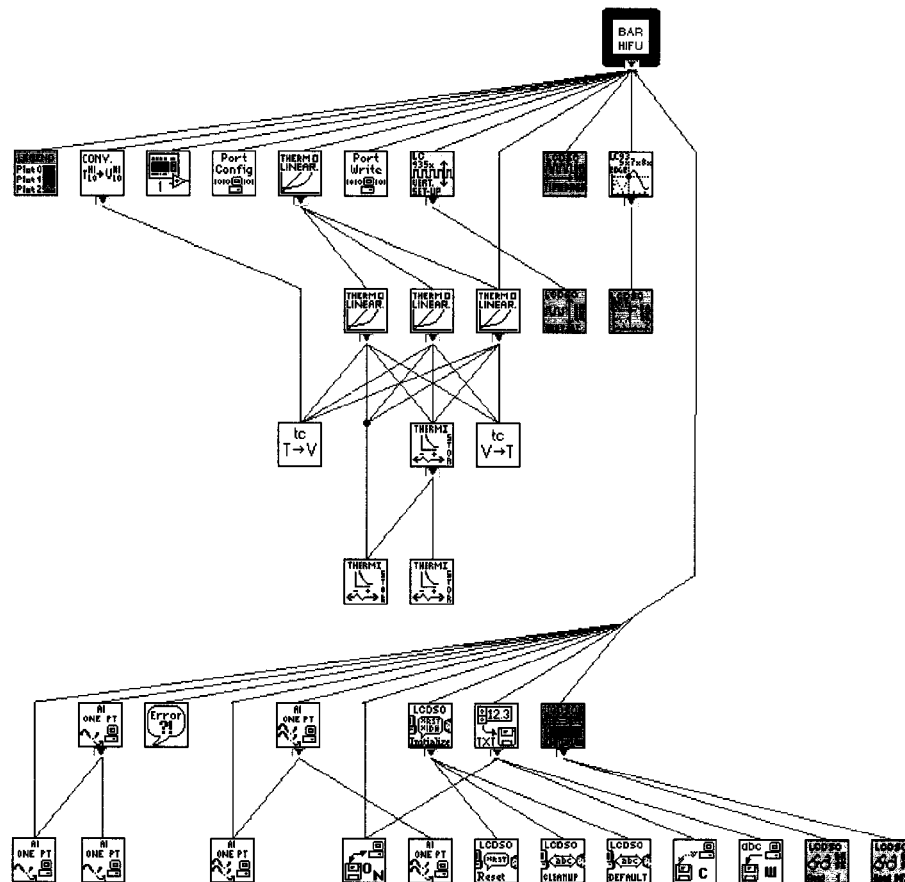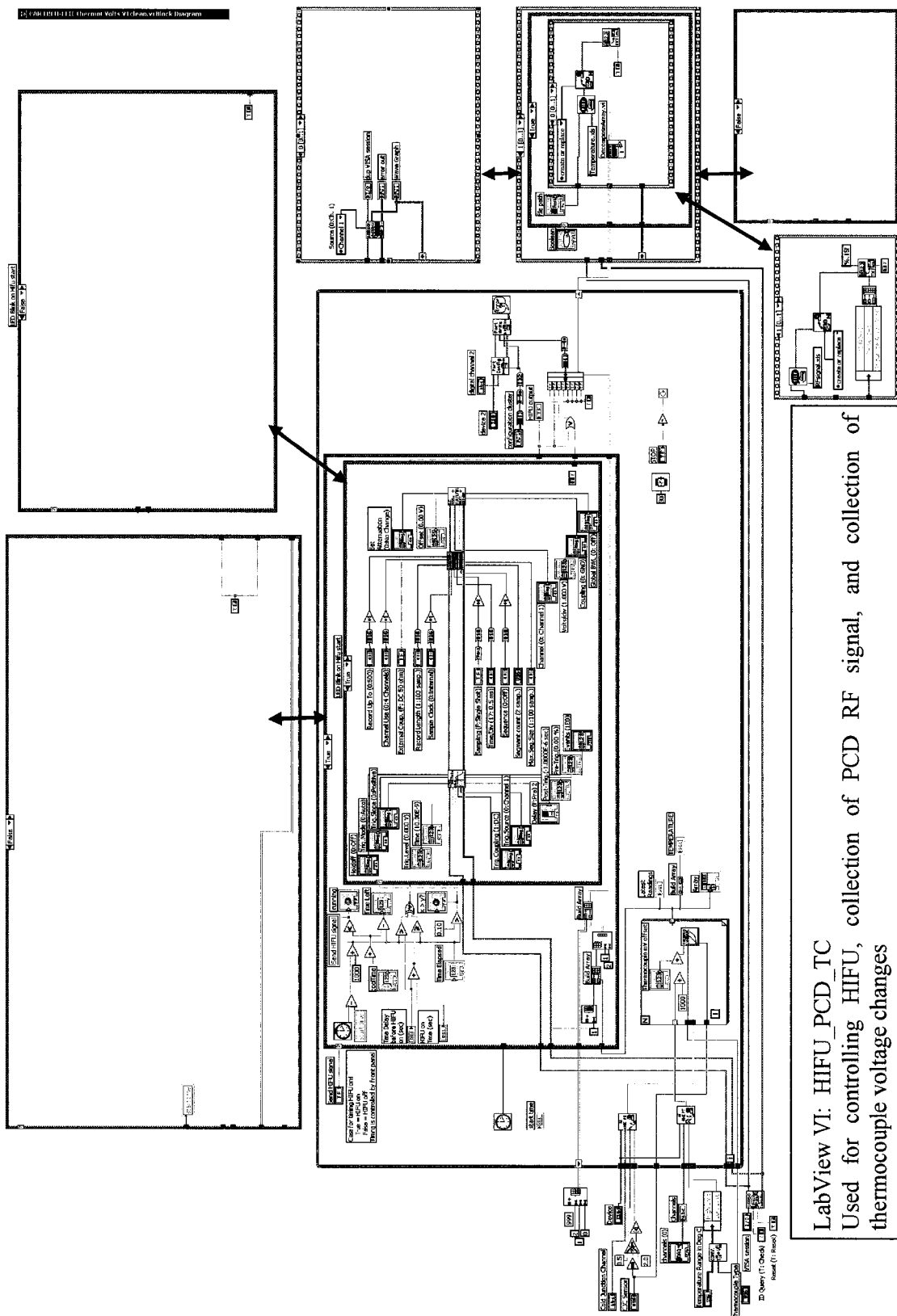
APPENDIX B: MATLAB ANALYSIS CODE

The following are scripts written in MATLAB and used for analyzing data:

RMS.m
```
% RMS Y = rms (U)
%
% Computes the root mean square of vector U
function  y = rms(u)
    mean_square = sum(u.^2)/length(u);
    y = sqrt(mean_square);
```

Active Cavitation Detection Analysis Scripts:

ACD_MasterControl.m

```
%%%%%%%%%%%%%%%%%%%%%%%
%%% ACD_MasterControl.m
%%% Brian A. Rabkin
%%% Created 12.15.03
%%% Last Updated: 01.25.04
%%%
%%% Used:  To manage the processing of all sample files at once through the use of a database
%%%
%%%%%%%%%%%%%%%%%%%%%%%


clear %Make sure no values are in memory


inFileRoot = '.txt';    % root of the input file
nFilesToRun = 1;        %number of files to process in an group


fileIN_Path = 'K:\Ultrasound\DATA\LF1_ProcessedData\ACD\';


%%%% GET THE INFORMATION FROM THE ACDmaster.txt DATABASE FILE  %%%%%%
%%% The file is setup with the following columns
%%% Tissue  Expt  Sample  [drive Volts]  [ACD use]  us/seg  ptsPerUs  SubWindowRes  numSegs  winstart
%%%    winstop  Split   get MaxppV
%%% PIG      8     BA1     300            0          1000    25        170           82       70
%%%    85       0        0


fileIN_dBASE = 'ACDmaster.xls';  %DATA BASE (dBASE) FILE NAME
fprintf(['Loading dataBase file (%s).\n\n'],fileIN_dBASE);


%%% Get the values for each column in the dBase file
[A1, A2, A3, A4, A5, A6, A7, A8, A9, A10, A11, A12, A13, A14] = .......
        textread(([fileIN_Path fileIN_dBASE]), '%s %d %s %d %d %d %d %d %d %d %d %d %d %f');


%%% Process Files associated with dBASE
tempMasterFile = [fileIN_Path, 'tempACDMaster', '.txt'];  %USED TO STORE THE TEMPORARY INFORMATION
                                                %OF WHAT HAS BEEN PROCESSED
    fidMasterOut = fopen(tempMasterFile ,'wt') ;


for cRow = 1:length(A1)   %RUN THROUGH ALL OF THE FILES AS POINTED TO BY EACH ROW OF THE
MASTER dBASE FILE
        dIN_Tissue         = char(A1(cRow));
        dIN_PIGnum         = A2(cRow);
        dIN_FILE           = char(A3(cRow));
        dIN_Voltage        = A4(cRow);
        dIN_RunSample      = A5(cRow);
        dIN_usPerSegment   = A6(cRow);
        dIN_ptsPerUs       = A7(cRow);
        dIN_SubWindowRes   = A8(cRow);
        dIN_numSegs        = A9(cRow);    %A9 = 1 if file has been split
        dIN_startWinPPAmp  = A10(cRow);   %A10 = 1 if file has been processed for maxppV
        dIN_stopWinPPAmp   = A11(cRow);


    file_current = [dIN_Tissue, num2str(dIN_PIGnum),' ', dIN_FILE];
    fprintf('Work on: %s \n', file_current);
    P_num = [dIN_Tissue, num2str(dIN_PIGnum)];  %pig number of tissue sample group
    fprintf('crow = %d \n', cRow);                  %print the dBase files row


    if (dIN_RunSample == 1)  %split file into time segments if supposed to and the file hasn't been split yet
        fprintf('PROCESS FILE %s\n', dIN_FILE);
```

```
        ACD_Split(fileIN_Path, P_num, dIN_FILE, dIN_usPerSegment, dIN_ptsPerUs);
        A12(cRow) = 1;

    elseif (dIN_RunSample == 1)  & (cRow >= 113) % Calculate the max peak-to-peak voltage at the focus
        %% Note: (cRow >= 113) in previous line is used to tell the
        %%     program to process only samples at line 113 or greater in
        %%     the dBase file
        dIN_FILE2 = dIN_FILE; %[dIN_FILE, 's', num2str(cSubFileIn)]
        ACD_GetMaxVpp(fileIN_Path, P_num, dIN_FILE2, dIN_Voltage, dIN_usPerSegment, .....
            dIN_SubWindowRes, dIN_ptsPerUs, dIN_numSegs, dIN_startWinPPAmp, dIN_stopWinPPAmp)
        A13(cRow) = 1;  %Change value to 1 since file has been split
    else
        fprintf('SKIP FILE\n');
    end
    fprintf(fidMasterOut, '%s\t %d\t %s\t %d\t %d\t %d\t %d\t %d\t %d\t %d\t\n', char(A1(cRow)), .....
            A2(cRow), char(A3(cRow)), A4(cRow), A5(cRow), A6(cRow), A7(cRow), A8(cRow), .....
            A9(cRow), A10(cRow));
end


    fclose(fidMasterOut);


clear all
```

ACD_Split.m

```
%%%%%%%%%%%%%%%%%%%%%%%
%%% ACD_Split.m
%%% Brian A. Rabkin
%%% Created 12.03.03
%%% Last Updated: 01.18.04
%%%
%%% Used:  To split the ACD raw files into time segments as collected by
%%%         the oscilloscope
%%%
%%% Input:  fileOUT_Path = 'E:\Ultrasound\DATA\LF1_ProcessedData\ACD\';
%%%     PIG_num = 'PIG8';
%%%     fileIN_segment = 'BA5';
%%% Output: Group of files each with one time segment in it.
%%%%%%%%%%%%%%%%%%%%%%%

function ACD_Split(fileOUT_Path, PIG_num, fileIN_segment, TimeWinRes, pntPerUs);

if nargin<1,  %Use these values if no input arguments
  fileOUT_Path = 'E:\Ultrasound\DATA\LF1_ProcessedData\ACD\';
  PIG_num = 'PIG8';
  fileIN_segment = 'BA5';
  TimeWinRes = 1000.000;    %Microseconds of time per a segment
  pntPerUs    = 25;             %Number of points per a microsecond
  fprintf(['Loading demo file (%s).\n'], [PIG_num, '\RAW\', fileIN_segment]);
end

  runGroup = [PIG_num, '.', fileIN_segment]
  fileIN_Root = '.txt';  % root of the input file
  fileIN_name = [PIG_num, '\RAW\', fileIN_segment, fileIN_Root];  %the input-file's name


  %%%%%%%%%%%%%%%%%%%%  GET DATA FROM FILE  %%%%%%%%%%%%%%%%%%%%%%%
  data_Incoming =load([fileOUT_Path fileIN_name]); %Get the data from the inputFile


  %%%%%%%%%%%%%%%%%%%%  PROCESS TIME DOMAIN DATA  %%%%%%%%%%%%%%%%%
  numPts=length(data_Incoming);              %# of points in scan
```

```
dataXAxis = data_Incoming(:,1);
dataYAxis = data_Incoming(:,2);

clear data_Incoming;   % clear data_Incoming since it is no longer used for this loop

xmin=min(dataXAxis(:,1));  %Minimum value on Xaxis
xmax=max(dataXAxis(:,1));  %Maximum value on Xaxis

%%%%% ADJUST TIME AXIS TO MICROSEC (us) %%%%%
rawDataTime= [];   %Raw data
rawDataTime = (dataXAxis - xmin)*1000000;  %Convert to secounds
dataTime = [];
dataAmp = [];
ptsStart = 1;

%%%%% NEW METHOD OF DETERMING WHEN TO SPLIT DATA   %%%%%
    numPtsPerSegment = TimeWinRes * pntPerUs + 2;
    %The following splits the Time and Yaxis into segements
    for cSplits = 1:(round(numPts/numPtsPerSegment)-1)
        dataTime = rawDataTime((cSplits*numPtsPerSegment-numPtsPerSegment +1): cSplits*numPtsPerSegment);
        dataAmp = dataYAxis((cSplits*numPtsPerSegment-numPtsPerSegment +1 ): cSplits*numPtsPerSegment);

        splitData = [dataTime, dataAmp];
        splitData2 = splitData.';

        splitFileName = [PIG_num, '\Split\', fileIN_segment,'s',num2str(cSplits),'.xls']
        splitFileAddress = strcat(fileOUT_Path, splitFileName)

        fidsplit = fopen(splitFileAddress ,'w');

        fprintf(fidsplit,'%6.4f \t %6.9f\n',splitData2);
        fclose(fidsplit);

    end %cSplits
```

ACD_GetMaxVpp

```
%%%%%%%%%%%%%%%%%%%%%%%%%%
%% ACD_GetMaxVpp
%% By: Brian A. Rabkin
%% Created 12.03.03
%% Last Updated: 01.18.04
%%
%% Used:  To calculate the maximum ppVoltage at the HIFU focus from the
%%        returning ACD RF signal
%%%%%%%%%%%%%%%%%%%%%%%%%%

function ACD_GetMaxVpp(fileIN_Path, PIG_num, fileIN_SubSegment, drive_Voltage, usPerSegment, .....
    SubWindowRes, pntPerUs, numSegs, startWinPPAmp, stopWinPPAmp);

%%%% PARAMETERS TO BE USED DURING THIS SCRIPT %%%%%
    fileIN_Root = '.xls';  % root of the input file

if nargin<1,   %IF DIDN'T GET ANY INPUT TO THE FUNCTION

    fileIN_Path = 'K:\Ultrasound\DATA\LF1_ProcessedData\ACD\';
    PIG_num = 'Gel2';
```

```
fileIN_SubSegment = 'GA08';
drive_Voltage = 300;
startWinPPAmp = 70;  %Leading window edge for where the focus is in time of flight
stopWinPPAmp = 85;  %Trailing window edge for where the focus is in time of flight

startSubFiles = 1;  %Run the first 40 files
stopSubFiles = 40;

usPerSegment = 200;
SubWindowRes = 200;
pntPerUs    = 25;
numSegs = 129;
fprintf(['Loading demo file (%s).\n'], [PIG_num, '\SPlit\', fileIN_SubSegment]);
else
   startSubFiles = 1;
   stopSubFiles = numSegs;
end

startWinPPAmp   = startWinPPAmp * pntPerUs;
stopWinPPAmp    = stopWinPPAmp * pntPerUs;

figNumber = 1;
arrayWinMaxPPAmp = [];
arrayWinPulseTime = [];

for cSubFileIn = startSubFiles:stopSubFiles
   runGroup = [fileIN_SubSegment,'s', num2str(cSubFileIn)]
   fileIN_name = [PIG_num, '\Split\', runGroup, fileIN_Root];  %the input-file's name


   %%%%%%%%%%%%%%%%%%%%  GET DATA FROM FILE  %%%%%%%%%%%%%%%%%%%%%%%%
          data_Incoming =load([fileIN_Path fileIN_name]);  %Get the data from the inputFile

   %%%%%%%%%%%%%%%%%%%%  PROCESS TIME DOMAIN DATA  %%%%%%%%%%%%%%%%%

   numPts=length(data_Incoming);                %# of points in scan

   dataXAxis = data_Incoming(:,1);
    dataYAxis = data_Incoming(:,2);

   clear data_Incoming;  % clear data_Incoming since it is no longer used for this loop

   xmin=min(dataXAxis(:,1));
    xmax=max(dataXAxis(:,1));

   dataTime = (dataXAxis - xmin);  %%%% USED FOR THE TIME AXIS
   dataAmp = dataYAxis;
   ptsStart = 1;

   TimeWinRes = usPerSegment *1.000;  %1000.000;      %us of time to split file by
   maxNumOfSubPlots = round(TimeWinRes/SubWindowRes) + 1;

   NumOfSubPlots = 7;
   cSubPlot = 1;

   cPlotsSaved = 1;  %%% COUNT THE NUMBER OF SUBPLOTS DONE

   %%%%%% PLOT TIME DOMAIN DATA  %%%%%%%%
          h = figure;
          figClosed = 1;  %to close figure after processing
```

```
subplot (NumOfSubPlots,1,1), plot(dataTime, dataAmp);
xlabel('Time (us)')
ylabel('Amplitude (Volts)')

figName = [runGroup,'.',num2str(figNumber)]
title(figName);
xmin=min(dataTime(:,1));
xmax= max(dataTime(:,1));
ymin=-1; %min(dataYAxis(:,1))
ymax= 1; %max(dataYAxis(:,1))
            %axis ([xmin, xmax, ymin, ymax])


%%%%%%%%%%%%%  GET SUBWindow %%%%%%%%%%%%%%%%%%
dataSubTime = [];
dataSubAmp = [];

numPtsPerSubWin = SubWindowRes * pntPerUs;

numPtsSubWin = length(dataTime);            %# of points in scan
ptsSubStart = (14.6 * pntPerUs);
stopSubWin = ptsSubStart + (numPtsPerSubWin + 1);
subFigNum = 1;
subPlotNum = 2;
findStartPulse = 0;

subArrayWinMaxPPAmp = [];  %array for getting the max Voltage per each subsegment

    %%%% SCAN THROUGH EACH SUBWINDOW %%%%
for cScanSubWin = 1:numPtsSubWin-1

        %%%% LOOK FOR THE INTERIGATION PULSE SENT BY THE PULSER-
        %%%% -RECIEVER
        if (dataAmp(cScanSubWin) <= -0.5) & (findStartPulse == 0)      %Find the first pulse signal in the train
            ptsSubStart = cScanSubWin;
            stopSubWin = ptsSubStart + (numPtsPerSubWin + 1);
            findStartPulse = 1;
        end

        %%%  CHECK NOT GOING PAST THE TOTAL TIME LENGTH
        if stopSubWin > numPtsSubWin-1      %USED TO MAKE SURE THAT THE LAST SUBWINDOW OF
                                            INTEREST DOESN'T EXCEED THE SUBSEGMENT LENGTH
            stopSubWin = numPtsSubWin-1;
        end


        if stopSubWin == cScanSubWin
            stopSubWin = stopSubWin + numPtsPerSubWin;
            ptsSubFinish = cScanSubWin;
            dataSubTime = dataTime(ptsSubStart:ptsSubFinish-1);
            dataSubTime = dataSubTime - dataSubTime(1);       %%% SET THE TIME BACK TO ZERO AT START
                                                              OF SUBWINDOW
            dataSubAmp = dataAmp(ptsSubStart:ptsSubFinish-1);  %%% GET SUBWINDOWS AMPLITUDE DATA
            ptsSubStart = cScanSubWin;                   %%% RESET ptsSubStart to start looking from here in time

        %%%% GET THE MAXppVOLTAGE BY USING AN EXTERNAL FUNCTION
        %%%% TO INSURE THE PEAKS (+,-) ARE ADJACENT TO EACH
        %%%% OTHER

        maxPeakAmp = max(dataSubAmp(startWinPPAmp:stopWinPPAmp));      %Get the max peak amplitude
                                                                       value
```

```
minPeakAmp = min(dataSubAmp(startWinPPAmp:stopWinPPAmp));    %Get the min Peak Amplitude
                                                                             value
subArrayWinMaxPPAmp = [subArrayWinMaxPPAmp (maxPeakAmp - minPeakAmp)];

subplot (NumOfSubPlots,1,subPlotNum), plot(dataSubTime,dataSubAmp)

if subPlotNum == 1
    figTitle = [figName, '.',num2str(SubWindowRes),'us.', num2str(cPlotsSaved)]
    title(figTitle)
end

xlabel(' ');
ylabel(subFigNum);
subFigNum = subFigNum + 1;

figFilename = [fileIN_Path, PIG_num, '\Images\', fileIN_SubSegment, 's', num2str(cSubFileIn)];  %the input-
                                                                             file's name
if subPlotNum == NumOfSubPlots

    mainFigFilename = [figFilename, '.tif']

    cPlotsSaved = cPlotsSaved + 1;

    print ('-dtiff', mainFigFilename)
    close(h);
    figClosed = 0;
    if subPlotNum < maxNumOfSubPlots
        h = figure
        figClosed = 1;
    end
    subPlotNum = 1;
else
    subPlotNum = subPlotNum +1;
end
    %close(h)
    end %stopSubWin
  end %cScanSubWin
  if figClosed == 1
    close(h);
  end

arrayWinMaxPPAmp = [arrayWinMaxPPAmp; cSubFileIn subArrayWinMaxPPAmp];  %Build array of
                                                                             subplotdata
    %arrayWinPulseTime = [arrayWinPulseTime; cSubFileIn];
  figNumber = figNumber + 1;

  end %for %cSubFileIn
  h2 = figure;
%hold on
plot (arrayWinMaxPPAmp(:,1), arrayWinMaxPPAmp(:,2), 'b')
%following used if want to print max for more then one ACD return
%pulse per a Time segment
        %       plot (arrayWinMaxPPAmp(:,1), arrayWinMaxPPAmp(:,3), 'r')
        %       plot (arrayWinMaxPPAmp(:,1), arrayWinMaxPPAmp(:,4), 'g')
        %       plot (arrayWinMaxPPAmp(:,1), arrayWinMaxPPAmp(:,5), 'y')
        %       plot (arrayWinMaxPPAmp(:,1), arrayWinMaxPPAmp(:,6), 'm')
        %       plot (arrayWinMaxPPAmp(:,1), arrayWinMaxPPAmp(:,7), 'k')
%plotTitle = ['Plot of maxVpp for:  %s at  %d Volts Figure: ', fileIN_SubSegment, drive_Voltage,];
```

```
title(sprintf('Plot of acoustic emmision for sample: %s %s at %d-mVpp', PIG_num, fileIN_SubSegment,
    drive_Voltage))

xmin = 0;
xmax = max((arrayWinMaxPPAmp(:,1)));
ymin = 0;
ymax = 1.5;
xlabel('Segment (170us/segment)')
        ylabel('Max Peak to Peak Amplitude (Volts)')
axis([xmin xmax ymin ymax]);

%hold off

maxPPVFileAddress = [fileIN_Path, PIG_num, '\MaxppV\', fileIN_SubSegment, '.MaxppV', '.tif'];

 print ('-dtiff', [maxPPVFileAddress, '.tif'])
 close(h2)

%%% PRINT FILE OF MAXVPP VALUES TO A FILE%%%%
maxPPVFileAddress = [fileIN_Path, PIG_num, '\MaxppV\', fileIN_SubSegment, '.MaxppV', '.xls'];
fidmaxPPV = fopen(maxPPVFileAddress ,'w');

fprintf(fidmaxPPV,'%6.0f \t %6.9f \t %6.9f \t %6.9f \t %6.9f \t %6.9f \t %6.9f\n',arrayWinMaxPPAmp');
fclose(fidmaxPPV);
```

Passive Cavitation Detection Analysis

PCD_MasterControl.m

```
%%%%%%%%%%%%%%%%%%%%%%%
%% PCD_MasterControl.m
%% Brian A. Rabkin
%% Created: 1.10.04
%% Updated: 5.05.04
%%
%% Used: To process and quantify the raw RF signal from the PCD detector into
%%        broadband and subharmonic components
%%
%%%%%%%%%%%%%%%%%%%%%%%%


%%---- Set the image parameters for display purposes
        set(0,'defaulttextfontsize',14, 'defaulttextfontweight', 'bold')
        set(0,'defaultaxeslinewidth',2);
        set(0,'defaultaxesfontsize',14)


%%---- set the window size and time spacing between windows. for FFT analysis

    global windowlength_microsec
    global windowspacing_microsec
        windowlength_microsec = 20;    %set the window width for FFT analysis
        windowspacing_microsec = 1;    %set the step to take between windows for FFT mapping

    global maxSpect %used to get max spectrum for normalization later.
        maxSpect = 0;


%%---- GET DATABASE FILE THAT SET PARAMETERS FOR ANALYSIS ----%%
    inFileRoot = '.txt';  % root of the input file
    nFilesToRun = 1;            %number of files to process in an group

    fileIN_Path = 'k:\Ultrasound\DATA\LF2_ProcessedData\';

%%%% GET THE INFORMATION FROM THE PCDmaster.txt DATABASE FILE  %%%%%%


    fileIN_dBASE = 'PCDmasterLF2.xls';
    fprintf(['\n\nLoading dataBase file (%s).\n\n'],fileIN_dBASE);
```

% Tissue exp#		Sample	DriveV	us/seg	pts/us	DutyCycle	dB		msDelay	Location		numSegs
FirstHIFUPulse	LastHIFUPulse	Run?Split		Mapped	USimageOnsetTime							
% PIG	8	BP1	300	1000	25	80	15	0	Front	80	7	69
1	1	0	1.20									
% A1	A2	A3	A4	A5	A6	A7	A8	A9	A10	A11	A12	A13	A14
A15	A16	A17										

```
[A1, A2, A3, A4, A5, A6, A7, A8, A9, A10, A11, A12, A13, A14, A15, A16, A17, A18] = .....
        textread(([fileIN_Path fileIN_dBASE]), '%s %d %s %d %d %d %d %d %d %s %d %d %d %d %d %f %f');


            %A12 =1 if file has been split
            %A13 = 1 if file has been processed for maxppV


        mAmpArray = [];  %collect the mean amplitude of each segment for each voltage
        got_mAmp = 0;  %used to plot mean data of amplitudes when they are processed (=1)


IntensityValues = [220, 490, 850, 1280, 1710];


    for cRepeat = 5:5
        VoltagePlot = 50 + cRepeat*50;
```

```
fprintf('Voltage: %s\t', VoltagePlot);
            h = figure;
hold
box on
cSamples = 0;

ProcessPigNum = 2;  %Which pig to process
runSplit = 0;
runMap = 1;
runMaxRMS = 0;
runSubMax = 0;
        idx_temp = find(A4 == VoltagePlot);
        idx_tempA = find(A14(idx_temp) == 1);
max_HifuFirstSeg = max(A12);
data_AmpStatsArray = zeros([max(A11)+1+max_HifuFirstSeg+1,length(idx_tempA)+1]);

for cRow = 1:length(A1)    %debug 10:10 %RUN THROUGH ALL OF THE FILES AS POINTED TO BY EACH
        ROW OF THE MASTER FILE
    dIN_Tissue    = char(A1(cRow));
    dIN_PIGnum    = A2(cRow);
    dIN_Sample    = char(A3(cRow));
    dIN_Voltage   = A4(cRow);
    dIN_usPerSegment = A5(cRow);
    dIN_ptsPerUs  = A6(cRow);
    dIN_DutyCycle = A7(cRow);
    dIN_dB        = A8(cRow);
    dIN_msDelay   = A9(cRow);

    dIN_ListenLocation = char(A10(cRow));
    dIN_numSegs   = A11(cRow);

    dIN_HifuFirstSeg = A12(cRow);    %First segment that HIFU is on
    dIN_HifuLastSeg = A13(cRow);     %Last segment that HIFU is on

    dIN_RunSample  = A14(cRow);
    dIN_Split     = A15(cRow);
    dIN_Mapped    = A16(cRow);

    dIN_USonsetTime = A17(cRow);

    file_current = [dIN_Tissue, num2str(dIN_PIGnum),' ', dIN_Sample];
    fprintf('Work on: %s\t\t', file_current);

    if (dIN_RunSample == 1) & (runSplit == 1) & (dIN_Split == 0) & (dIN_Mapped == 0)
            %split if supposed to and the file hasn't been split yet
        P_num = [dIN_Tissue, num2str(dIN_PIGnum)];
        filePath_current = [fileIN_Path, 'PCD', P_num, '\Split\'];
        fprintf('SPLIT FILE \n');
        ACD_Split(filePath_current , P_num, dIN_Sample, dIN_usPerSegment, dIN_ptsPerUs);
        dIN_Split = 1;

    elseif (runMap == 1) & (dIN_PIGnum == ProcessPigNum) %% Map the FFT of the RF signal
        P_num = [dIN_Tissue, num2str(dIN_PIGnum)];
        filePath_current = [fileIN_Path, 'PCD', P_num, '\Split\'];
        fprintf('FFT MAP FILE \n');
        max_SpectrumArray = [];
        rms_Image = zeros((1000/windowspacing_microsec - windowlength_microsec), dIN_numSegs);
        subHarm_image = zeros((1000/windowspacing_microsec - windowlength_microsec), dIN_numSegs);
        %%% FOLLOWING "FOR" LOOP TAKES THE RAW RF AND MAKES AN FFT
        %%% MAP OF IT, ALSO GETS THE RMS AND SUBHARMONIC DATA
```

```
for cFiles=1:dIN_numSegs      %loop to get segment of the sample

    [rms_ArrayGet,         subHarm_ArrayGet,         time_Axis,         max_Spectrum]         =
PCD_FFTMapSegmentsMCLF2(fileIN_Path, P_num, dIN_Sample, cFiles, dIN_Voltage, dIN_ptsPerUs, dIN_dB);

        pack
        rms_image(:,cFiles) = rms_ArrayGet(:,2);
        subHarm_image(:,cFiles) = subHarm_ArrayGet';
        max_SpectrumArray = [max_SpectrumArray, max_Spectrum];
    end %cFiles
    dIN_Mapped = 1;
    rms_Time = rms_ArrayGet(:,1)+windowlength_microsec; % flipud(rms_ArrayGet(:,1));
    subHarm_Time = rms_Time;   %Get the time frame of the subHarmonic

    figSubH = figure;

        imagesc(1:dIN_numSegs, subHarm_Time, subHarm_image);
        colormap;
        colorbar;
        axis xy;
            fileout_Figure_Name = [P_num, '.', dIN_Sample, '.SUBmap']

        title(fileout_Figure_Name);
        filePath= [fileIN_Path, P_num, '\SUB\'];
        title_figure = [filePath, fileout_Figure_Name]
        %saveas(figSubH, [title_figure, '.fig'], 'fig');
        saveas(figSubH, [title_figure, '.tif'], 'tif');
    close(figSubH);

    figSubH = figure;
        axisXarray = (2-dIN_HifuFirstSeg:1:80-dIN_HifuFirstSeg);

        subHarm_max = mean(subHarm_image(65:890, :));
        axisX = [0-dIN_HifuFirstSeg, 79-dIN_HifuFirstSeg];
        axisY = [-80, -40];
        plot(axisXarray, subHarm_max, '-ko', 'MarkerEdgeColor','k','MarkerFaceColor','k', 'MarkerSize',4);

        fileout_Figure_Name = [P_num, '.', dIN_Sample, '.SUBmax']

        title(fileout_Figure_Name);
                                        ylabel('Level');
        xlabel('HIFU Pulse Number');
        filePath= [fileIN_Path, P_num, '\SUB\'];
        title_figure = [filePath, fileout_Figure_Name]
        saveas(figSubH, [title_figure, '.tif'], 'tif');

        maxRMSFileAddress = [filePath, P_num,'.',dIN_Sample, '.SubHar', '.xls'];
        dlmwrite(maxRMSFileAddress, subHarm_max', '\t');
    close(figSubH);

    rms_image = 20*log10((rms_image/0.03)+1e-4);
    %scans the whole pulse for 20 ms interval with max RMS
    rms_WindowMax = max(rms_image(65:length(rms_image), :));
    figH = figure;
        rms_image(1,1) = 0;
        rms_image(1,2) = -80;

        imagesc(1:dIN_numSegs, rms_Time, rms_image);
        colormap;
        axis xy;
```

```
        fileout_Figure_Name = [P_num, '.', dIN_Sample, '.RMSmap']  %% NAME FIGURE OUTPUT FILE
    title(fileout_Figure_Name);
    xlabel('HIFU Pulse Number');
    ylabel(sprintf('\\musec [%i \\musec window length %i\\musec window spacing]',...
        windowlength_microsec, windowspacing_microsec));

    h = colorbar;
    axes(h);
    ylabel('Level','rotation',270);


        filePath= [fileIN_Path, P_num, '\RMS\'];
        title_figure = [filePath, fileout_Figure_Name]
        saveas(figH, [title_figure, '.fig'], 'fig');
        saveas(figH, [title_figure, '.tif'], 'tif');

    close(figH);
    figRMS_Ave = figure;
        fileout_Figure_Name = [P_num, '.', dIN_Sample, '.RMSmax']  %% NAME FIGURE OUTPUT FILE
            title_figure = [filePath, fileout_Figure_Name]

        plot(1:length(rms_WindowMax), rms_WindowMax, '-ko', 'MarkerEdgeColor','k',...
        'MarkerFaceColor','k', 'MarkerSize',4);
        title(fileout_Figure_Name);
                                        ylabel('Level');
        xlabel('HIFU Pulse Number');
        axis([0, length(rms_WindowMax), -80, 0]);
            saveas(figRMS_Ave, [title_figure, '.fig'], 'fig');
            saveas(figRMS_Ave, [title_figure, '.tif'], 'tif');

    maxRMSFileAddress = [filePath, P_num,'.',dIN_Sample, '.MaxRMS', '.xls'];

        dlmwrite(maxRMSFileAddress, rms_WindowMax', '\t');
    close(figRMS_Ave);

elseif (runMaxRMS == 1) & (dIN_RunSample == 1) & (dIN_Split == 1) & (dIN_Voltage == VoltagePlot)
    P_num = [dIN_Tissue, num2str(dIN_PIGnum)];
    filePath_current = [fileIN_Path, 'PCD', P_num, '\Split\'];
    got_mAmp = 1;

    remove_BackGround = 0;  %---- used to remove the backgound
    [data_Time, data_Amp]  =  PCD_AnalyzeMaxRMSLF2(fileIN_Path, P_num, dIN_Sample, dIN_Voltage,
        remove_BackGround);

    timeGraph = (1:(length(data_Amp)+max_HifuFirstSeg+1));
    timeGraph = (timeGraph*0.1596 - (max_HifuFirstSeg+1)*0.1596);

    data_Amp = data_Amp';

    lineX = [dIN_USonsetTime, dIN_USonsetTime];
    lineY = [-65, 0];
    lineBGX = [min(timeGraph), max(timeGraph)];
    lineBGY = [-56.31, -56.31];
    plot(timeGraph((max_HifuFirstSeg-dIN_HifuFirstSeg+1):((max_HifuFirstSeg- .....
        dIN_HifuFirstSeg+1)+length(data_Amp)-1)), data_Amp, '-ko', 'MarkerEdgeColor','k',...
        'MarkerFaceColor','k',...
        'MarkerSize',4)

    xlabel('Time (sec)')
    ylabel('Amplitude (dB)')
```

```
figName = ['Driving Voltage', num2str(dIN_Voltage), '-mVpp']
    NameTitle = [num2str(IntensityValues(cRepeat)), ' W/cm^2  (I_S_P_T_A)', ' ', file_current];
title(NameTitle);


    xmin=min(timeGraph);
    xmax=max(timeGraph)+0.5;% 82;
   ymin=-65; %min(dataYAxis(:,1))
  ymax= 0; %max(dataYAxis(:,1))
  axis ([xmin, xmax, ymin, ymax]);



   if length(data_AmpStatsArray) > length(data_Amp)
      zerA = zeros([(max_HifuFirstSeg-dIN_HifuFirstSeg+1), 1]);
      zerB = zeros([((length(data_AmpStatsArray)-(max_HifuFirstSeg-dIN_HifuFirstSeg+1)-1).....
            - length(data_Amp)), 1]);
      data_Amp = [zerA; data_Amp'; zerB];
      data_Amp = data_Amp';
   end
   cSamples = cSamples + 1;
   if cSamples == 1
      data_AmpStatsArray(:,cSamples)= [0; timeGraph'];
      cSamples = cSamples + 1;
   end

   data_AmpStatsArray(:,cSamples)= [cRow; data_Amp'];

elseif (runSubMax == 1) & (dIN_RunSample == 1) & (dIN_Split == 1) &  .....
            (dIN_Voltage == VoltagePlot)  & (dIN_PIGnum == 2)
    P_num = [dIN_Tissue, num2str(dIN_PIGnum)];
   filePath_current = [fileIN_Path, 'PCD', P_num, '\Split\'];
   got_mAmp = 1;
    [data_Time,  data_Amp]  =  PCD_AnalyzeSubMaxLF2(fileIN_Path,  P_num,  dIN_Sample,  dIN_Voltage,
                        remove_BackGround);


    timeGraph = (1:(length(data_Amp)+max_HifuFirstSeg+1));
   timeGraph = (timeGraph*0.1596 - (max_HifuFirstSeg+1)*0.1596);


    data_Amp = data_Amp';


   lineX = [dIN_USonsetTime, dIN_USonsetTime];
   lineY = [-65, 0];
   lineBGX = [min(timeGraph), max(timeGraph)];
   lineBGY = [-56.31, -56.31];
   plot(timeGraph((max_HifuFirstSeg-dIN_HifuFirstSeg+1):((max_HifuFirstSeg- ....
          dIN_HifuFirstSeg+1)+length(data_Amp)-1)), data_Amp, '-ko', 'MarkerEdgeColor','k',...
          'MarkerFaceColor','k',...
          'MarkerSize',4) ;
   xlabel('Time (sec)')
   ylabel('Amplitude (dB)')

   figName = ['Driving Voltage', num2str(dIN_Voltage), '-mVpp']
    NameTitle = [num2str(IntensityValues(cRepeat)), ' W/cm^2  (I_S_P_T_A)', ' ', file_current];
title(NameTitle);

xmin=min(timeGraph);
xmax=max(timeGraph)+0.5;% 82; %
 ymin=0; %min(dataYAxis(:,1))
 ymax= 1.5*1e-3; %max(dataYAxis(:,1))
axis ([xmin, xmax, ymin, ymax]);
```

```
            if length(data_AmpStatsArray) > length(data_Amp)
                zerA = zeros([(max_HifuFirstSeg-dIN_HifuFirstSeg+1), 1]);
                zerB = zeros([((length(data_AmpStatsArray)-(max_HifuFirstSeg-dIN_HifuFirstSeg+1)-1).....
                        - length(data_Amp)), 1]);
                data_Amp = [zerA; data_Amp'; zerB];
                data_Amp = data_Amp';
                %data_Amp = [data_Amp; zeros([((length(data_AmpStatsArray)-1) - length(data_Amp)), 1])];
            end
            cSamples = cSamples + 1;
            if cSamples == 1
                data_AmpStatsArray(:,cSamples)= [0; timeGraph'];
                cSamples = cSamples + 1;
            end

            data_AmpStatsArray(:,cSamples)= [cRow; data_Amp'];
            %figure
        else
            fprintf('SKIP \n');
        end
    end %for cRow

    hold off;
    fileout_Figure_Name= ['RMSmax', '.', num2str(VoltagePlot), 'mVpp', '.tif'];
    title_figure = [fileIN_Path, fileout_Figure_Name];

    maxOutTitle = [fileIN_Path, P_num, '\RMS\', 'RMSmax', '.', num2str(VoltagePlot),'mVpp', '.xls'];
    dlmwrite(maxOutTitle, data_AmpStatsArray, '\t');
    if got_mAmp ==1
        mAmp = mean(data_AmpStatsArray(2:length(data_AmpStatsArray),:)');
        mAmpTime = (1:length(mAmp))*0.1596;

        mAmpArray = [mAmpArray, mAmp'];
    end

end %for cReapet for counting number of voltages to analyze




PCD_FFTMapSegmentsMC.m

%%%%%%%%%%%%%%%%%%%%%%%
%%% PCD_FFTMapSegmentsMC.m
%%% Brian A. Rabkin
%%% Created: 1.10.04
%%% Updated: 2.19.04
%%%
%%% Used:  To process and quantify the raw RF signal from the PCD detector into
%%%       broadband and subharmonic components
%%%
%%%%%%%%%%%%%%%%%%%%%%%

function [rms_Array, subHarm_Array, time_axis, maxSpectrum]    = PCD_FFTMapSegmentsMC(filePath, pig_Name,
IN_Sample, cFiles, IN_Voltage, IN_ptsPerUs, IN_dB);


    %%%---- Set the image parameters for display purposes
            set(0,'defaulttextfontsize',12, 'defaulttextfontweight', 'bold')
            set(0,'defaultaxeslinewidth',2);
```

```
            set(0,'defaultaxesfontsize',12)

global windowlength_microsec;     %FFT Window Length
global windowspacing_microsec;    %Spacing between the start of each FFT window

inFileRoot = '.xls';


  if nargin<1,    %IF DIDN'T GET ANY INPUT TO THE FUNCTION
    filePath = 'C:\MATLAB6p5\work\Ultrasound\TestData\';
    IN_dB = 20;
    pig_Name = '\PCDPig7'; %'\Metal';
    fileIN_SubSegment = 'BP12'%'Metal1.50mv1';
    IN_Sample = 'BP12'%'Metal1.50mv1'
    cFiles = 11
    spectrum_BackGr =0;
    windowlength_microsec = 25;
    windowspacing_microsec = 1;
  end

filePath_current = [filePath, pig_Name, '\Split\'];
filePath_Figures = [filePath, pig_Name, '\FFTImages\'];


    save_Image = 1;    % 1 = yes

  file = [IN_Sample,'s', num2str(cFiles), inFileRoot]; % INCOMING FILE NAME

            %%%%%%%%%%%%%%%%%%%  GET DATA FROM FILE   %%%%%%%%%%%%%%%%%%%%%%%%
            input_data = load([filePath_current file]);  %% LOAD DATA

            %%%%%%%%%%%%%%%%%%%  PROCESS TIME DOMAIN DATA   %%%%%%%%%%%%%%%%%
                     dataXAxis = input_data(:,1);
                     dataYAxis = input_data(:,2);

    %%%%% ADJUST TIME AXIS TO us  %%%%%%


                     xmin=min(dataXAxis(:,1));
    dataXAxis2 = (dataXAxis - xmin);  %Adjust X axis to useconds
    dataXAxis = dataXAxis2;
    input_data(:,1) = dataXAxis;

    %% FIGURE of TIME DOMAIN RAW DATA  %%


            fileout_Figure_Name = [pig_Name, IN_Sample,'s', num2str(cFiles), 'mapFFT']   %% NAME
FIGURE OUTPUT FILE

    %%%% PROCESS DATA INTO FFT MAP  %%%%
      sampling_rate_mhz = 25;
            sampling_rate_hz = sampling_rate_mhz*1e6;
      firstWindowPoint = 1*sampling_rate_hz/1e6;
      lastWindowPoint = length(input_data); %windowlength_microsec*sampling_rate_hz/1e6 + firstWindowPoint
+2*windowspacing_microsec; %length(input_data)

    [time_axis,     frequency_axis,     frequency_image,     rms_Array,     maxSpectrum]     =
PCD_getFFTseriesMCLF2(input_data(firstWindowPoint:lastWindowPoint, :), IN_dB);

      RMS_Plot = 0;
    if RMS_Plot == 1
      figH1 = figure
```

```
        plot (rms_Array(:,1), rms_Array(:,2));
    close(figH1);
end


    dataXAxis = input_data(firstWindowPoint:lastWindowPoint,1);
                        dataYAxis = input_data(firstWindowPoint:lastWindowPoint,2);


    figH  =  figure ;
        subplot(2,1,1), plot(dataXAxis, dataYAxis);
        title(fileout_Figure_Name);
                                xmin=min(dataXAxis(:,1));
                                xmax=max(dataXAxis(:,1));
            ymin=-1; %min(dataYAxis(:,1))
                                ymax= 1; %max(dataYAxis(:,1))
                                    axis ([xmin, xmax, ymin, ymax]);
                            h = colorbar;
                            axes(h);

%%%% MAKE FFT MAP FIGURE %%%%


        lineX = [ 0 45];
        lineY_subH = [1.66 1.66];
        lineY_fundH = [3.32 3.32];
        lineY_ultraH = [4.98 4.98];
        lineY_harmH = [6.64 6.64];


    subHarm_Array    =    max(frequency_image(35:36,:))    -    mean((max(frequency_image(33:34,:))    +
max(frequency_image(37:38,:)))/2); % frequency_axis(35)


    frequency_image  =  20*log10((frequency_image)+1e-4);  %+1e-4   71.5857   /max(max(frequency_image)
(LF2.Pig2 maxSpec = 2.024803e+001)


        idx = find(frequency_image > -40);
        frequency_image(idx) = -40;
        clear idx;
        frequency_image(1,1) = -40;
        frequency_image(1,2) = -80;


        subplot(2,1,2), imagesc(time_axis, frequency_axis, frequency_image), line(lineX, lineY_ultraH, 'color', 'r'),...
        line(lineX, lineY_fundH, 'color', 'r'), line(lineX, lineY_harmH, 'color', 'r'), line(lineX, lineY_subH, 'color',
'r'), axis([0, 1000, -120, 0]);


        colormap; %(gray);
        ylabel('MHz');
        xlabel(sprintf('\\musec [%i \\musec window length %i\\musec window spacing]',...
        windowlength_microsec, windowspacing_microsec));


        xmin=0; %min(time_axis)
        xmax=max(time_axis);
        ymin=0.2; %min(frequency_axis);
        ymax=7; %max(frequency_axis)


        axis ([xmin, xmax, ymin, ymax]);
        hold on;
        axis xy;
        hold off;


        h = colorbar;
        axes(h);
```

```
if save_Image == 1
   title_figure = [filePath_Figures, fileout_Figure_Name];
   saveas(figH, title_figure, 'tif');
   close(figH);
else
   %close(figH);
                        end % save_Image

plot3D = 0;
if plot3D == 1

   figure
   idx = find(frequency_image > -50);
   frequency_image(idx) = -50;
   clear idx;

   surf(time_axis, frequency_axis, frequency_image);
   shading interp;
   colormap(jet);
   xmin=0; %min(time_axis)
   xmax=max(time_axis);
   ymin=0.2; %min(frequency_axis);
   ymax=10; %max(frequency_axis)
   zmin = -80;
   zmax = 0;

   axis ([xmin, xmax, ymin, ymax, zmin, zmax]);
end


 subHarm_Array_Plot = 0;
if subHarm_Array_Plot == 1
  figH1 = figure
   plot (time_axis, subHarm_Array);
end

FreqStep                    =                    frequency_axis(10)-frequency_axis(9)
```

Thermal Model

```
%%%%%%%%%%%%%%%%%%%%%%%
%% LF2_Thermal_Cavitation.m
%% Brian A. Rabkin
%% Created: 8.21.04
%% Updated: 10.30.04
%%
%% Used: To calculate the temperature at the HIFU focus in tissue during and after a
%%       HIFU exposure and compare it to the Cavitation and US image
%%       echogenicity
%%
%%%%%%%%%%%%%%%%%%%%%%%
    clear all
    inFileRoot = '.txt';  % root of the input file

    %%---- GET DATABASE FILE THAT SET PARAMETERS FOR ANALYSIS ----%%
    fileIN_dBASE = 'PCDmasterLF2.xls';
    fprintf(['\n\nLoading dataBase file (%s).\n\n'],fileIN_dBASE);

    %%%%% Sample group to analyze %%%%%%%%%
    animal = 2;
    %pig 1:  2,3, 5-13, 15
    %pig 2:  2, 4,5, 7-32
    runthis = 7;
    runStop = 8 %runthis;
    TCdistance = 0.0;
    sampleGroup = ['LF2PIG', num2str(animal)];
    usFile     = ['LF2P', num2str(animal),'US'];
    fileIN_Path = 'k:\Ultrasound\DATA\LF2_ProcessedData\';
                filePath   = [fileIN_Path , sampleGroup, '\'];

    %% ARRAYS FOR CONVERTING DRIVE VOLTAGE (mVpp) to HIFU INTENSITY
    mVpp        =[50,  60,  70,  80,  90, 100, 110, 120, 130, 140, 150, 160, 170, 180, 190, 200, 210,  220,  230,  240,
250, 260, 270, 280, 290, 300]
    IntensityValues =[50,  80,  110, 140, 180, 220, 260, 310, 360, 430, 490, 550, 620, 690, 770, 850, 920, 1010, 1110,
1170, 1280, 1370, 1460, 1540, 1640, 1710]

    %%%%% PLOT VARIABLES TO ADJUST  %%%%%%%%%%%
    plotStartTime = -1;
    plotStopTime = 15;
    plotThermLow = 0;  %min Temperature to plot
    plotThermHigh = 120;  %max temperature to plot
    plotRMSmin = 0; %-60;
    plotRMSmax = 1; %-20;
    plotVideoMin = 0;
    plotVideoMax = 2500;
    heatingTime = 10;
    coolingTime = 0; %plotStopTime - heatingTime;
    %%%% END

    %%---- Set the image parameters for display purposes
        set(0,'defaulttextfontsize',14, 'defaulttextfontweight', 'bold');
        set(0,'defaultaxeslinewidth',2);
        set(0,'defaultaxesfontsize',14);

%%% Start Analysis %%%
for cFile = runthis:1:runStop  %% SAMPLES TO RUN FROM THE GROUP BEING ANALYZED
        %figH = figure;  %open first figure

    %%%%%%%% GET THERMAL DATA FOR EACH FILE  %%%%%%%%%%%%%%%%%%%
```

```
fileIN = ['T', num2str(cFile)];
inData = load([filePath, fileIN, '.xls']);   %% LOAD TEMPERATURE FILE

TC_Time = [];   %% Thermocouple temperature time
TC_Amp = [];    %% Thermocouple temperature amplitude

TC_Time = inData(:,1)/1000 - 1.5;   %% CONVERT TO ms and for the 1.5 sec of background recording before
start of HIFU
                        TC_Amp = inData(:,2);
    cImage = 0;
    clear inData;


%%%%%%% PLOT RMS VALUE FOR BROADBAND NOISE  %%%%%%%%%%%%%%%%%%%%%%%%%%%%

%%%%% GET THE INFORMATION FROM THE PCDmaster.txt DATABASE FILE  %%%%%%%
```

% Tissue		exp#	Sample	DriveV	us/seg	pts/us	DutyCycle	dB		msDelay	Location	
	numSegs		FirstHIFUPulse	LastHIFUPulse	Run?		Split		Mapped	USimageOnsetTime		
% PIG	8		BP1	300	1000	25	80	15	0		Front	80	7	69
1	1		0	1.20									
% A1	A2	A3	A4	A5	A6	A7	A8	A9	A10	A11	A12	A13	A14
A15	A16		A17										

```
[A1, A2, A3, A4, A5, A6, A7, A8, A9, A10, A11, A12, A13, A14, A15, A16, A17, A18] = textread(([fileIN_Path
    fileIN_dBASE]), '%s %d %s %d %d %d %d %d %d %s %d %d %d %d %d %d %f %f');

%A12 =1 if file has been split
%A13 = 1 if file has been processed for maxppV

    cSamples = 0;

    max_HifuFirstSeg = max(A12);
    idx_temp = find(A4 == 300); % TEMPORARY REMOVE find(A4 == VoltagePlot);
    idx_tempA = find(A14(idx_temp) == 1);

    data_AmpStatsArray = zeros([max(A11)+1+max_HifuFirstSeg+1,length(idx_tempA)+1]);

        for cRow = 1:length(A1)   %debug 10:10 %RUN THROUGH ALL OF THE FILES AS POINTED TO BY
EACH ROW OF THE MASTER FILE
            dIN_Tissue      = char(A1(cRow));
            dIN_PIGnum      = A2(cRow);
            dIN_Sample      = char(A3(cRow));
            dIN_Voltage     = A4(cRow);
            dIN_usPerSegment = A5(cRow);
            dIN_ptsPerUs    = A6(cRow);
            dIN_DutyCycle   = A7(cRow);
            dIN_dB          = A8(cRow);
            dIN_msDelay     = A9(cRow);

            dIN_ListenLocation = char(A10(cRow));
            dIN_numSegs     = A11(cRow);

            dIN_HifuFirstSeg = A12(cRow);   %First segment that HIFU is on
            dIN_HifuLastSeg = A13(cRow);    %Last segment that HIFU is on

            dIN_RunSample   = A14(cRow);
            dIN_Split       = A15(cRow);
            dIN_Mapped      = A16(cRow);

            dIN_USonsetTime = A17(cRow);
```

```
file_current = [dIN_Tissue, num2str(dIN_PIGnum),' ', dIN_Sample];

P_num = [dIN_Tissue, num2str(dIN_PIGnum)];

volts = dIN_Voltage

%%%% START PROCESSING CAVITATION FILES  %%%%%%%%%%%%%%%%%%%
fileToGet = ['RF',num2str(cFile)];          %% RF file to get
sampleGroupToGet = strcmp(P_num, sampleGroup);  %% Make sure the right sample group is being
analyzed
sampleToGet = strcmp(dIN_Sample, fileToGet);    %% Make sure the right sample within the group is being
analyzed

if (sampleToGet == 1) & (sampleGroupToGet == 1) %& (dIN_USonsetTime < 90) %(dIN_Mapped == 0) &

    remove_BackGround = 0;  %NOT used anymore so leave == 0
    [data_Time, data_Amp] = PCD_AnalyzeMaxRMSLF2(fileIN_Path, P_num, dIN_Sample, ....
            dIN_Voltage, remove_BackGround);

    timeGraph = (1:(length(data_Amp)+max_HifuFirstSeg+1));
    timeGraph = (timeGraph*0.1596 - (max_HifuFirstSeg)*0.1596);

    data_Amp = data_Amp';

    %data_Amp = data_Amp(dIN_HifuFirstSeg:(dIN_HifuFirstSeg+62));

    lineX = [dIN_USonsetTime, dIN_USonsetTime];
    lineY = [-65, 0];
    lineBGX = [min(timeGraph), max(timeGraph)];
    lineBGY = [-56.31, -56.31];
    RMS_Amp = ((data_Amp+54.3)/(54.3 - 13.3389)-0.1)/0.9;     %56.7747normalize to 0-1
    idx = find(RMS_Amp <= 0);
    RMS_Amp(idx) = 0;
    RMS_Time = timeGraph((max_HifuFirstSeg-dIN_HifuFirstSeg+1):((max_HifuFirstSeg- ....
            dIN_HifuFirstSeg+1)+length(data_Amp)-1));

    idx = find(RMS_Time <= 10);
    idxStop = max(idx)
    idxStart = find(RMS_Time == 0);
    RMS_Time = RMS_Time(idxStart:idxStop);
    RMS_Amp = RMS_Amp(idxStart:idxStop);
    figName = ['Driving Voltage', num2str(dIN_Voltage), '-mVpp'];

%%% GET THE HIFU INTENSITY FOR THE INPUT DRIVE VOLTAGE %%%
    voltage  = num2str(dIN_Voltage)
    dIN_Voltage = str2num(voltage)
    idxIntensity = find(mVpp == dIN_Voltage);        % GET ARRAY INDEX FOR THE DRIVE VOLTAGE
    HIFUintensity =  IntensityValues(idxIntensity)       % get the HIFU intensity

        %NameTitle = [sampleGroup, '-', fileIN, ' ', num2str(dIN_Voltage), '-mVpp'];
    NameTitle = [sampleGroup, '-', fileIN, ' ', num2str(HIFUintensity), ' W/cm^2 (I_S_P_T_A)'];
    figTitle = [fileIN];

    if length(data_AmpStatsArray) > length(data_Amp)
        zerA = zeros([(max_HifuFirstSeg-dIN_HifuFirstSeg+1), 1]);
        zerB = zeros([((length(data_AmpStatsArray)-(max_HifuFirstSeg-dIN_HifuFirstSeg+1)-1) - ....
                length(data_Amp)), 1]);
        data_Amp = [zerA; data_Amp'; zerB];
        data_Amp = data_Amp';
    end
```

```
        cSamples = cSamples + 1;
        if cSamples == 1
            data_AmpStatsArray(:,cSamples)= [0; timeGraph'];
            cSamples = cSamples + 1;
        end

        data_AmpStatsArray(:,cSamples)= [cRow; data_Amp'];

%%% Get Video Data
    filePath = [fileIN_Path, sampleGroup, '\'];
    fileIN = [usFile, num2str(cFile)];
    inData = load([filePath, fileIN, '.xls']);   %% LOAD TEMPERATURE FILE

    VID_Time = [];
    VID_Amp = [];
    VID_Time = inData(:,1);
    VID_Amp = inData(:,2);

    clear inData;

    modelTemperature = [];
    for cMT = 1:1  %get the Model predicted temperature for this many locations near the focus
        [modelTime, modelTemperatureIN] = ThermalModel(HIFUintensity, (TCdistance), heatingTime, ....
            coolingTime);
        modelTemperature = [modelTemperature; modelTemperatureIN];
    end

%%% PLOT Thermal Vs. Video
figDouble2 = figure;
    hold on;
    for cMT = 1:1  %get the Model predicted temperature for this many locations near the focus
        hl1 = line(modelTime, modelTemperature(cMT,:), 'LineStyle', '--', 'Color', 'k', 'LineWidth', 1);
    end
    hl1 = line(TC_Time, TC_Amp,'Color','b', 'LineWidth' , 1);

    xlabel('Time (s)');
    ax1 = gca;
    set(ax1,'XColor','b','YColor','b');
    axis([plotStartTime, plotStopTime, 35, plotThermHigh]);
    title(NameTitle);
    ylabel('Temp (degC)');

    if max(VID_Amp) >= 120
        idx = find(VID_Amp > 120);
            hold on;
        %fprintf (['%s the Time of Hspot onset = %f.\n\n'], figTitle, VID_Time(idx(1)));
        pLineX = [VID_Time(idx(1)) VID_Time(idx(1))];
        pLineY = [119 plotVideoMax];
        line(pLineX, pLineY, 'Color', 'k');
    else
        %fprintf (['%s the Time of Hspot onset = %f.\n\n'], figTitle, 0);
    end

    ax2 = axes('Position',get(ax1,'Position'),...
        'YAxisLocation','right',...
        'Color','none',...
        'YColor', 'r'); % green [ 0.251 0.502 0.502 ]);

    hl2 = line(RMS_Time, RMS_Amp, 'Color', 'r', 'marker', 'o', 'MarkerEdgeColor', 'r',...
        'MarkerFaceColor', 'r',...
```

```
                        'MarkerSize',4,'Parent',ax2);
                    axis([plotStartTime, plotStopTime, plotRMSmin, plotRMSmax]);
                    title_figure = [filePath, 'Thermal\P', num2str(animal), '_', figTitle, '_TCvVIDvMvIC_COMB'];

                    saveas(figDouble2,[title_figure, '.tif'], 'tif');
                %  close(figDouble2);


                    end
                end

            %%%% Print values in array format for pasting into excell sheet
            if max(VID_Amp) >= 120
                idx = find(VID_Amp > 120);
                fprintf(['%f\t'], VID_Time(idx(1)));
            else
                fprintf(['%d\t'], 999);
            end

            if max(TC_Amp) >= 100
                idx = find(TC_Amp > 100);
                fprintf(['%f\t'], TC_Time(idx(1)));
                fprintf(['%f\n'], max(TC_Amp(:,1)));
            else
                fprintf(['%d\t'], 999);
                fprintf(['%f\n'], max(TC_Amp(:,1)));
            end
end
```

ThermalModel.m
```
%%%%%%%%%%%%%%%%%%%%%%%%
%% ThermalModel.m
%% Brian A. Rabkin
%% 10.15.04
%%
%% Used: To calculate the temperature at the in tissue during and after a
%%       HIFU exposure
%%
%% Input: intensity = HIFU Intensity
%%        TCdistance = hermocouple distance from focus
%%        heatTime = Time HIFU is on
%%        coolTime = Time to calculate after HIFU is off
%% Output: TimeOut      = Array of time during and after HIFU
%%        TemperatureOut = Array of temperature at TimeOut
%%%%%%%%%%%%%%%%%%%%%%%%

function [TimeOut, TemperatureOut] = ThermalModel(intensity, TCdistance, heatTime, coolTime);
    %RETURNS [modelTemperature, modelTime]

    if nargin<1,   %IF DIDN'T GET ANY INPUT TO THE FUNCTION
        TCdistance = 0;
        intensity = 100;
        heatTime = 10;
        coolTime = 20;
        showPlot = 1; %  show plot
    else
        showPlot = 0;  % don't show plot
    end

    Dist = TCdistance/1000;  % distance in m from the HIFU axis
```

```
%% Tissue properties of MUSCLE
frequency   = 3.32;      %MHz  HIFU Frequency
Density     = 1.07*1000;  %g/cm3
SpeedSound  = 1.566*1e+2; %cm/s  rho
Alpha       = 0.15e2;    % Np/cm/MHz from Christensen 1988
ThermalK    = 0.0048e2;  %4.8 %%(W/cm degC)
                         %J*s-1*cm-1*degC-1 %The Journal of Physiology (2000), 524.2, pp. 603-615
SpecificHeat = 3.59e3;   % (J/g degC) [Cv]
                 %The Journal of Physiology (2000), 524.2, pp. 603-615
                 % also in Journal of Physiology (2001), 536.3, pp. 947-956
GausRad     = 0.038/100; %(cm) symble = a


ThermalDiffus = ThermalK/(Density*SpecificHeat);


TemperatureOut = [];    % Temperature array
TimeOut = [];           % Time array
bodyTemp = 36;          % Number used to start the model at body temperature


Intensity = intensity*1e4; % Convert to W/m2


cTime = 1;       % For Indexing array


    %%%% CALCULATE THE TEMPERATURE RISE DURING HIFU
for  time = 0:0.01:heatTime
    TemperatureOut(cTime) =
        ((2*Alpha*frequency*Intensity)/(Density*SpecificHeat))*((GausRad^2)/(4*ThermalDiffus)) *exp(-
        Dist^2/GausRad^2)*log(1+((4*ThermalDiffus*time)/GausRad^2));

    TempPeak = TemperatureOut(cTime);

    TimeOut(cTime) = time;
    cTime = cTime +1;  % index array
end


%% Get temperature at end of HIFU
TempPeak = TemperatureOut(cTime-1);


%%%% CALCULATE THE TEMPERATURE AFTER HIFU
for  time = (heatTime+0.01):0.01:(heatTime+coolTime)
    timeAfter = time - heatTime;  % How long it has been since heating stopped

    TemperatureOut(cTime) = TempPeak/(1+((4*ThermalDiffus*timeAfter)/GausRad^2));

    TimeOut(cTime) = time;
    cTime = cTime +1;
end


TemperatureOut = TemperatureOut + bodyTemp;  % Adjust temperature to start at body temperature


if showPlot == 1;
    plot (TimeOut, TemperatureOut, 'MarkerSize', 10, 'color' , 'r');
end
```

VITAE

BRIAN ALAN RABKIN

EDUCATION

University of Washington, Ph.D., (Bioengineering) December 2004

Thesis: *High-Intensity Focused Ultrasound (HIFU) Induced Hyper echoic Regions for the Ultrasound Guidance of HIFU Therapy.*

University of Washington, M.S., (Bioengineering) August 2002

Thesis: *Discrete Isoelectric Fractionation: The fractionation of proteins in free solution by discrete pH intervals.*

University of California, Santa Barbara, B.A., (Aquatic Biology) 1995

RESEARCH EXPERIENCE

University of Washington, Graduate Research Assistant   Sept. 2002 – Dec. 2004

Prof. Shahram Vaezy at the Department of Bioengineering and Center for Industrial and Medical Ultrasound, Applied Physics Laboratory.

- Research into the role of acoustic cavitation in the formation of a hyperechoic region in real-time ultrasound images during high intensity focused ultrasound (HIFU) therapy.
- Development of a real-time Color-Doppler ultrasound imaging method for the guidance and monitoring of HIFU therapy.
- Assessment of HIFU therapy for the intra-operative treatment of ovarian cancer.
- Development of an immunocompetent orthotropic isograft mouse model of ovarian cancer for HIFU treatment.

University of Washington, Graduate Research Assistant   Oct. 2000 – Aug 2002

Prof. Deirdre Meldrum at the Genomation Laboratory, Department of Electrical Engineering and Department of Bioengineering, University of Washington, Seattle Washington

- Development of a protein separation and analysis systems for discrete isoelectric fractionation of proteins.
- Development of a capillary isoelectric focusing device for protein separation and quantification.

NASA-Ames Research Center, Research Assistant   Aug. 1997 – Sept. 2000

Prof. Bernard Halloran, Department of Medicine, University of California, San Francisco at Moffett Field, California.

- Design of an in-vivo strain gauge telemetry system.
- In-vivo strain analysis of the rat femur, humerus and tibia.
- In-vitro remodeling of bone specimens by cultured osteoblasts and osteoclasts.

Stanford University, Research Assistant   Apr.1998 – Jul.1999

Stanford Human Genome Center, Department of Genetics, Palo Alto California

- Mapping and sequencing of Human Chromosome 4.
- Molecular biology and genetic analysis - High-density Filter Hybridization, PCR and Gel Electrophoresis.
- Development of a cultured bacteria library for tracking human artificial clones.

- Computational biology - Data analysis and manipulation, setup and tracking of experiments, design of static and dynamic web pages using CGI script. Languages include PERL, C++ and HTML for data analysis and tracking of biological samples.

NASA-Ames Research Center, Moffett Field, Research Assistant   Feb.1997 – Jan. 1998
Prof. Emily R. Morey-Holton, Department of Medicine, University of California, San Francisco.
Research into the effects of loading, hyper-loading and unloading on bone mineralization in rats.
- Necropsy of experimental animals including histomorphometry.
- Maintained laboratory, data analysis and acquisition computer systems, including both software and hardware.

University of California, Santa Barbara, Research Assistant   Mar.1993 – Jan. 1995
Prof. James J. Childress, Marine Sciences Institute.
- Research into the ecological physiology of deep-sea animals.
- Assays on glycolytic enzymes, measured respiration rates and dissected specimens.
- Field research aboard vessels in the North-East and Mid Pacific Ocean.
- Collected, identified and maintained midwater animals.

Oceanographic Research Expeditions   Mar. 1993 – Jun.1994
Chief Scientist: Dr. James J. Childress, Marine Sciences Institute, University of California, Santa Barbara.
- 5 Expeditions aboard the Research Vessel, New Horizon, Scripps Institute of Oceanography, San Diego, California.
- Expeditions aboard the Research Vessel, Point Sur, Moss Landing Marine Laboratories, Moss Landing, California.

TEACHING EXPERIENCE
- Teaching Assistant in Inorganic Chemistry at the University of Washington, spring quarter, 2002
- Mentoring of undergraduate student and high school summer intern, University of Washington, June 2001 – August 2002

GRANTS
Schonfeld J, Halloran B, **Rabkin B**, Szivek J. "Development of a system for quantifying in vivo bone strains in rodents in normal and altered gravity environments." Co-Investigator, NASA Ames Research Center, Directors Discretionary Fund, 1999

PUBLICATIONS
Ph.D.Thesis: Discrete Isoelectric Fractionation: The fractionation of proteins in free solution by discrete pH intervals. Dec. 2004

Rabkin B, Zderic S, Vaezy S. Hyperecho in ultrasound images of HIFU therapy: involvement of cavitation. Ultrasound Med. Biol. Requested for resubmission, Dec. 2004

Chou S, **Rabkin B**, Dowling S, Theiss P, Vaezy S. An immunocompetent orthotopic isograft mouse model of ovarian cancer for high-intensity focused ultrasound (HIFU) treatment. Comparative Medicine, Accepted June 2004

M.S. Thesis: "Discrete Isoelectric Fractionation: The fractionation of proteins in free solution by discrete pH intervals." Dept. of Bioengineering, University of Washington: August 2002

Rabkin B, Szivek JA, Schonfeld J, Halloran BP. Long-term measurement of bone strain in vivo: the rat tibia. J. Biomed. Mater. Res. May 1 ;58(3):277-81, 2001.

Dehority, W, Halloran BP, Bikle DD, Curren T, Kowtenuik PJ, Wronski TJ, Shen Y, **Rabkin BA**, Bouraoui A, Morey-Holton E. Bone and hormonal changes induced by skeletal unloading in the mature male rat. Am. J. Physiol. 276 (Endocrinol. Metabolism. 39): E62-E69, 1999.

Rabkin B, Szivek JA, Schonfeld J, Halloran BP. An *in-vivo* model for long term assessment of bone strain. J Bone Mineral Res. Sept;14(Sup 1):S316, 1999

Abstracts, Mini-Papers and Posters:
Rabkin B, Zderic V, Vaezy S. Real-time color-Doppler guidance of HIFU for the selective avoidance or occlusion of blood vessels. 4th International Symposium on Therapeutic Ultrasound, Kyoto, Japan: 2004

Rabkin B, Zderic V, Vaezy S. HIFU-induced hyperecho in ultrasound images: cavitation activity and thermal behavior. 4th International Symposium on Therapeutic Ultrasound, Kyoto, Japan: 2004

Rabkin B, Zderic V, Vaezy S. Involvement of cavitation in the appearance of hyperechoic regions in ultrasound image visualization of high intensity focused ultrasound therapy: in-vivo results. IEEE UFFC Ultrasnoics Symposium, Montreal, Canada, Aug 23-7: 2004

Holl M, Friedman N, **Rabkin B**, Gibbons E, Kosar T, Meldrum D. Fluorescence-based quantitative PCR for determining minimal residual disease using disposable microfluidic cartridges. Biomedical Engineering Society Annual Meeting, October 2000, Washington.

Holl M, Paulson T, **Rabkin B**, Gibbons E, Kosar T, Meldrum D. Integrated microsystem for classification, sorting, and storage of cellular nuclei based on DNA content from a tissue biopsy. Biomedical Engineering Society Annual Meeting, October 2000, Washington.

Rabkin B, Szivek JA, Schonfeld J, Halloran BP. *In-Vivo* method for chronic assessment of bone strain. Grav Space Bio Bull. Oct;13(1):17, 1999.

Komarova, SV, **Rabkin B**, Booker JD, Ataullakhanov FI, Globus RK. Changes in energy metabolism of primary rat osteoblasts during differentiation. BioThermoKinetics In The Post Genomic Era, Proceedings of the 8th international meeting on Biothermokinetics, July 1998, Sweden. 58-61, 1998.

Komarova, SV, **Rabkin B**, Booker JD, Ataullakhanov FI, Globus RK. Regulation of glycolytic and oxidative phosphorylation pathways in mature osteoblasts. BioThermoKinetics In The Post Genomic Era, Proceedings of the 8th international meeting on Biothermokinetics, July 1998, Sweden. 62 – 65, 1998.

Technical Skills

- **Surgical:** Animal model development and surgery including mice, rats, rabbits and pigs.
- **Analytical Laboratory Techniques:** Acoustic cavitation detection, capillary isoelectric focusing, high-density filter hybridization, PCR and gel electrophoresis, spectrophotometry, gas chromatography, blood-gas analysis, flourometry, microscopy, column chromatography, respiromotry, histology.
- **Computers:** Programming languages – Java, Perl, CGI script, Matlab and HTML. Unix, Macintosh and Windows; word processing, spreadsheets, statistical analysis.
- **Data acquisition:** systems development including hardware and software (LabView).
- **Mechanical Skills:** Metal work. Design and constructing of surgical instruments, cell culturing devices, sensor equipment, strain gauge test equipment and other research devices. SolidWorks design software.